2014

GENERATION OF MULTICOMPONENT POLYMER BLEND MICROPARTICLES USING DROPLET EVAPORATION TECHNIQUE AND MODELING EVAPORATION OF BINARY DROPLET CONTAINING NON-VOLATILE SOLUTE

Venkat N. Rajagopalan
University of Kentucky, venkatnarayanis@gmail.com

STUDENT AGREEMENT:

I represent that my thesis or dissertation and abstract are my original work. Proper attribution has been given to all outside sources. I understand that I am solely responsible for obtaining any needed copyright permissions. I have obtained needed written permission statement(s) from the owner(s) of each third-party copyrighted matter to be included in my work, allowing electronic distribution (if such use is not permitted by the fair use doctrine) which will be submitted to UKnowledge as Additional File.

I hereby grant to The University of Kentucky and its agents the irrevocable, non-exclusive, and royalty-free license to archive and make accessible my work in whole or in part in all forms of media, now or hereafter known. I agree that the document mentioned above may be made available immediately for worldwide access unless an embargo applies.

I retain all other ownership rights to the copyright of my work. I also retain the right to use in future works (such as articles or books) all or part of my work. I understand that I am free to register the copyright to my work.

REVIEW, APPROVAL AND ACCEPTANCE

The document mentioned above has been reviewed and accepted by the student's advisor, on behalf of the advisory committee, and by the Director of Graduate Studies (DGS), on behalf of the program; we verify that this is the final, approved version of the student's thesis including all changes required by the advisory committee. The undersigned agree to abide by the statements above.

Venkat N. Rajagopalan, Student

Dr. Asit K. Ray, Major Professor

Dr. Thomas D. Dziubla, Director of Graduate Studies

GENERATION OF MULTICOMPONENT POLYMER BLEND MICROPARTICLES USING DROPLET EVAPORATION TECHNIQUE AND MODELING EVAPORATION OF BINARY DROPLET CONTAINING NON-VOLATILE SOLUTE

DISSERTATION

A dissertation submitted in partial fulfillment of the
requirements for the degree of Doctor of Philosophy in the
College of Engineering
at the University of Kentucky

By
Venkat Narayan Rajagopalan

Lexington, Kentucky

Director: Dr. Asit K. Ray, Professor of Chemical Engineering

Lexington, Kentucky

2014

ABSTRACT OF DISSERTATION

GENERATION OF MULTICOMPONENT POLYMER BLEND MICROPARTICLES USING DROPLET EVAPORATION TECHNIQUE AND MODELING EVAPORATION OF BINARY DROPLET CONTAINING NON-VOLATILE SOLUTE

Recently, considerable attention has been focused on the generation of nano- and micrometer scale multicomponent polymer particles with specifically tailored mechanical, electrical and optical properties. As only a few polymer-polymer pairs are miscible, the set of multicomponent polymer systems achievable by conventional methods, such as melt blending, is severely limited in property ranges. Therefore, researchers have been evaluating synthesis methods that can arbitrarily blend immiscible solvent pairs, thus expanding the range of properties that are practical. The generation of blended microparticles by evaporating a co-solvent from aerosol droplets containing two dissolved immiscible polymers in solution seems likely to exhibit a high degree of phase uniformity. A second important advantage of this technique is the formation of nano- and microscale particulates with very low impurities, which are not attainable through conventional solution techniques. When the timescale of solvent evaporation is lower than that of polymer diffusion and self-organization, phase separation is inhibited within the atto- to femto-liter volume of the droplet, and homogeneous blends of immiscible polymers can be produced. We have studied multicomponent polymer particles generated from highly monodisperse microrddroplets that were produced using a Vibrating Orifice Aerosol Generator (VOAG). The particles are characterized for both external and internal morphology along with homogeneity of the blends. Ultra-thin slices of polymer particles were characterized by a Scanning Electron Microscope (SEM), and the degree of uniformity was examined using an Electron Dispersive X-ray Analysis (EDAX). To further establish the homogeneity of the polymer blend microparticles, differential scanning calorimeter was used to measure the glass transition temperature of the microparticles obtained. These results have its significance in the field of particulate encapsulation. Also, better control of the phase morphologies can be obtained by simply changing the solvent/solvents in the dilute solutions.

Evaporation and drying of a binary droplet containing a solute and a solvent is a complicated phenomenon. Most of the present models do not consider convection in the droplet phase. In this dissertation work, a model is developed that incorporates convection inside the droplet. The results obtained are compared to the size obtained

from experimental results. The same model when used with an aqueous solution droplet predicted concentration profiles that are comparable to results obtained when convection was not taken into account. These results have significance for more rigorous modeling of binary and multicomponent droplet drying.

KEYWORDS: Polymer blend microparticles, microdroplets,
droplet evaporation technique

VENKAT NARAYAN RAJAGOPALAN
Student's Signature

10/17/2014
Date

GENERATION OF MULTICOMPONENT POLYMER BLEND MICROPARTICLES AND MODELING EVAPORATION OF BINARY DROPLET CONTAINING NON-VOLTAILE SOLUTE

By

Venkat Narayan Rajagopalan

Dr. Asit K. Ray
Director of Dissertation

Dr. Thomas D. Dziubla
Director of Graduate Studies

10/17/2014
Date

To My Family and Dr. Asit K. Ray

ACKNOWLEDGEMENT

Words at my command are not adequate to express my gratitude towards my Ph.D. advisor Dr. Asit K. Ray for his unrelenting support throughout the visualization of this work. He has always been an inspiration and has always motivated me and supported me even during the most challenging times. I have always been a big fan of his strong command in the chemical engineering principles and his teaching capabilities and I had the privilege to experience it first hand.

I would also like to thank Dr. Eric Grulke for helping me and giving me appropriate suggestions during my research work in regards to polymer blends.

I would also like to thank my Ph.D. committee (Dr. Douglas Kalika, Dr. Zach Hilt and Dr. Kozo Saito) for their time and effort to comment and review my research work. I would like to thank James Begley and Mary Ingle (Histology Lab, University of Kentucky) for their help in providing me with ultramicrotomed samples for my research work and helping me with confocal microscopy and Larry Rice (Electron Microscopy lab, University of Kentucky) for helping me get acquainted with scanning electron microscopy.

I would also like to take this opportunity to thank all my fellow lab mates with whom I have had numerous discussions regarding different subjects both academic and otherwise. I would also like to thank all my friends at Lexington, KY who have made my stay here memorable.

Last but not the least, I would also like to thank my parents Mr. R. Rajagopalan & Mrs. Sandhya Rajagopalan, my brother Shankar and my wife Sonal for their unconditional love and support throughout my research work.

TABLE OF CONTENTS

LIST OF FIGURES

LIST OF TABLES

CHAPTER 1

1. INTRODUCTION

Droplet drying techniques have been widely used for the production of food and dairy products using spray drying in one form or the other. The end products in such processes are particulate powders. Droplet drying methods offers several advantages over other bulk methods and size reduction methods. They offer continuous productions, high throughputs, very large surface areas and hence high drying rates. They are easy to handle and transport and are space efficient in terms of packaging and storage. Spray drying is one of the most widely used methods for the production of particulate powders. Spray drying involves atomizing the liquid solution feed into fine droplets. These droplets are made to come in contact with a dry gas, usually air (or N_2 to prevent oxidation in some cases), at a certain temperature, either co-currently or counter-currently in a drying column. The droplets are dried to form particles and are usually collected at the bottom by using cyclones and additional filters. Particles of different morphologies are obtained from such processes depending upon the operating conditions and nature of the feed. Particle morphology mainly dictates the various properties of the powder obtained. This is pictorially shown in figure 1.1 where the desired particle/powder characteristics are a function of morphology in one way or the other. For example, the strength and hardness of the particles obtained depends on the particle size, its density and also on the degree of porosity present in the particles. Differences in strength can be observed for hollow and solid particles. Depending on the structure of the particle formed, either skin forming, crystalline or agglomerates, may determine the strength of

the particles. A sodium chloride solution droplet would dry to form a particle with crystallites in the outer shell whereas a skim milk droplet would form an impermeable thin skin. Volatile content in the particles are important when applied to food and perfume industry. The degree of retention depends again on the thickness of the crust and how well the vapors are trapped inside the particles.

The morphology or structure of the particles depends mainly on the process variables such as feed concentration, drying temperature, method of atomization, etc. Low feed concentrations and slow evaporation rates results in solid particles whereas rapid evaporation rates may yield hollow particles. Some particles require after treatment methods such as making pellets or grinding the particles to further reduce their sizes. These operations also alter the morphologies of the resultant particles formed.

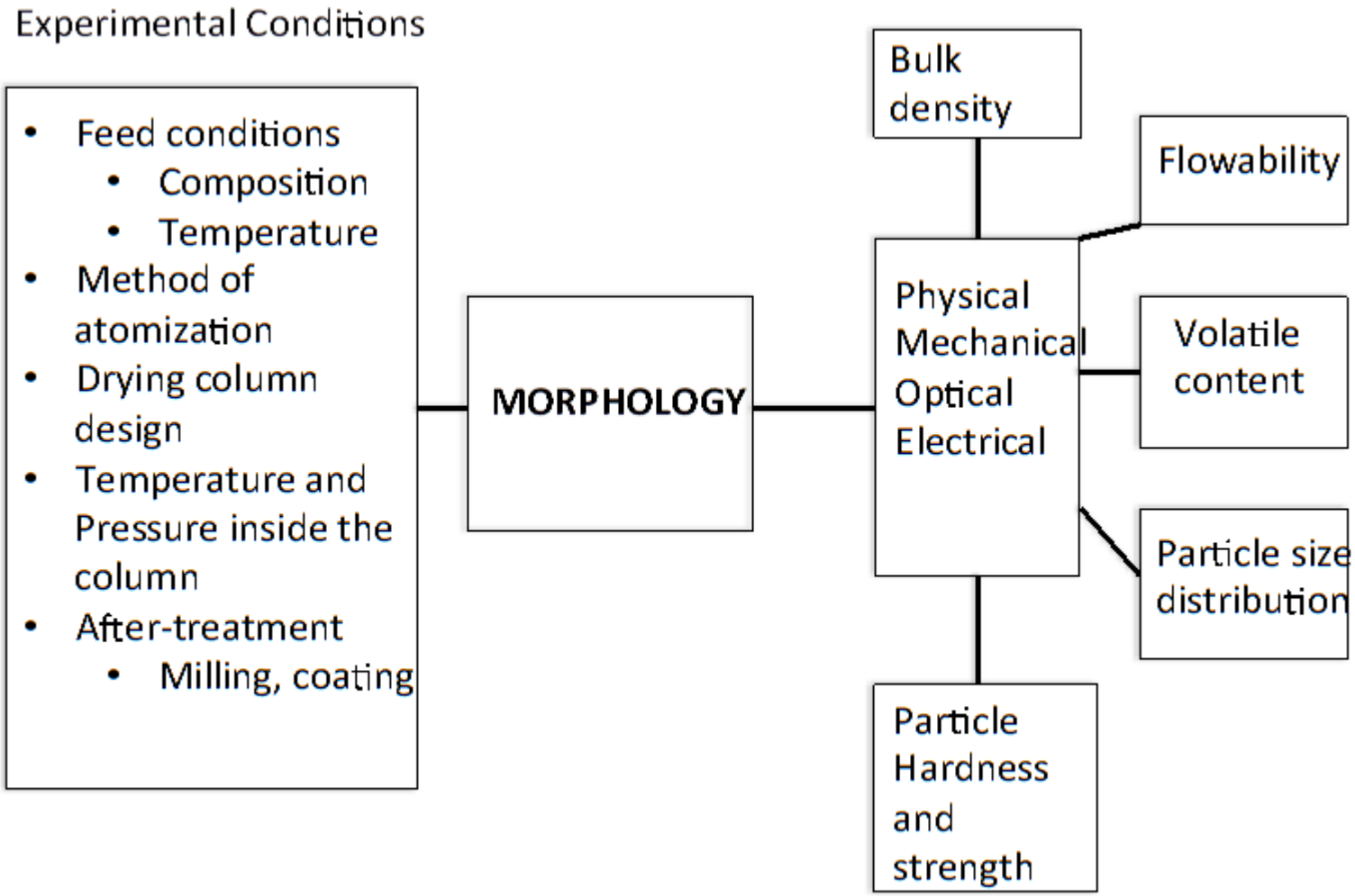

Figure 1.1: Dependence of particle properties on morphology and process variables

Various particles morphologies can result during spray drying depending on the process variables and nature of the materials at hand. Most of the particles produced via spray drying are hollow due to the high temperatures and drying rates. The hollow nature of the particles makes them ideal for encapsulation applications. Also, depending on the porosity of the particles, they can be used for timed release in drug-delivery, reactions involving catalyst particles, encapsulation of aroma, etc. An area where such a production may play a major role in controlling the morphologies and properties of the microparticles is polymer blends. Not enough research is available in the field of polymer blends in microparticle form and most of the research involved concentrates on thin films. Several advantages of the polymer blends in microparticle forms have been identified and this has prompted us to study polymer blend microparticles.

Many theoretical models have been developed over the years from simple characteristic drying curve models that uses semi-empirical expressions derived from experiments to highly complex models involving transport phenomena equations in single droplets extrapolated to the whole of the drying column in a computational fluid dynamic models. These models describe the particle formation mechanisms by considering the drying behavior of single solution/slurry/colloidal droplet and correlating these with the operating variables.

The purpose of this thesis is two-fold. The first part of the thesis deals in using the droplet drying technique to produce homogeneous polymer blend microparticles. Chapter 2 starts with a brief introduction of the thermodynamic aspects of polymer blends along with some background on preparation and characterization of polymer

blends. Some background on preparation of microparticles is also discussed along with their characterization.

Chapter 3 discusses the experimental set-up used for the preparation of the polymer blend microparticles in detail. The polymer blend systems chosen are also presented. In Chapter 4, the particle morphologies obtained, effect of various operating parameters such as initial concentration, orifice size, and temperature on morphology and homogeneity of the blends is discussed in the results and discussion section. Several conclusions are drawn based on the results obtained and also future work related to the production of polymer blend microparticles and better characterization techniques to understand the phase separation in polymer blends is also discussed.

Chapter 5 deals with the modeling of single polymer solution droplet consisting of a highly volatile solvent. A brief literature review on the previous single droplet drying models have been discussed. Most of the theoretical research in modeling single droplet drying is based on the diffusion equation that represents the concentration inside the droplet. Evaporation of a highly volatile solvent introduces a convective velocity inside the droplet and the droplet density varies along with the concentration inside the droplet. First, the drying of the droplet is modeled until the onset of skin formation. The results obtained when the convection is not taken under consideration for the same solution droplet is also compared to show that the surface concentration is under-predicted in the latter case. Conclusions and further relaxation of modeling assumptions for better prediction of the drying behavior is also discussed.

CHAPTER 2

2. BACKGROUND

2.1 Introduction

Polymer blends may be defined as physical mixtures of two or more polymeric systems. Traditionally, the interest in polymer blends arose due to the economic advantages of blending a cheaper polymer with an expensive one. Blending also results in altering the properties of the polymers and yielding a blend that has properties of both the polymers. In most cases there is an inherent phase separation when mixing two polymers. Most of the polymers are immiscible in each other, i.e., they phase separate when mixed together. This phase separation is usually seen as domains of the polymer rich phases otherwise known as the morphology of phases. The morphology of these separated phases governs the properties of the blend. Recent advances in polymer science and its application in various other fields such as drug delivery, electro-optical devices, solar cells, membrane sciences, etc. have propelled the research in polymer blends. An excellent review on the application and advantages of polymer blends is given by Favis (1991). Most of his work reviews the synthesis of polymer blend using melt processing. He discusses the factors that affect the interfacial adhesion and morphology of the polymer blends during blending. Ajji and Utracki (1996) discuss the effect of poor adhesion between the two polymer phases by reviewing the theoretical models, and how compatibilizers (mainly copolymers) can be used to lower the interface thickness. Increased application of polymer blends in other fields paved way for understanding the polymer blend phase separation using experiments and simulation.

Theoretically, if one can have a highly supersaturated solution of the polymer blends such that the composition of both the polymers lie in the region where the blend exists as a single phase then a uniform blend can be achieved. Phase separation is a relative term. Ideally, a homogeneous blend will be obtained when there is no separation at molecular level. This is not always possible in polymers as molecular weight plays a major role in determining the size of the chains in the confined space. However, the need to test the above hypothesis forms the basis of this dissertation. Several methods such as freeze-drying and spin casting have been employed to obtain homogeneous polymer blends with little or no success. All these non-equilibrium processes involve achievement of supersaturation of the components in the blend so that the mobility of the polymers is highly reduced. This supersaturation may also be achieved by droplet evaporation technique if the time scale of solvent evaporation is comparatively less than the time scale of phase separation. If such a state can be achieved then the mobility of the polymers will reduce considerably and the diffusion process will be inhibited, thus inhibiting phase separation in the blend. This will lead to a uniform mixing of the chains of the two polymer components. A simple pictorial representation is shown below in figure 2.1. Initially the droplet contains a completely homogeneous solution containing two polymers dissolved in common solvent. As the solvent evaporates, the droplet shrinks in size. If the evaporation of the solvent is very slow, then the polymers have enough time to diffuse and separate out to form a core-shell microparticle as shown in figure. A moderately slow evaporation might yield a structure that has domains of each polymer. Rapid evaporation might produce particles that inhibit the diffusion process and

the polymer chains remain uniformly distributed yielding well-mixed polymer blend microparticles.

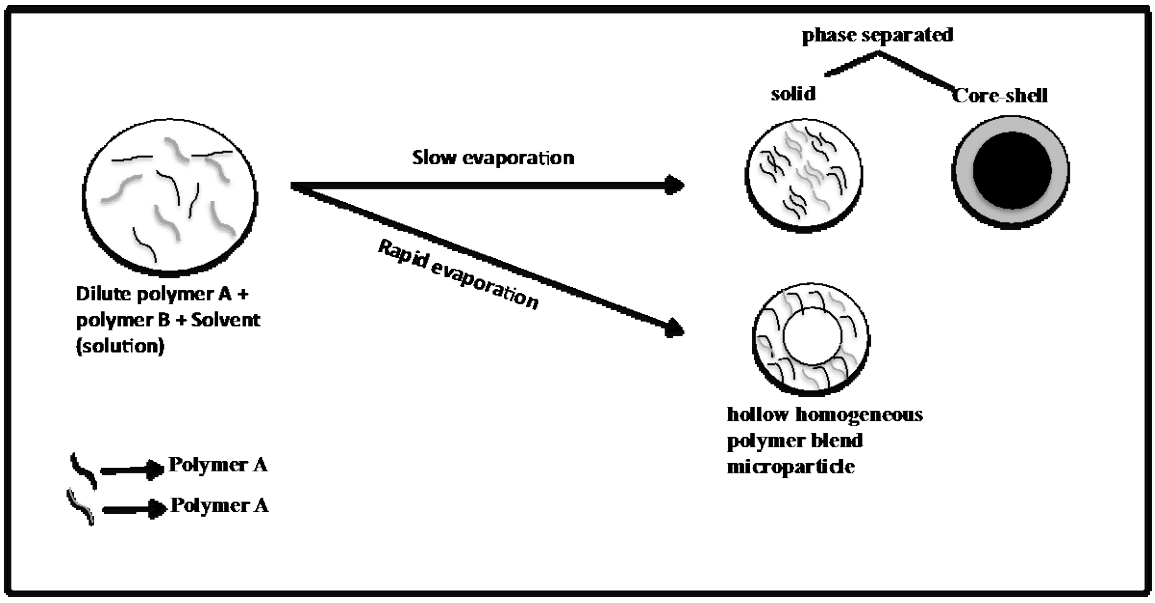

Figure 2.1: Schematic representation of formation of polymer blend microparticles from dilute polymer solutions.

In the present work, polymer blend microparticles have been prepared using the microdroplet evaporation technique. The droplets are generated using a modified vibration orifice aerosol generator that produces a uniform monodispersed linear array of microdroplets. The blend microparticles obtained are characterized for their morphology and homogeneity using electron microscopy (SEM, TEM) techniques and Differential scanning calorimeter (DSC). DSC was used to obtain the glass transition temperature of the blends. The internal morphology of the blends was investigated either by using ultra-microtomed slices or by confocal microscopy when one of the polymer components had fluorescence.

Section 2.2 discusses the thermodynamic viewpoint of the theory of phase separation in polymer blends. The two commonly explained phenomena of phase separation namely; nucleation and growth and spinodal decomposition are explained briefly. Also, different methods of controlling or inhibiting the phase separation in bulk systems is presented along with the introduction of mechanism of phase separation from a ternary system wherein a solvent is evaporated from the homogeneous blend solution to form polymer blend thin films. Section 2.3 discusses the various methods for preparation of polymer blends including solvent induced preparation techniques like spin casting into thin films.

Section 2.4 starts with a review of the general applications of microparticles with the focus shifting towards polymer blend microparticles and their applications. In this chapter, various aerosol based methods used for the production of microparticles and microspheres have been discussed along with the numerous characterization techniques employed to study the morphologies of such materials.

2.2 Phase separation/miscibility in polymer blends

This chapter briefly reviews and discusses the theory of miscibility and phase separation in polymer blend mixtures. The criteria for two polymers to be homogenously mixed, or in other words, be in a single phase, is that the Gibbs free energy of mixing (ΔG_m) is negative, i.e.,

$$\Delta G_m = \Delta H_m - T\Delta S_m < 0 \quad (2.1)$$

where ΔH_m & ΔS_m are the changes in enthalpy and entropy of mixing respectively and T is the absolute temperature. Equation 2.1 suggests that for two or more components (either polymer-polymer, or, polymer–solvent or all the three) to exist as a single phase either the change in enthalpy should be very small or the entropy of mixing and/or temperature needs to be very high. The contribution towards the enthalpy function comes from the interaction between the different components in the blend solution. The entropy from mixing is always positive but for polymers it is usually small when compared to the enthalpy term and hence most of the polymers tend to phase separate. Different phase diagrams are possible based on the nature of the polymers, their intra and inter-polymer interactions. Different possible phase diagrams are shown in Fig 2.2. Typically, it is a plot of temperature vs. composition of one of the components in a binary mixture.

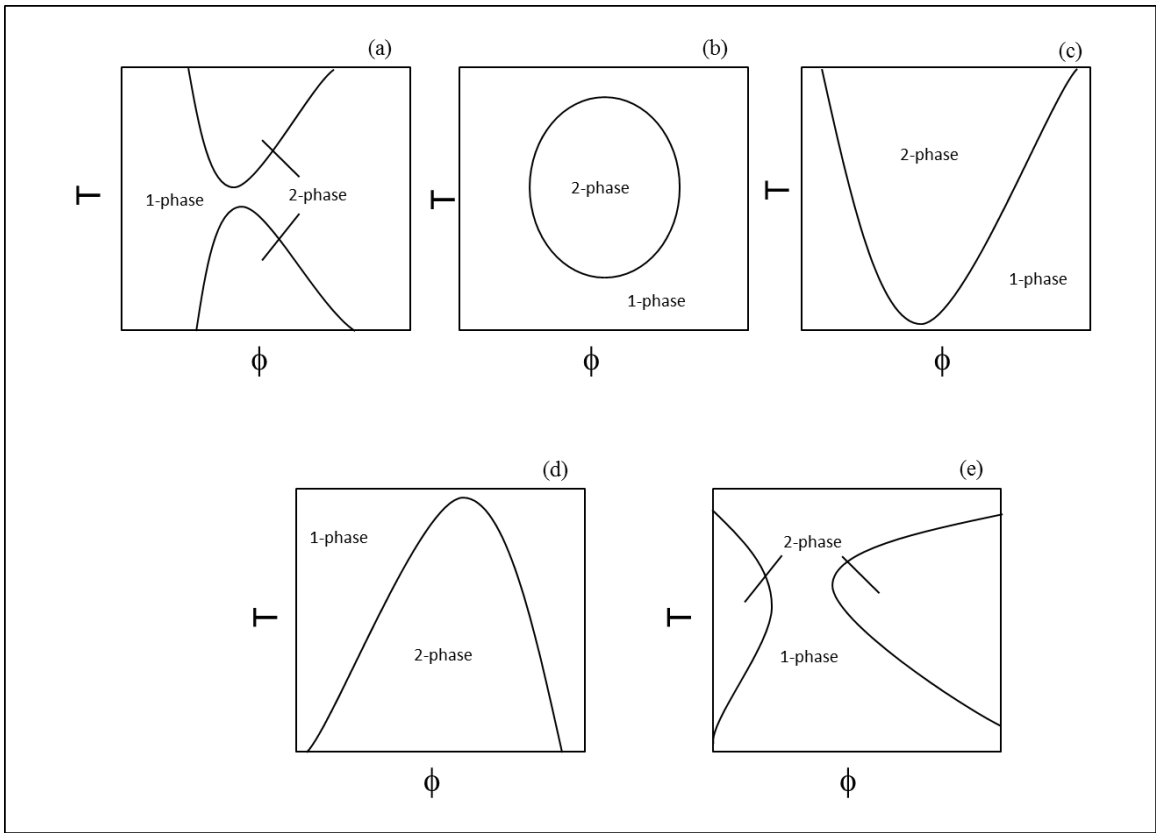

Figure 2.2: Phase diagrams of different polymer blend systems as a function of Temperature (T) and compostition (ϕ). (a) LCST above a UCST, (b) LCST below a UCST, (c) LCST, (d) UCST and (e) a blend having higher solubility at an intermediate temperature range (adapted from (Qian, Mumby et al. 1991))

Figure 2.2 clearly show the existence of regions where the blend exists as a homogeneous single phase and otherwise. According to Figure 2.2, some polymer mixtures exhibit Upper Critical Solution Temperature (UCST) as shown in Figure 2.2 (d), some exhibit Lower Critical Solution Temperature (LCST) as in Figure 2.2 (c) and some mixtures tend to exist in single phase at a moderate temperature range (Figure 2.2 (e)). This representation gives an idea of the regions in which one can operate to yield a homogeneous or phase separated polymer blends.

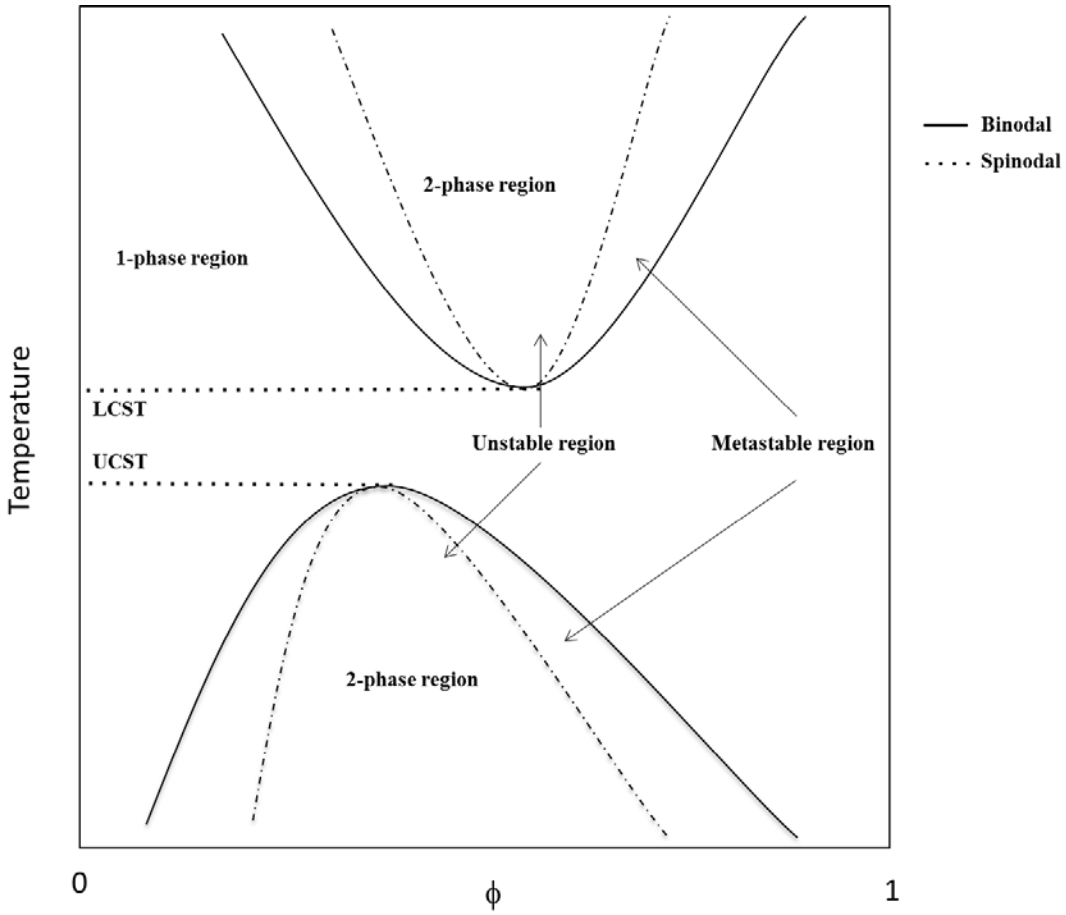

Figure 2.3: A typical phase diagram for a polymer blend showing different regions of stability.

A general schematic representation of the different regions of a phase diagram is shown in figure 2.3. Kinetics of phase separation mainly proceeds in a direction governed by the phase diagram. The solid curve is called the "binodal" or the "co-existence" curve and the dotted lines represent the "spinodal". This leads to a more important criterion for phase separation given by inequality 2.2.

$$\frac{\partial^2 G_m}{\partial \emptyset^2} > 0 \qquad 2.2$$

The critical point, which is either an LCST or a UCST, is given by inequality 2.2 when the RHS equals zero. The region in between the binodal and spinodal is the “metastable” region and the one enclosed by the spinodal is the “unstable” region.

Rate processes associated with phase separation are an important aspect in studying polymer blends as this gives an idea of the mechanism of phase separation due concentration fluctuations. These two regions and the energy fluctuations due to an infinitesimal change in composition are the primary reasons in defining which mechanism contributes towards phase separation and the final morphology of phase separated domains. The mechanisms that occur in both the metastable and unstable regions are strikingly different. In the metastable region, the infinitesimal fluctuations in composition wear out easily and hence a large fluctuation in composition is required for the phases to form. This large fluctuation is called a nucleus and the morphology obtained is more structured and defined. This is called Nucleation and Growth (NG). In the unstable region however, the mixture is unstable to even very small fluctuations. Since there is no thermodynamic barrier to phase growth, the phase separation occurs more spontaneously. Also, the growth of the fluctuations occurs in a direction opposite to the concentration gradient created by small composition fluctuations. The growth of the phase depends upon the diffusion distance and hence the decomposition or phase separation occurs in finer length scales. Sections 2.2.1 and 2.2.2 will very briefly discuss the nucleation and growth and spinodal decomposition in polymer blends.

2.2.1 Nucleation and Growth

When a system of a homogenous solution of two polymer blends is cooled from a high temperature equilibrium state to non-equilibrium one below the phase transition region, the system will eventually evolve into a new equilibrium state. Ordered phases of both the polymers will be formed during the process. During this process, local ordered domains of the ordered phases tend to grow if the sizes of these ordered phases are greater than the critical nucleus size. Continuous growth of these nuclei and ordered interfaces results in structures similar to that shown in figure 2.4 (a). Most of the nucleation and growth phenomena yield spherical domains but under certain conditions the nucleation and growth process can be controlled to yield several other morphologies such as lamellar or cylindrical. In the nucleation and growth, the process is usually very slow. This results in a more uniform and structured phase separated domains. Figure 2.4 (a) clearly demarcates the phase-separated domains of PVC and PS blend films prepared in our lab. PS forms the continuous phase and PVC forms the discrete circular domains. (The films were prepared by dissolving a 2wt% PS-PVC (equal weight ratios) in THF and pouring the dissolved solution in a petri dish. The solution was dried for more than 3 days at room temperature and further dried under vacuum for 48 hrs. The dried films were observed under SEM.)

2.2.2 Spinodal Decomposition

In contrast to nucleation and growth phenomena, when a single-phase system of polymer blend is forced to jump into the spinodal region, phase separation is more spontaneous and random microstructures are formed. A pictorial representation of polymer blend morphology from such a process is shown in figure 2.4 (b). Figure 2.4 (b) is just a representation, as we did not make any films that resulted in spinodal decomposition. Since the morphology obtained from a spinodal decomposition process is a highly interconnected network of polymer chains, the properties of polymer blends are superior in many cases when compared to the blends obtained from nucleation and growth processes. Spin casting and freeze drying of polymer blend solutions into thin films takes advantage of the spinodal decomposition process.

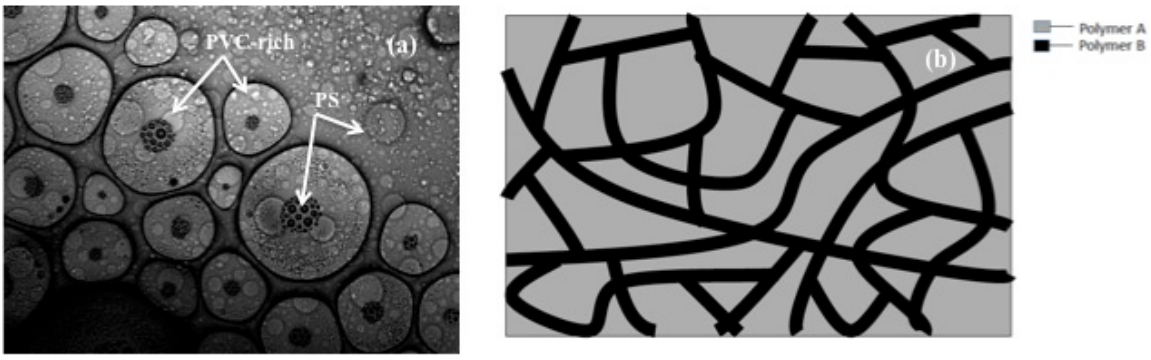

Figure 2.4: Visual representation of different phase separation processes in polymer blends (a) SEM images of PVC-PS film showing Nucleation and Growth (b) Spinodal Decomposition forming co-continuous phases.

2.3 Methods for preparing polymer blends

Polymer blends are generally prepared either from the molten state or by compatibilizing one or both the polymers to increase the interaction between each phase or by introducing a solvent to prepare thin films via spin casting.

2.3.1 Melt Processing

Conventionally, polymer blends were prepared from melts. It is the most economical process and offers high degree of mixing. The polymers are heated above their melting points until both the polymers are in molten liquid state and then quenched to yield a solidified polymer blend. Most of the times the quenching is carried out in combination with an extrusion process. Usually, the polymers are raised above their melting points and then passed through an extruder for obtaining fibrous end products with lateral phase separations (Scott and Macosko (1991), Chapleau and Favis (1995)). The basic idea behind these processes was to induce mixing and breaking up of the phase separated domains into smaller sizes.

2.3.2 Compatabilization

Most of the polymer pairs are immiscible in each other and the interfacial tension between the two phases plays a major role during phase separation. The reduction of the interfacial tension either by altering the surface properties of one or both of the polymers or, by adding a third component (co-polymer) is called compatibilization in polymer literature. The resulting blend is sometimes referred to as “polymer alloys”. An excellent review on polymer alloys is given by Utracki (Utracki 2002). Compatabilization is either

induced using physical mixing of a third component or by chemically bonding the third component to increase the mutual interactions between the polymers to be blended. For example, Li and Hu (2000) have compared compatablized and uncompatabilized blends of polypropylene and polyamide 6 made using melt mixing. Si et. al. (2006) have used organoclays to compatibilize polymer blends of PS/PMMA and PC/SAN. Cao et. al. **(2011)** studied the compatibilization of immiscible blends of polyamide (PA) and polyphenylene oxide (PPO) using grapheme oxide sheets. Vast literature is available for these processes but they are not the scope of the present work and hence are not discussed here.

2.3.3 Solvent induced

As discussed earlier, most polymer blends are immiscible over a wide range of temperature and composition that is of practical importance. Even though the starting polymer blend mixture is homogeneous in its molten state, when it is cooled to temperatures of operable range, due to the slow diffusion process, the phase separation is more pronounced and the phase morphologies are more or less segregated with domain of one polymer-rich phase in the other. Improving the melt mixing and the rate of quenching can reduce the domain sizes but not to a large extent. Also, the properties of the blend obtained are not continuous throughout. High molecular weight polymers tend to be immiscible because of very low enthalpic and entropic contributions when blended together. Using a solvent to dissolve the polymers increases the entropic contributions and hence a homogeneous mixture of the polymers and the solvent is formed. Removal of the solvent from this solution aids in precipitation and/or phase separation in the polymer blends. If the solvent is removed rapidly enough to prevent phase separation then one can

ideally achieve a homogeneous blend. The process by which the solvent is removed governs the final morphology of the blends obtained. The blends obtained are in a non-equilibrium state and are kinetically frozen in time. Freeze-drying, supercritical fluid precipitation and spin coating are processes that use solvent evaporation as the basis for preparing homogenous blends. Most of these methods are coupled with spin casting of polymer blends. The following section will briefly review the literature on the various preparation methods along with their shortcomings.

Another solvent evaporation technique and the most widely used among all of the above is spin casting from a homogeneous solution onto a substrate. Thin and ultra thin films of polymers and polymer blends are generated using this technique. Here, a homogeneous solution of the polymers in a solvent is added to a rotating substrate. Simultaneous centrifugal force due to rotation and solvent evaporation yields a thin film. The morphology of the films obtained depends on the nature of the solvent, interactions between the polymer and solvent and polymers and the nature of the substrate. Many investigators have tried to use spin coating as a means of creating kinetically frozen particles for various applications. The spin casting process is a diffusion process and is relatively slow due to the dimensional constraints posted by the substrate during solvent evaporation. Over the past decade, preparation and characterization of such films have been the subject interest of many researchers in the field of polymer blends. Due to the ease of operation, most of the solvent induced phase separation has extensively been studied in thin films. Many researchers have tried to probe and understand the mechanism of phase separation in polymer blends using solvent evaporation. Earlier research involved polymers mixed in a common solvent and then dried in atmosphere. Later, Spin

coating process has been used extensively to get thin and ultra thin films of polymer blends for various applications. The films produced were much thinner than the bulk evaporation produced films. Also, the interactions between component chains (due to confinement effects) are much pronounced due to the reduction in dimension of the films. With the advent of various characterization techniques such as SEM, TEM, light scattering and AFM, several researchers have probed the kinetics of polymer blend thin films. The following paragraphs will briefly discuss the efforts of various researchers in the field. Dalnoki-Veress et. al. (1996) studied the phase separation of PS/PI by dissolving the polymers in a common solvent toluene. The solution was quenched at room temperature by rapid evaporation of the solvent. They prepared three different surfaces and found out that the affinity of the polymeric phases to the substrate and free surface has a significant influence on the final morphology of the polymer blends along with the solvent used. Areas of the polystyrene rich domains were used to measure the extent of phase separation. It was concluded that the wetting properties of polystyrene was the major factor in large differences in domain sizes in different substrates.

In another similar kind of work, Walheim et. al. (1997) also studied the effect of spin cast films of PS/PMMA from toluene, MEK and THF as solvents. Effects of three different solvents and substrate surfaces on the phase morphologies were studied using the topographies obtained by atomic force Microscopy (AFM). Lateral phase separation was observed with PMMA phase rich near the surface as PMMA gets depleted of solvent more rapidly than PS. They showed that this was due to the affinity of toluene and THF towards PS. They also concluded that if the solvent is a better solvent for the polymer with lower surface tension then the surface exhibit sharp well-defined edges. The reverse

was observed when MEK was used. Spin cast films of PVC/PS were prepared by Fang et. al. (2000) and their morphologies were studied using DSC and Electron microprobe analysis. They compared their results to the blends prepared by melt processing. They also concluded that the phase-separated domains follow sea-island like structures when nucleation and growth mechanism was followed.

Mokarian-Tabari et. al. (2010) prepared polymer blend films of PS/PMMA using spin casting from toluene solution. They quantified the evaporation rate by relating it to change in film thickness. They showed that when evaporation rate is higher the structure starts to develop into a co-continuous phase and very quickly reaches a fixed pattern. Since the evaporation was fast, higher concentration gradients existed in the phases and hence marangoni instabilities were present during formation of the phases which result in laterally phase separated structures. At slower evaporation rates, there are no such instabilities observed and also layered structures are formed and followed NG mechanism of phase separation.

Zhang and Taekoda (2012) have fabricated ultra thin films of PS/PMMA and then selective leaching of one of the polymers was used to get a nanoporous structure. They used a sacrificial PVA film on substrate which can be removed so that the films can be freestanding (i.e. the films can be removed from the substrate and transferred to any other surface). This also aided in the study of the bottom surface which otherwise adhered to the substrate. Cross-sectional views of the films showed that decreasing the thickness of the films can significantly increase the pore areas.

Newby and Composto (2000) studied thin film polymer blends of PMMA and SAN prepared by evaporation of Methyl isobutyl ketone (MIBK) for the effect of the

lateral confinement of the substrate by tracking the dynamics of phase separation. They divided the phase separation into early, intermediate and late stages where the wetting layer thickness increases along the center of the film, slows down and then approaches a constant value. A similar research was also done by Wang and Composto (2000) who studied the phase separation kinetics by inducing phase separation at the critical point. They selectively removed one of the components and used AFM to study the layered structures. Jukes et. al. (2005) have studied the phase separation in thin films of semiconducting polymer blends of PS/PMMA by spin-coating.

Several researchers have recently used confocal microscopy coupled with Raman spectroscopy and AFM to study the phase morphology of ultra thin films (Schmidt-Hansberg et. al, 2005, Campoy-Quiles et. al., 2008, Yeo et. al., 2009, Li et. al., 2004). All these studies were for applications involving opto-electronic membranes and one of the polymer components exhibited photoluminescence.

2.4 Preparation and Characterization of Microparticles

Microparticles find wide range of applications in the field of microelectronics, catalysis, drug delivery, polymer coatings and membrane sciences. Production of these microparticles and tuning of their size and morphology play an important role in these applications. Microparticles vary widely in quality, sphericity, uniformity of particle and particle size distribution. Spherical microparticles are often referred to as microspheres. Preparation of these microspheres includes emulsification methods, sol-gel methods, spray drying/droplet evaporation, or a combination of these. Morphology and structure of the microparticles play an important role in determining the properties for various applications. Hence, the effective characterization of these particles is equally important

as their production. This section briefly describes the methods used to produce microparticles along with different characterization techniques used to study such particles. The emulsification and sol-gel methods are bulk methods. These methods yield a broad distribution of particle sizes and are time-consuming as the physical and chemical processes associated with such processes are quite slow. Other downstream processing such as removal of solvent, washing of impurities, filtration of residues, etc. are always associated with such processes. Aerosol based processes such as electro-spraying and spray drying are favorable when compared to the above processes. The next section will discuss the micro-droplet based processes for microparticle production and also discuss the various characterization studies used to study their external and internal morphology.

2.4.1 Microdroplet based techniques

Solvent evaporation from micron and sub-micron droplets offer several advantages over the methods discussed above to prepare polymers blends and other microparticles from homogeneous solutions. High surface-to-volume ratios enhance evaporation in microdroplets and proper choice of solvents can lead to better control of the morphology obtained via such a process. Also, since the process of evaporation in these droplets proceed radially, different particle morphologies can be obtained by controlling the radial profiles of the components. Other pre-treatment and post treatment processes can be avoided and particles can be produced with ease by a single step of manufacturing. The method can be scaled-up for bulk production of microparticles and microspheres with minimum difficulty.

Conventional bulk processes used to produce microparticles are sol-gel methods and emulsion techniques. These techniques have been studied by many researchers and are not the scope of this dissertation. The major disadvantages of these bulk processes are (a) scale-up and bulk production, (b) very large particle size distribution and (c) costly.

Basic steps involved in aerosol based processes are the break-up of the liquid solution into small droplets and carrying out the necessary processes, such as drying, reactions, precipitation, crystallization, etc., within these droplets to obtain the desired particle sizes and morphologies. Atomization of the liquid solution can be achieved by several different techniques but can be classified as gas atomization, ultrasonic and electrical. Gas atomization involves very high shear force, using a high velocity gas, to breakup liquid into small droplets. The droplets obtained from such a process are highly polydisperse.

Ultrasonic atomization involves breaking up of the liquid jet using ultrasonic vibration of the nozzle or orifice through which the liquid is ejecting out. In ultrasonic atomization, low velocities result in less mechanical stress on the materials and hence less prone to deactivation when comes to bioactive materials, spray coatings and drug delivery (Barba et. al. 2012, Friend et. al. 2008, Friedas et. al. 2004). Ultrasonic atomization usually is preferred for low-viscosity solutions and low-temperature applications. When used for prolonged periods, the temperature of the system increases considerably and the temperature sensitive materials cannot be used in conjunction with such methods (Biskos et. al. 2008).

Another process associated with microdroplets is electrospraying. Electrospraying operates on the principle of applying high voltage to a nozzle or an orifice, through which

the liquid passes, and in the process highly fine charged droplets are formed. Bock et.al. 2011, Liu et. al. 2008, have produced polymer particles using electrospraying/ electrospinning techniques for different solution concentrations. Hollow microspheres of polymethylsilsequioxane (PMSQ) has been prepared by electrospraying the precursor solution into a core-shell droplet (Chang et. al 2010). Subsequent evaporation of the core (a volatile solvent) yields a hollow microsphere. The internal morphology was obtained by sectioning the microspheres and observing them under an SEM.

Droplets formed by atomization of the liquid solution subsequently are dried, along with chemical reactions (such as polymerization, degradation, etc.), if necessary, to yield the required products of certain morphology. Various methods are incorporated and these can be classified as spray drying, spray pyrolysis, spray freeze-drying and supercritical fluid extraction. All these processes involve solvent evaporation or extraction of the solvent by different processes.

Spray drying uses an atomizing nozzle to produce microdroplets by introducing a high velocity, high temperature, air stream along with the solution that need to be atomized for particle production. Spray drying has been extensively used in the food industry for the production of milk powders (J Kim et. al. (2009), Sharma et. al. (2012)), concentrated fruit juice powders (Abadio et. al. 2004, Chegini and Gobidian 2007, Solval et. al. 2012) and proteins. It is also used in pharmaceutical industries for the preparation of amorphous drugs and their encapsulations for controlled release. Yang et. al. 2010 produced spray-dried encapsulated hematoporphyrin by polymeric micelles. The prepared films were dissolved in ethanol and then spray dried to get particles of size 2.3μm. The distribution of the drug was studied using fluorescence imaging. Desai and

Park (2005) have prepared chitosan microspheres that encapsulates acetaminophen. The surface morphology was studied by varying the cross-linking in chitosan. Particles of about 5μm size were formed but with large agglomerates. Sun et. al. 2009 produced hollow hydroxyapatite microparticles with a mean particle size of 5 μm. A large distribution in particle size is obtained in the process, as the droplet break-up is not uniform. Several researchers have attempted to use different nozzle/atomizer designs to improve the particle size distributions from spray dryers (Okuyama and Lenggoro 2003). An excellent review on spray drying in pharmaceutical engineering is given by Vehring (2007). He has also given the effect of spray drying conditions that govern final particle morphologies.

Spray pyrolysis is another process wherein microdroplets undergo chemical changes at high temperatures. Pingali et. al. (2005) prepared silver nanoparticles from aqueous silver nitrate solution by spray pyrolysis. The solution was atomized into droplets using an ultrasonic atomizer and a large particle size distribution was obtained. Effect of solution concentration on the final particle sizes was studied and it was shown that the particle sizes increased with increase in solute concentration. A linear fit was also obtained for mean particle size and concentration with a regression co-efficient of 0.95. Hollow microspheres of TiO_2 were prepared by Dwivedi and Dutta (2012) using ultrasonic spray pyrolysis. Very fine particles were formed but most of them were sticking to each other and formed agglomerates. The fractured particles were looked under SEM for confirmation of hollow microspheres.

All the above-mentioned atomization methods produce large particle size distributions. Agglomerates are formed in most cases as the spraying cannot be controlled

or made uniform in these cases. Economically, the energy required for bulk productions are quite high and the temperatures involved sometimes are not suitable for most of the materials involved. These shortcomings can be avoided with the use of a highly monodispersed droplet generator, such as a vibrating orifice aerosol generator, in which the size of the droplets can be controlled precisely. The following section 2.4.1.1 briefly discusses the research work on production of particles using a vibrating orifice aerosol generator.

2.4.1.1 Microparticles prepared using Vibrating Orifice Aerosol Generator

Vibrating orifice aerosol generator (VOAG) uses a periodic disturbance to break-up the liquid solution jet emerging out of an orifice. High number concentration of particles obtained from a VOAG makes it an ideal method for bulk production of microparticles. Wide range of particles can be formed from either homogeneous or colloid precursor solutions. Bergland and Liu (1973) have showed that the aerosol droplets generated using a VOAG can be highly uniform in size with standard deviations of about 1%. Since a VOAG can produce uniform monodispersed droplets of aerosols, they were mainly used for aerosol sampling and measurement. A conventional Berglund-Liu VOAG has been the most widely used droplet generator to study different processes associated with these droplets. Bergland et. al. (1974) have studied the response of several optical particle counters using VOAG. Recently, however, studies have been conducted using Vibrating orifice Aerosol generator for determining the evaporation rates of highly volatile substances. Devarakonda and Ray (1998) have extensively studied the evaporation of ethanol droplets produced by VOAG using laser light scattering techniques. Since a VOAG produces monodispersed droplets with very small size, it has

been looked at as a micro-reactor to produce ordered structures. A wide range of microparticle morphologies have also been observed that are produced using a VOAG. Liu (1976) observed that crystalline NaCl when crystallized from solution either formed polycrystalline particles or crystallized into hollow particles whereas amorphous compounds resulted in a solid spherical particle. With a controlled evaporation rate of the solvent from the evaporating droplet, porous particle morphology can also be obtained as observed by Auvermann (1979). He obtained porous potassium chlorate particles produced by VOAG. Leong (1981) has worked on studying different particle morphologies. He examined the effect of evaporation rate; solute composition and solubility on the final particle shape obtained from crystallization of suspended droplets produced using a VOAG. Esen and Schweiger (1996) have produced spherical polymer particles by photopolymerization of monomer SOMOS dissolved in a volatile solvent, ether. Esen et. al. (1997) further continued the work on the same lines to produce a layered structure consisting of glycerol encapsulated in a polymer matrix. They showed that manipulating the parameters of a VOAG can precisely control the thickness of the polymer layer. Gao et. al (2007) have also produced polymer microspheres using a VOAG. Researchers have also made attempts to produce structured porous catalyst particles using a VOAG as shown by Rama Rao et. al. (2002). They produced mesoporous silica by evaporating ethanol from the precursor solution droplets of TEOS, HCL and water and allowing the precursor solution to react at high temperatures. Rathod et. al. (2003) has also used VOAG to produce highly monodispersed mesoporous silica particles of 10 μm with a pore size of 2 nm and a specific surface area of 900 m^2/gm. Monodispersed Uranium oxide microparticles were produced by Erdmann et. al. (2000).

The particles obtained were spherical and dense. They used secondary ion mass spectroscopy to calculate the isotopic composition of U^{235}/U^{238}.

In the present study, a vibrating orifice aerosol generator has been used to produce monodispersed polymer blend microparticles. The vibration frequency and liquid flow rate was optimized to get uniform particles.

2.4.2 Characterization of Microparticles

Microparticles produced by various methods are characterized for their internal and external morphologies using several techniques. Choice of the characterization techniques depends upon the nature and size of particles formed. Scanning electron microscopy and transmission electron microscopy are most widely used direct techniques for the visual observation of particle size and shape. External morphology of microparticles using SEM and TEM is quite common nowadays. Walton (2002) has shown different morphologies of ferrite particles and tungsten chloride, yogurt powders and the agglomerates formed and skimmed milk hollow particles produced by industrial spray dryers using SEM. The particle size is either measured manually or by using image analysis software and an average value is obtained as shown by Liu et. al. (2008) who prepared chitosan particles by spray drying.

The internal morphologies of particles can be visually observed by either fracturing the microparticles and viewing them in an SEM or by using ultramicrotomy. Fracture in a particle can be achieved by cryo-milling, polishing, etc. (Li Yan et. al. 2005). The particles are introduced to ultra low temperatures (usually in liquid Nitrogen) and broken down by some kind of milling operation. The fractured particles thus obtained are observed under an electron microscope to observe the internal morphology of the

microparticles. Ultramicrotomy is a process in which the microparticles are embedded in a matrix and using a diamond knife ultra thin slices (about 60 nm) are obtained which are further analyzed by microscopy techniques. Ehtazazi et. al. (1999) have prepared microspheres of poly (D-L, lactide) using a double emulsion method. The internal morphology of the pores inside the microparticles was characterized by sectioning the microspheres under low temperatures. The sectioned samples had a thickness of 20 μm. The size of the actual microspheres formed was about 40 μm and the microspheres formed were quite rigid for sectioning to be done easily.

In-situ sectioning of microparticles can also be done using focused ion beams. A highly coherent and focused ion beam cuts through the particle when inside the electron microscope chamber. This allows direct observation of the microparticle cross-sections. Moghadam et. al. (2006) have used the technique to observe the internal structure of poly (lactic acid) (PLA) loaded with naltrexone. Sequential and controlled depth analysis of a single microparticle can be performed using such a technique (Kamino et. al. 2004, Steer et. al. 2002).

In case of fluorescent samples, the confocal microscopy is an effective non-destructive tool for studying the distribution of the fluorescent component in the microparticles. Confocal microscope scans the microparticle along its depth and yields images across its cross-sections, at each depth, showing the distribution of the components. Ming Na et. al. (2012) have produced drug loaded polymer microspheres. In the case of polymer blend thin films, especially in the case of photo-luminescent materials, confocal microscopy has been extensively used. Zammarano et. al. (2011) detected fluorescein labeled cellulose using a laser confocal microscope. Distribution of

components can also be obtained by using an Energy Dispersive X-Ray Spectrum (EDS) on the ultramicrotomed samples. This approach is mainly used in the study of polymer nanocomposites and surface modified polymers.

If the samples are a mixture of polymers, then a more important aspect of the study is the homogeneity of the samples. An important property that is used universally is the glass transition temperature. When both the polymers are amorphous, a single glasss transition temperature (T_g) suggests that the polymers are miscible in each other whereas two distinct T_g's represent a phase separation in the blends. (Fang 2000). In a polymer blend with one amorphous and one crystalline component the glass transition can be used to determine the degree of crystallinity of that blend (Xuan and Yang 1985, Agarwal et. al. 2010).

2.4.3 Polymer Blend Microparticles

Majority of the current research in polymer blends is restricted to thin and ultra thin films but recently polymer microparticles find wide range of applications in the field of drug delivery, opto-electronic devices, polymer nano-composites, fuel cells, optical sensors, membrane sciences, etc. Having a co-polymer or a polymer blend as an encapsulation offers several advantages over a single polymer as one can control the release kinetics of the drug by varying the composition of each polymer in the blend. For example, polymer electrolyte membrane is sometimes doped with a hydrophobic material (such as PTFE) to inhibit water crossover in fuel cells. An excellent review on the subject is given by Siepmann et. al. (2008) wherein they discuss the advantages of having a polymer blend as drug coatings. Also, as the size decreases, the swelling characteristics increase and hence the solubility of the drug increases during its release. Sullad et. al.

(2010) have used a blend of biodegradable polymers PVA and hydroxypropyl cellulose to encapsulate the drug theophylline using a water-in-oil (w/o) emulsion method to cross-link both polymers. The swelling characteristics and release efficiency was studied. Reddy et. al. (2013) has encapsulated an anti-cancer drug 5-fluoroucil using chitosan and hydroxypropylmethyl cellulose. Diferential Scanning Calorimeter (DSC) was used to corroborate the uniform distribution of the drug in the polymer blend microspheres. Alhan and Basit (2011) have also showed the influence of polymer blend distribution and interaction on the release characteristic of the drug prednisolone. They encapsulated the drug with Euragrit S and Euragrit RS/RL or ethylcellulose and extended the drug release characteristics in acidic environment. Most of the work in encapsulation of drugs is related to cross-linking the two polymers via an emulsion polymerization technique.

Recently, polymer blend microspheres have also been studied in the field of fuel cells, wherein the microspheres are embedded onto a polymer electrolyte membrane for controlling the diffusion and electronic properties of the membrane. These can have direct impact on the efficiency of the fuel cells. Wang et. al. (2011) has showed that adding polymeric microcapsule fillers onto a membrane matrix can enhance water retention of membranes. In a similar study, Guo et.al. (2012) showed that by embedding a hydrophilic hollow polymer microparticles (0.5 wt% loading) onto a Nafion membrane one could increase the proton exchange across the membrane and yield a increase in power density of about 106% at nominal operating conditions when compared to pure Nafion membranes.

Another exciting field in which polymer blend microspheres might play an important role are the organic opto-electronic devices such as solar cells and organic-

LED's. Main focus is on the bilayer heterojunctions that need to have excellent electron-hole mobility. With various configurations of the conjugated polymers, one can achieve different electronic properties depending on the nature of the polymers and solvents used. Kietzke et. al. (2007) have used a miniemulsion process wherein they have produced nanoparticle polymer blends from bulk aqueous solutions. They showed that the nanoparticles obtained from the process had bi-phasic morphology. They also used the same approach to produce P3HT and PPV blend particles and the same result was seen. Schmidt-Hansberg et. al. (2011) has probed the structure formation in fullerene-polymer solvent cast blend films for application in organic solar cells.

Most of the research advances in polymer blend systems uses bulk solution techniques. There are several disadvantages to these bulk methods such as scaling-up and bulk production, large distribution in particle sizes, etc. Particle formation from solution droplets offers quite a lot of advantages when compared to bulk methods. Micron sized droplets have large surface-to-volume ratio when compared to bulk methods. There is no substrate interaction as in the case of thin films. Nature of the solvent, composition and initial size of the droplets along with the confinement effects play a major role in determining the morphology and in turn the final properties of the particles obtained. Polymer blend microparticles have been produced using techniques such as supercritical fluid extraction and spray-freeze drying.

In freeze drying, a homogeneous solution of two or more polymers dissolved in a common solvent is cooled rapidly to obtain a frozen solvent matrix containing the polymers. Once the solvent is frozen (solid), direct sublimation of the solvent from the solid to gas phase leads to solid polymer blends. Several researchers have worked on

producing polymer blends from freeze-dried solutions. Allan and Young (1980) have prepared polymer blends of poly (methyl methacrylate) (PMMA) and poly (vinyl alcohol) (PVA) freeze-dried from naphthalene solutions and studied the blend using differential scanning calorimeter (DSC). They showed a single glass transition temperature for their first heating scans and subsequent heating scans resulted in two separate glass transition peaks. Also, at a high heating rate i.e. 40 ^{0}C/min, they observed pronounced maxima and minima in the glass transition zone. They concluded that these features of the DSC data could be used to study the effects of preparation history of the blend. Risbud et. al. (2000) produced pH sensitive chitosan-polyvinyl pyrrolidone (PVP) hydrogels for controlled drug delivery. The process formed large moieties and the pore diameters were about 39.20 ± 2.66 μm. This in turn resulted in highly swollen hydrogels when used in acidic environment.

Freeze drying incorporates lowering the temperature to freeze the solutions whereas when high pressures are used to compress and liquefy a gas to dissolve the solutes and the gas is expanded, the process is called supercritical fluid extraction (SCF). An excellent review on particle formation using supercritical fluids is given by Tom and Debenedetti (1991). They have discussed in detail the theory, operation and working of such equipment along with the applications of such systems in the field of ceramics, microencapsulation in drug delivery and thin films. Shine (1994) has prepared polymer blends using the supercritical extraction of solvents from the homogeneous polymer blend solution of poly (methylmethacrylate) and poly (ethylmethacrylate) in chlorodifluoromethane. The method is used to make bulk scaffolds, thin films and particles from sprays. Several studies have been conducted to produce polymer blends in

supercritical fluids (Domingo et. al., 2003, Chang et. al., 2004) and to study the effects of supercritical gases like CO_2 on polymers or polymer blends (Walker et. al., 1999, Watkins et. al., 1999, Zhou et. al., 2003). The energy involved for compression is sufficiently large and the pre-treatment processes involved are quite cumbersome.

Recently, Barnes et.al. (1999) showed that two immiscible polymers can be dissolved in a common solvent and a single homogenous polymer blend microparticle can be obtained. They used an on-demand droplet generator to yield a single suspended drop and showed that the refractive indices of the single polymer blend microparticle is an average of that of the pure components. They studied the fraunhauffer diffractions from the particles and calculated the refractive indices of the particles. They found that the refractive index of a single blend particle obtained was equal to the mass average of the respective components in the blend and this, concluded that the particles are homogeneously mixed. The limitations to their study are (1) bulk production of particles- they only studied a single particle and (2) the droplet/ particle obtained was always spherical as the charge on the droplets was quite high which held the particle together. Also, there was no experimental evidence of homogeneity or phase separation in the blends.

In the present work, a more practical approach for production of polymer blend microparticles has been proposed. The microparticles of the homogeneous polymer blend solution was generated using a VOAG and the obtained microparticles were studied for their internal and external morphologies using electron microscopy techniques. The glass transition temperature for the blend was also obtained using differential scanning calorimetry.

CHAPTER 3

3. EXPERIMENTAL

This chapter presents a detailed description of the experimental set-up used in the present work to produce polymer blend microparticles from dilute polymer blend solutions.

3.1 Experimental set-up

The schematic representation of the experimental set-up used for the production of polymer blend microparticles in this study is shown in figure 3.1 below. The experimental set-up can be divided into two parts, namely,

1) droplet generation system-VOAG along with liquid feed supply and electronics

2) drying column with particle collection

The liquid from the reservoir is pressure fed through an orifice placed inside a piezoelectric crystal (PZT) cup to form a liquid jet. The jet is broken down into highly monodisperse droplets by applying a periodic disturbance to the PZT. These droplets are passed through a drying column, maintained at a certain temperature, where subsequent evaporation of the solvent and drying of the droplet result in microparticles of the polymer blends which are then collected at the bottom of the drying column using a particle collector. Each of these parts are discussed in detail in the following sections below.

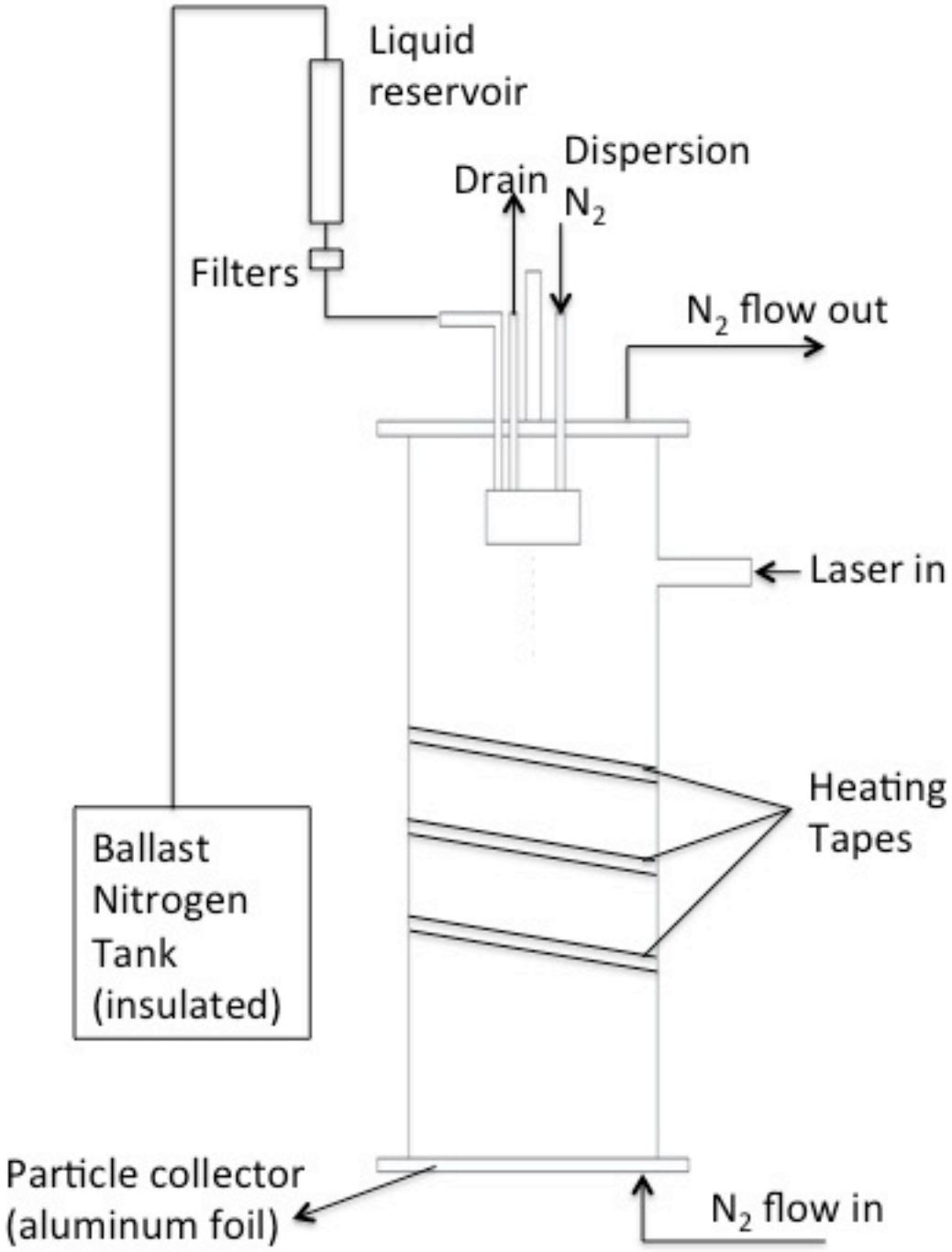

Figure 3.1:Schematic representation of the experimental set-up used to generate multicomponent polymer blend microparticles

3.1.1 Droplet generation system

The droplet generation system used in the present work consists of a modified vibrating orifice aerosol generator (VOAG) along with the liquid feed supply system. Droplets generated by a VOAG are highly monodispersed. The working of a VOAG is based on the principle that when a cylindrical jet is forced to become unstable under the influence of axi-symmetrical periodic disturbances, then the jet breaks down into small droplets. The number of droplets produced in unit time is equal to the frequency of the periodic disturbance, *f*. The same principle is used in our studies for generating linear stream of droplets.

The first VOAG used capillary tubes as nozzles and these nozzles were vibrated to break the liquid into chain of droplets. Different droplet sizes were produced by varying the size of the capillary tubes. Over the years, the design of a VOAG has been considerably modified. The recently and most widely used one is the Bergland and Liu (1973) VOAG. Over the years, the principle behind generation of the droplets remains the same but the design has considerably been improved to produce highly monodispersed droplets. They incorporated stainless steel pinholes instead of capillary tubes. The initial droplet size was varied by varying the size of the pinholes. Figure 3.2 shows a simple cross-sectional representation of the droplet generator head.

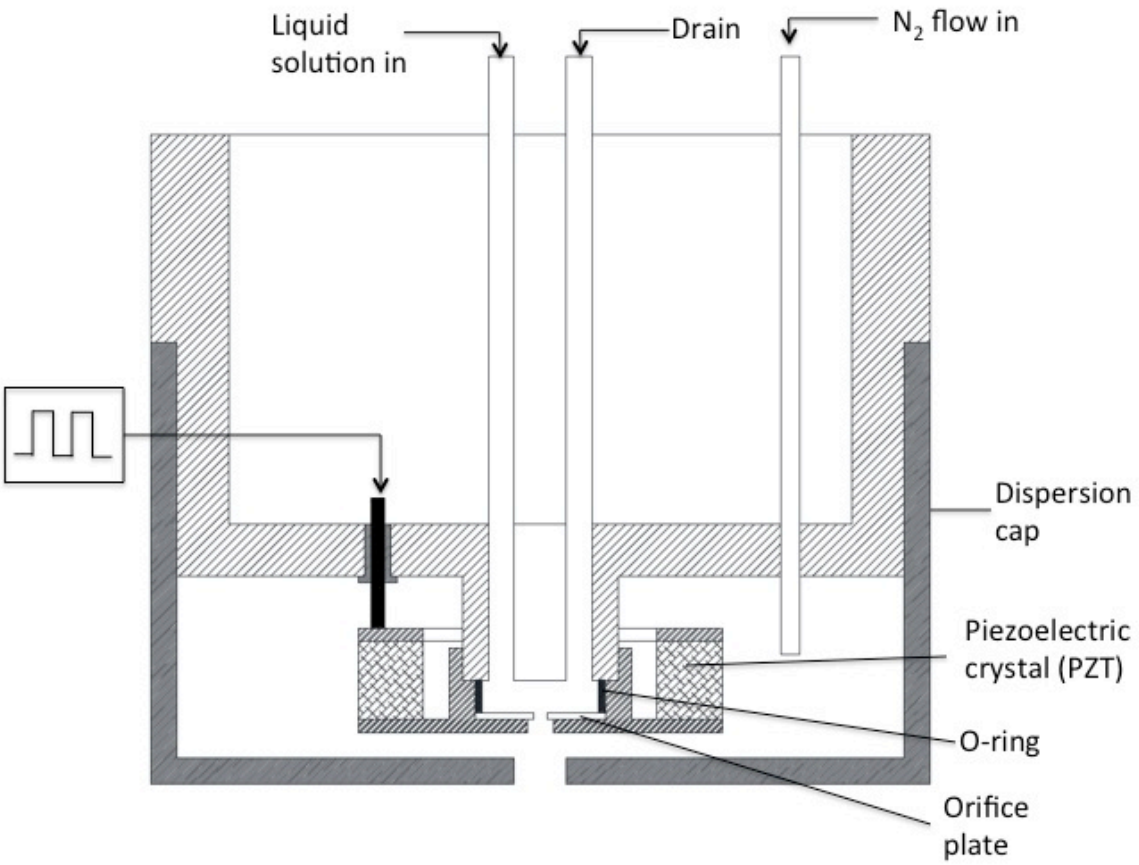

Figure 3.2: Cross-sectional view of the droplet generator head (VOAG)

The liquid solution is forced through the liquid line and the liquid collects in the cavity made between the orifice plate (i.e. the pin hole) and the teflon o-ring. The air gap is removed by purging the liquid through the drain and then liquid is allowed to flow through the pinhole as a cylindrical jet. A periodic frequency is applied to the orifice plate, which breaks the liquid jet into droplets. The size of the droplets generated through such a system can be calculated from equation 3.1 given below,

$$a = \left[\frac{3Q}{4\pi f}\right]^{1/3} \qquad (3.1)$$

where, a is the size of the droplet, f is the frequency of vibration of the orifice plate and Q is the liquid flow rate through the orifice plate. Equation 3.1 demonstrates that a highly monodispersed stream of droplets can be generated by maintaining a constant flow rate, Q and constant frequency of vibration, f. Stabilization of the flow rate and frequency of vibration resulted in several important modifications to the VOAG. The liquid feed system and the periodic disturbances applied to the PZT will now be discussed in detail.

Liquid feed system

The conventional VOAG used by Berglund and Liu uses a syringe pump to force the liquid through the orifice. The syringe pump has good long-range stability but has instantaneous fluctuations (few μm ranges) that are inherent due to its operational characteristics. Mitchell et. al. (1987) developed a pneumatic liquid pump to minimize the fluctuations. Leong (1986) modified the liquid feed system by replacing the liquid syringe pump with a gas pressurized liquid flow system. The syringe pump was replaced by a liquid reservoir, which was connected to the gas ballast tank. The gas pressure in the tank was used to control the flow rate of the liquid. The volume of the ballast gas tank was very large when compared to that of the liquid reservoir and hence the pressure in the ballast tank controlled the flow rate of the liquid through the orifice. Leong used different solutions with different concentrations and showed that the flow rate remained constant with a deviation of 0.3% to 3 %. He also reported that the partial clogging of the orifice can result in change in flow rate and diameter of the liquid jet and may play a role in the loss of monodispersity of the generated droplets.

In the present study similar modifications incorporated by Devarakonda (1998) has been used. The liquid flow system consists of a gas ballast tank that is connected to

the top of a stainless steel liquid reservoir (130 ml) using a 1/4" teflon tubing. The sample solution is pre-filtered using a syringe filter to remove the large impurities and is stored in this reservoir. The ballast tank is filled with nitrogen from storage upto the desired pressure and then isolated. From ideal gas law, pressure is directly proportional to temperature of the gas in the ballast tank and even a small change in pressure can affect the change in temperature of the gas, i.e.

$$\frac{\Delta P}{P} \sim \frac{\Delta T}{T} \tag{3.2}$$

Also, according to Bernoulli's theorem, the effect of pressure can be related to the change in the flow rate and in turn to the droplet size (equation 3.1) as given by equation 3.3.

$$\frac{\Delta P}{2P} \sim \frac{\Delta Q}{Q} \sim \left(\frac{\Delta a}{a}\right)^3 \tag{3.3}$$

From equation 3.3 it is apparent that the fluctuations in flow rate will affect the monodispersity of the droplets. To avoid such variations in size, the ballast tank is well insulated from the ambient atmosphere using fiberglass insulation pads. A pressure gauge is attached to the tank for monitoring the pressure.

The liquid is pressurized from the top and is allowed to flow through a 0.45μm filter (FHLP 02500) to remove large dust particles from the solution and then through a 0.2μm filter (FGLP 02500) to remove the finer particles of dust or other contaminants. Two more 0.45 μm filters (FHLP 01300) are used very close to the orifice to assure complete removal of contaminants. The liquid collects in the cavity between the o-ring

and the orifice plate in the piezoelectric ceramic crystal (PZT) cup (shown in figure 3.2) and once the air bubbles are flushed out, a liquid jet issues from the orifice. The flow rate, *Q*, can be controlled by adjusting the pressure of the gas inside the ballast tank.

Frequency of vibration

Once the liquid jet emerges out of the orifice, a periodic disturbance is applied to the orifice to break up the liquid jet. As discussed above, this is another important criterion for generation of monodispersed droplets. This is accomplished by using a frequency synthesizer HP 3335 A. The instantaneous fluctuations from the synthesizer are about 0.1 Hz. The signal from the synthesizer is a sinusoidal wave with very low amplitude. In a sine wave the amplitude rises and drops gradually to and from the peak amplitude over a period of several hundred nanoseconds. This means that the PZT receives the highest amplitude only for a very short duration. To avoid this, the signal is passed through an in-house converter where the sine wave is converted to a square wave. The signal from the square wave is more sudden as the time taken by square wave to reach its highest amplitude is only a few nanoseconds when compared to a sine wave. The signal is then amplified using a linear amplifier (Piezo Systems Inc. Linear Amplifier Model-EPA 104) and sent to the PZT. The top and bottom ends of the PZT are glued to two stainless steel plates and the circuit is designed such that a square wave of constant voltage (15V) is applied to the top plate whereas the bottom plate is grounded. Particles ranging from few microns to about 100 microns can be produced using the modified VOAG using various combinations of orifice diameters and frequencies but there is only a certain operational window for producing monodispersed droplets while doing so. The theoretical frequency

range in which monodispersed droplets can be produced is given by Schneider and Hendricks (1964) as presented below in equation 3.4. Berglund and Liu further demonstrated this operational window with respect to the voltage applied to the piezoelectric ceramic crystal and the ratio of the disturbance wavelength to the liquid jet diameter (λ/D_j). Even though equation 3.4 predicts the operational range to quite an extent but the true operational range (or optimum frequency) depends on factors like the nature of the solution (density, viscosity, etc.), actual frequency of vibration of the orifice, etc.

$$\frac{v_{jet}}{7D_{jet}} < f < \frac{v_{jet}}{3.5D_{jet}} \tag{3.4}$$

where, v_{jet} and D_{jet} are the liquid velocity and the diameter of the jet, respectively. An He-Ne laser beam was used to illuminate the linear droplet stream. The light scattering from the droplets directly opposite the laser beam was observed on a screen. The monodispersity of the droplets generated was confirmed by observing the 2D diffraction lines. When the droplets generated are not stable the diffraction lines would fluctuate and when the droplets are stable and monodispersed the diffraction lines are very bright, distinct and without fluctuations. Figure 3.3 shows the difference in diffraction lines obtained when a highly monodispersed droplet is generated from a polymer blend solution and otherwise. Another method that was used to detect stable monodispersed droplet generation is the jet deflection method. In this method, a gas is passed perpendicular to the falling droplet stream with very low flow rate (say 500-700 ml/min). If the jet deflects uniformly without forming any secondary jets then it can be concluded

that the droplet stream is monodispersed. The secondary jets arise due to the presence of satellite drops (drops having different sizes than the primary droplets) that are generated due to fluctuations in the system. The monodispersed droplets produced are quite close to each other and since the droplets fall under gravity, farther away from the generator these droplets combine and coalesce to form larger drops. To avoid this, nitrogen gas is used to disperse these droplets as soon as they are produced. This is achieved by incorporating a dispersion cap. The cross-sectional view of the droplet generator head with the dispersion cap is already shown in figure 3.2. The dispersion N_2 flow rate was optimized for segregation of produced monodispersed droplets. If the dispersion flow rate is too high, then either the droplet residence time in the evaporation chamber is reduced resulting in incomplete drying or the droplets can break-up into smaller satellite droplets that might not settle and if the flow rate is too low then the droplets are not uniformly dispersed and droplet coalescence occurs yielding polydispersed droplets. The N_2 gas flow was adjusted to lie in the range of 1000-2000 ml/min for optimum dispersion of the droplets. Once the droplets are generated and dispersed they are passed through the drying column for evaporation and drying of the microdroplets to obtain polymer blend microparticles.

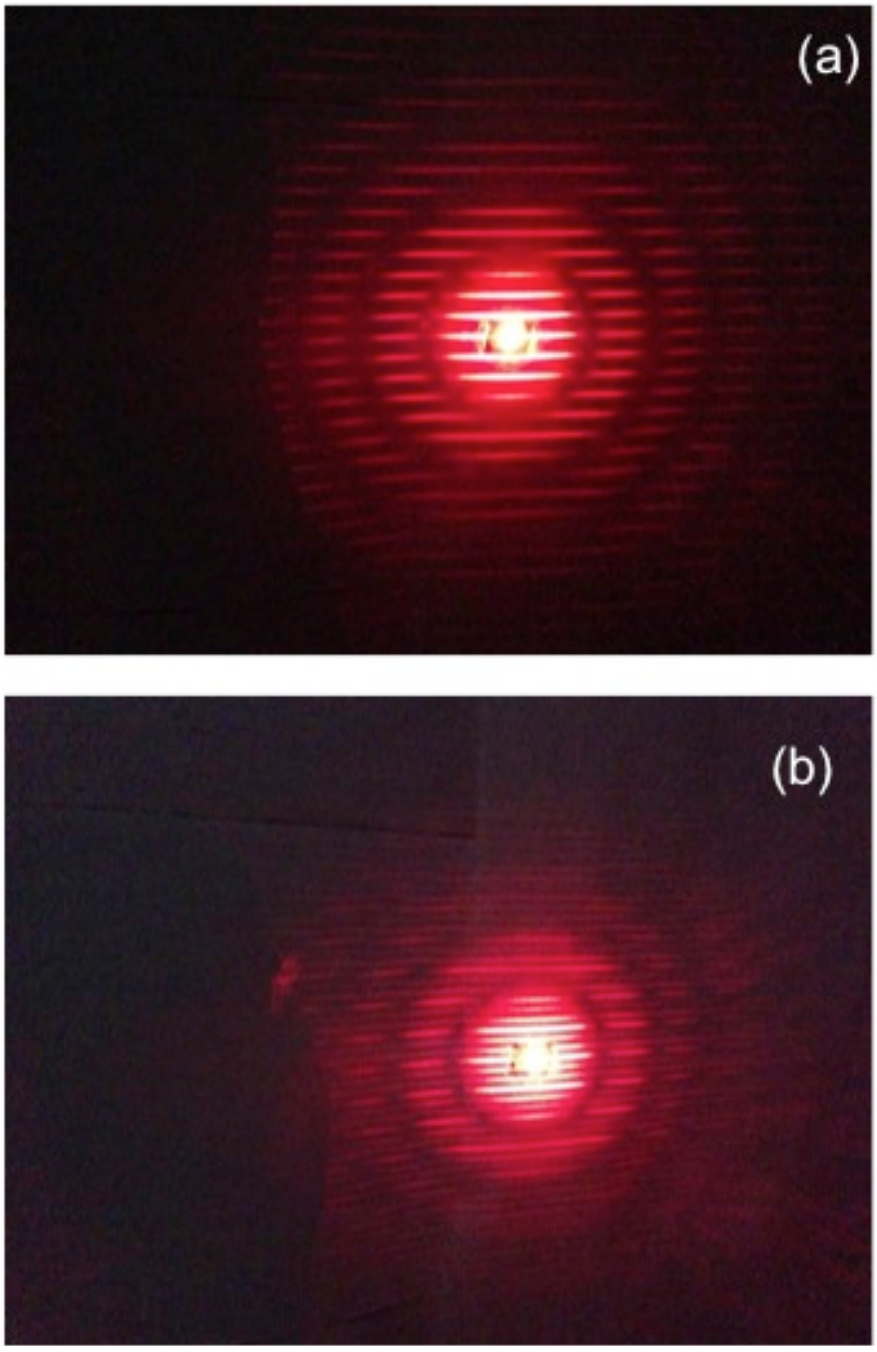

Figure 3.3: Image of the diffraction lines from a linear stream of droplets generated using VOAG with 15μm orifice. (a) highly monodispersed droplets generated at a frequency of 100kHz (b) droplets generated at a lower frequency (40 kHz) with fluctuating diffraction lines. Flow rate was kept constant.

3.1.2 Drying column

In the present work two drying columns are used. Except for particles generated for DSC study, all the other experiments were carried out using the drying column shown in Figure 3.1. The drying column consists of two cylindrical sections, top section was made of plexi-glass that supports the VOAG and the bottom section was a quartz tube 10” in diameter and 4 ft. in height. The quartz tube was equipped with heating tapes to raise the temperature to facilitate fast drying conditions. Heating tapes are controlled by using variable transformers. A thermocouple was suspended inside the column to obtain the drying gas temperature. Also, to facilitate uniform drying conditions and to prevent saturation of the solvent vapor in the column, a counter-current flow of N_2 gas was established by passing the gas through the bottom of the cylindrical quartz tube. This gas will be referred to as the dilution gas from now onwards. A controlled temperature bath/circulator (Thermo NesLab RTE 7) was used to preheat the gas, if required. Two rotameters, (Omega) Model 1447-S and 1467-G were used to adjust and maintain the flow rate of the dispersion and dilution gas, respectively. Since the diameter of the tube is very large, hence laminar flow prevails inside the drying column. The terminal settling velocity can be determined using stokes equation given in equation 2.7.

$$v_s = \frac{2}{9} \frac{(\rho_d - \rho_g)}{\mu} g R^2 \tag{3.5}$$

where, v_s is the terminal settling velocity of the droplet, ρ_d and ρ_g are the densities of the droplet and the gas respectively, μ is the viscosity of the gas, g, the gravitational acceleration and R is the radius of the droplet/particle falling under gravity. An

approximate residence time of the droplets can be obtained by using the height of the column and the velocity of the droplets. As the droplets fall to the bottom, the solvent evaporates and the solid particles are collected at the bottom of the cylindrical column using an aluminum foil. Certain problems were encountered during the drying process. At room temperatures, the droplets did not achieve complete evaporation and the particles were sticking to the aluminum foil. When the temperature was raised, negligible amount of particles were collected on the aluminum foil and instead the particles either deposited on the walls or moved upwards and settled on the dispersion cap. Once the temperatures were decreased, the particles started to settle at bottom again. Such a behavior of the particles could be due to the thermal gradients inside the cylindrical column. Most of the experiments were conducted using this drying column. Only a few milligrams of microparticles were collected using this process.

Even though characterization techniques such as SEM, TEM and confocal microscopy required very few particles but for obtaining the glass transition temperature using DSC method atleast 7-10 mg of sample is required. To increase the collection of these particles, a new drying column was built with a cyclone separator at the bottom for increasing the collection of particles. Figure 3.4 shows the schematics of the new drying column along with its salient design features. The idea behind construction of the new drying column was to introduce N_2 gas radially and from the top so that the droplets/particles are pushed and carried to the bottom of the drying column and are then separated by a cyclone separator.

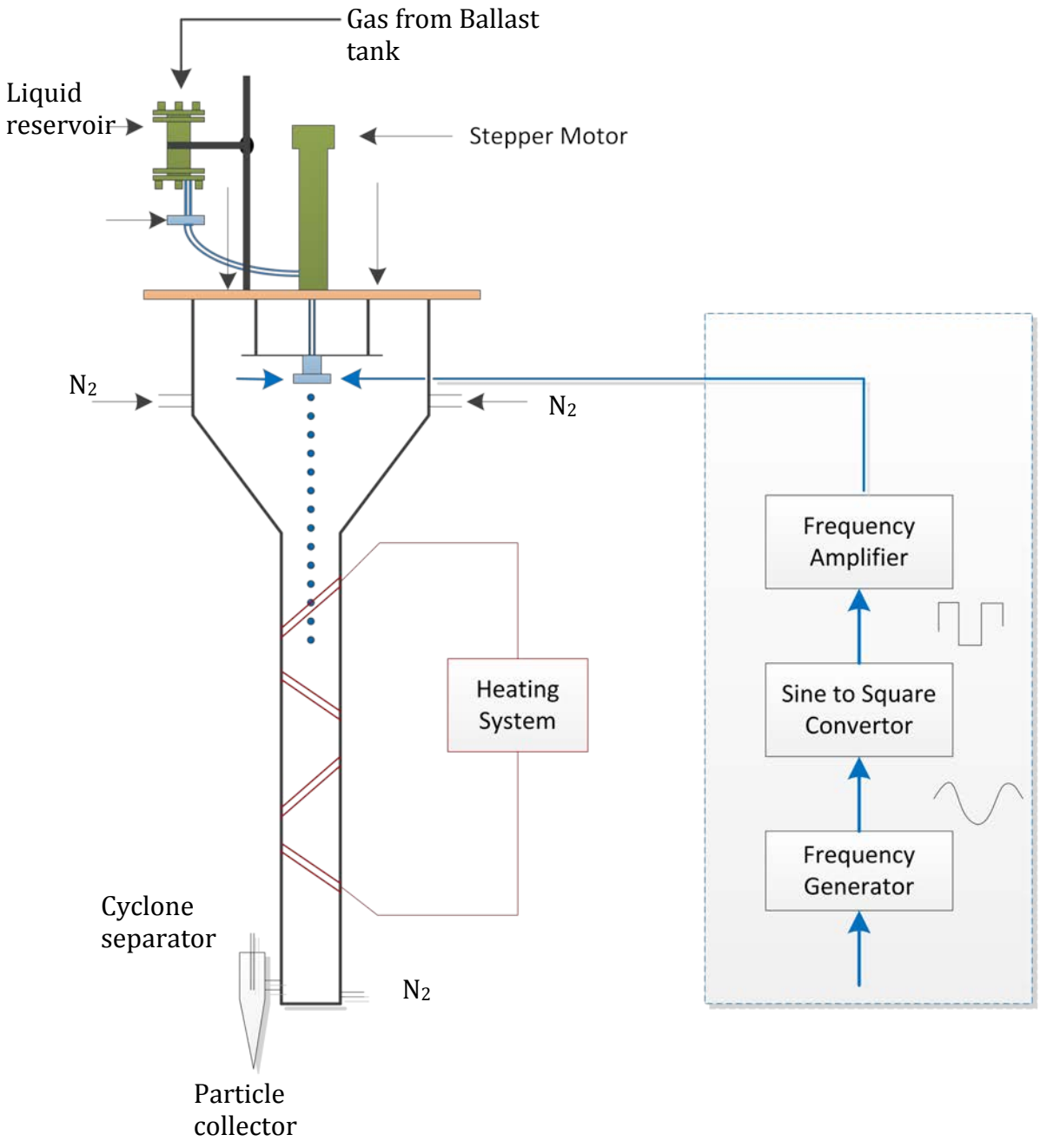

Figure 3.4: Schematic representation of the new drying column with cyclone separator at the bottom

The new drying column has a plastic tank (15 gallon) with a cylindrical section at the top and a conical section at bottom. The cylindrical portion houses the VOAG at the top and the conical section is connected to a 4 ft. glass tube, 2.25" diameter, via a stainless steel cajun style fitting designed and fabricated in-house. The glass tube is heated using three heating tapes wound round it. The heating tapes are connected to respective variable transformers for controlling the temperature inside the drying column. A thermocouple was suspended from the top to the center of the glass tube using a connecting wire. At the bottom, a cyclone separator is connected to the glass tube to collect the particles. The N_2 gas flows co-currently from the two ¼" diameter ports on the top of the cylindrical tank. To prevent the droplets from striking the surface of the tank, gas was also passed radially through eight equal sized 1/8" ports that extend to 4" inside the tank. Even though this prevented the impact of particles on the cylindrical surface but due to the charge on the droplets produced by VOAG it was observed that the droplets started to settle on the conical section of the tank as shown in figure 3.5. To prevent this from happening, an anti-static liquid (Sprayon SP 610) was sprayed all over the inside walls of the tank.

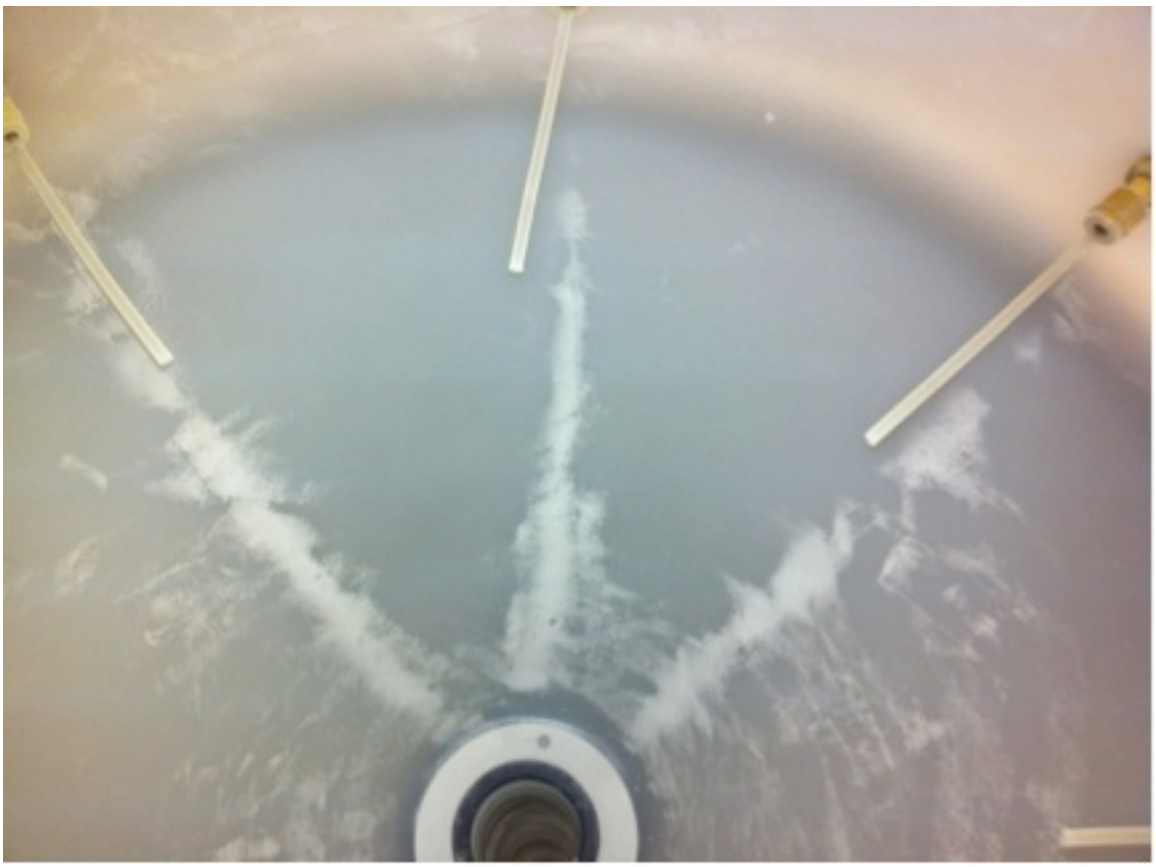

Figure 3.5: Photograph of the inside surface of the conical section of drying column showing polymer blend particles settled on its surface.

Once the droplets are generated using the VOAG and checked for its monodispersity, it was placed on top of the tank and sealed off. Both the dispersion gas and the dryer gas were switched on and passed through the chamber. The particle/droplet-laden gas passed through the glass tube and then through the cyclone separator where the particles settle down into the particle collector, which was a 1.5 ml centrifuge vial, and the gas escaped from the top.

3.2 Chemicals used

Polystyrene (Mw 280,000) and poly(vinyl chloride) (Mw 180,000) was bought from Sigma Aldrich, USA. Poly (vinyl carbazole) (Mw 90000) was purchased from Scientific Polymer Products. The solvents, Tetrahydrofuran (THF) (99.9%), Ethanol (200 proof) and Dichloromethane (99.9%) were purchased from Sigma Aldrich.

3.3 Production of multicomponent polymer blend microparticles

In the present study, binary polymer blend microparticles are prepared using microdroplet evaporation method. Binary combinations of polystyrene (PS), poly (vinyl chloride) (PVC), poly (methyl methacrylate) (PMMA) and poly (vinyl carbazole) (PVK) were used for generation of each of the polymer blends. All the binary polymer pairs are immiscible in each other under normal conditions. PVK was chosen in the present study so that the natural fluorescence of PVK can be used to study the distribution of PVK inside the blend microparticles.

For a particular experimental run, two polymers were chosen and co-dissolved in a solvent. The criterion for the choice of the solvent was that the vapor pressure of the solvent is sufficiently high that the evaporation proceeds rapidly. Tetrahydrofuran has been used in our studies as it dissolves all the polymers and also has a very high vapor pressure. Different dilute concentrations of the polymer blend solutions were prepared. Dilute solutions offer several advantages:

a) both the components in the solution are completely and uniformly mixed in the solvent.

b) break-up of the liquid jet into droplets is achieved easily (low viscosity of solution).

The solutions prepared were checked for optical clarity, pre-filtered to avoid any impurities and stored in airtight glass bottles so that the solvent vapors cannot escape into the atmosphere.

Characterization of the particles was divided into two parts. The first one was the external particle morphology, i.e., the shape and size of the particles formed. Particle internal morphology and phase separation was either done by ultramicrotoming the particles and studying them under a transmission electron microscope or by using a confocal microscope to check the distribution of polymers inside the microparticles using fluorescence of one of the polymers. Differential scanning calorimeter was used to check the glass transition temperature of the polymer blend microparticles.

CHAPTER 4

4. RESULTS AND DISCUSSION

The results of this study are divided into two parts. The first part deals with the microparticle morphologies obtained by the droplet evaporation technique. This involves studying the effects of process variables such as initial concentration, orifice size and chamber temperature on the morphology of different polymer and polymer blend microparticles prepared. The effect of dispersion flow was also studied. In the second part, homogeneity of the blends is discussed by either performing an Energy Dispersive X-ray Analysis (EDAX) on an ultra thin section of a sample or by using the conventional DSC or by using confocal microscopy. The particles obtained, in general, are irregular and non-spherical. The average diameters of the particles were obtained by simply averaging the length of major and minor axis of 10 microparticles from an SEM micrograph. The scales on the micrographs were used as a reference to calculate the lengths.

4.1 Morphology of polymer/polymer blend microparticles

4.1.1 Effect of initial polymer(s) concentration

Three different concentration (1, 2 and 3 wt%) solutions of different immiscible polymer/polymer mixtures were prepared to study the effect of initial polymer concentration on the morphology of the microparticles obtained. Each experiment involved careful and proper control of the frequency of the vibrating orifice as well as the flow rate to yield a stream of monodisperse droplets. The chamber temperature was measured by means of a thermocouple and the chamber was maintained at about 40 ^{0}C.

The conditions and the polymer and polymer blend microparticles generated using a vibrating orifice aerosol generator are given in Table 2.1. Concentration of polymer solutions higher than 3wt% were tried but monodispersity was not achieved. This can be due to the fact that the break-up of the jet not only depends on the frequency and the flow rate but also on the viscosity and surface tension of the solution. Orifice sizes of 10, 15, 20 and 25μm were used for obtaining different initial sizes. It was observed that no droplets were collected on the aluminum foil collector at the bottom with a 10μm orifice. Several experiments were repeated to ensure that this is not due to any experimental artifacts. With this observation, further use of a 10μm orifice was avoided. Also, with a 20μm and 25μm orifice, the frequency range for generating droplets was very narrow and the droplets did not dry completely as they impinged on the aluminum foil at the bottom. Stable droplets were generated using 15μm orifices without any glitches and hence all the other experiments were conducted using orifices of these sizes.

Table 4-1:Experimental conditions used for generation of polymer/polymer blend microparticles

Polymer/ Polymer blend system	Solvent used	Conc (wt%)	Chamber Temp. (^{0}C)	Orifice (μm)
PS	THF	2	40	15
PS/PVC	THF	2	40	15
PS/PVC	THF	3	40	15
PS/PMMA	DCM	2	40	15
PS/PVC	THF-Ethanol	2	40	15
PS/PVK	THF	2	40	15

Pure PS microdroplets generated using a 10μm orifice and 1wt% concentration had high monodispersity but no particles were collected at the bottom of the chamber. Very small droplets tend to evaporate faster and the precipitation starts within a few milliseconds.

Visual observation of the walls of the chamber revealed that most of the particles settled on the walls and careful observation of the dilution N_2 gas outlet using a laser revealed that the particles were also escaping from the top. The former observation can be a result of a thermophoretic force developed during the heating of the chamber walls. The chamber walls are at a higher temperature than the center of the chamber. This can cause the droplets/particles to move to higher temperature zones. The effect of thermophoresis was confirmed when the droplet were allowed to dry in ambient atmosphere without supplying any heat. Immediately, the droplet reached the bottom of

the aluminum foil but as expected did not dry completely. Also, droplets from 1wt% solution have ultra low densities and hence, the velocity of the dilution N_2 would be enough to carry the particles along with it. From these observations, the production of microparticles was limited to 2wt% and 3wt% concentration solutions. Figure 4.1 shows the scanning electron micrographs of microparticles (equal ratio of both polymers) of polystyrene-polyvinyl chloride blend microparticles produced with 2wt% and 3wt% total polymers' concentrated solution in THF. In general, there is folding and crippling of the microparticles formed by evaporation of polymer blend solution droplets of PVC and PS as shown in the figure. An explanation for the formation of such particles is that when the solution droplet is formed, THF, being highly volatile, starts to evaporate instantaneously. As the THF evaporates, the droplet shrinks and the polymer crust starts to form at the surface. Rapid drying of the droplet results in this crust being a thin skin or shell due to the low concentrations of the solids in solution droplet. Further loss of solvent reduces the volume of the droplet while the surface maintains a constant area. Eventually the shell collapses due to the density difference and implodes. This results in surface hollows and indentations. Several researchers have observed such morphology in spray-dried particles (Vehring et.al. 2008, Wang et.al. 2009). The indentations on the particles are marked and shown in figure 4.1 (a). Even though the microparticles of polymer blends of a 2 and 3wt% look similar in structure, there are some important dissimilarities. Microparticles of polymer blends formed from a 2wt% polymer solution were more crippled and collapsed than the microparticles produced from a 3wt% solution.

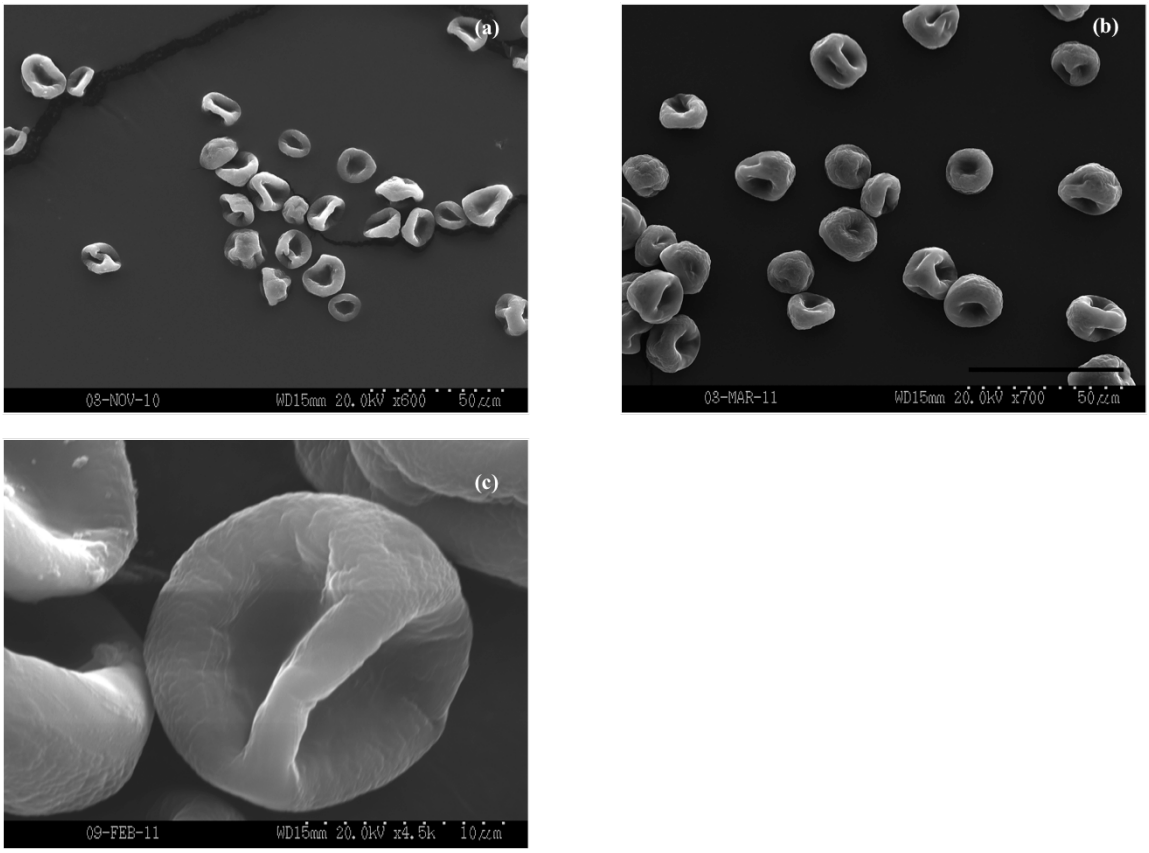

Figure 4.1:SEM micrographs of polymer blend microparticles of PS-PVC produced using (a) 2wt% and (b) & (c) 3wt% polymer concentration in THF

This was due to the fact that as the concentration increased the crust formed would be slightly thicker and rigid and would be able to prevent the walls from collapsing. Even though folding of the microparticles is observed in a 3wt% solution as shown in figure 4.1 (c), the surface was much close to spherical. The average size of 2wt% microparticles formed was calculated to be about 14.58μm and that from a 3wt% solution was 16.74μm. Theoretically, after complete evaporation of the solvent from a solution droplet, if the particle obtained is a non-porous, spherical solid then the final particle size depends on the initial solids concentration as given in equation 4.1.

$$D_p = D_0(C)^{1/3} \quad (4.1)$$

where, D_p is the final particle diameter, D_0 the initial droplet diameter and C is the initial concentration of the solution droplet. The initial droplet diameter from our experiments is about 40 μm and the initial concentration of the solution droplet is 2wt%. The final particle size calculated from equation 4.1 is about 10μm. But as mentioned earlier the average particle sizes obtained from SEM images are 14.58 μm. This is significantly larger than the theoretical particle sizes for a solid (not hollow), spherical, non-porous microparticles obtained. Hence it can be concluded that the particles obtained are hollow. Also, no apparent pores were observed on the surface of the particles. The average particle sizes of blend microparticles obtained from 2wt% solution droplets are slightly smaller than that obtained from 3wt% solution droplets. The ratio of the average particle sizes obtained from a 2wt% and 3wt% solutions was 0.871. The ratio of the theoretical particle sizes (for these two concentrations) for spherical, solid non-porous particles was calculated to be 0.874. This further confirmed that the microparticles generated from lower concentration solution droplets have smaller sizes when compared with the droplets generated from higher concentration solutions. The polymer concentration at the surface reaches the skin forming concentration at an earlier time due to higher initial concentration.

4.1.2 Effect of Evaporation rate

Evaporation rate of the solution microdroplets plays a major role in deciding the final morphology of the microparticles formed. Evaporation rates can be controlled either by changing the temperature, or by using solvents with various volatilities. As discussed in

section 4.1.1, for the drying column used in the present work, the drying of particles and their settling was related to temperature. To collect enough particles for analysis it was necessary to maintain the temperature at around 40 ^{0}C. Lowering the temperature resulted in incomplete evaporation and wet particles were obtained at the bottom. The particles were confirmed to be wet based on the fact that these particles stuck to the aluminum foil and cannot be separated. Due to the limitations imposed by the temperature, the more convenient parameter to control was the solvent. To study the morphology of microparticles under different evaporating conditions, solvents of various volatilities were considered. Most important criteria for the choice of the solvents were (i) high volatility and (ii) dissolves both the polymers. Most of the solvents used to dissolve two immiscible polymers usually have low volatilities. Hence, to study the effect of evaporation rate, a single polymer blend system was almost impossible to consider. Two polymer blend systems were chosen namely, (i) PS-PVC and (ii) PS-PMMA. Dichloromethane (DCM) dissolves both PS and PMMA. Also, DCM has a higher volatility than THF and hence higher evaporation rates can be achieved. It has to be noted here that PS and PVC do not have a common solvent with volatility lower than THF but fast enough to obtain completely dried particles. To achieve this, a solution of THF and Ethanol was used to dissolve the polymer blend system. This was used to achieve two purposes. The first purpose was to study the effect of evaporation rate on the surface morphology and shape of the microparticles obtained. Secondly, both PS and PVC do not dissolve in ethanol. The effect of ethanol on phase separation is discussed in section 4.2.1.

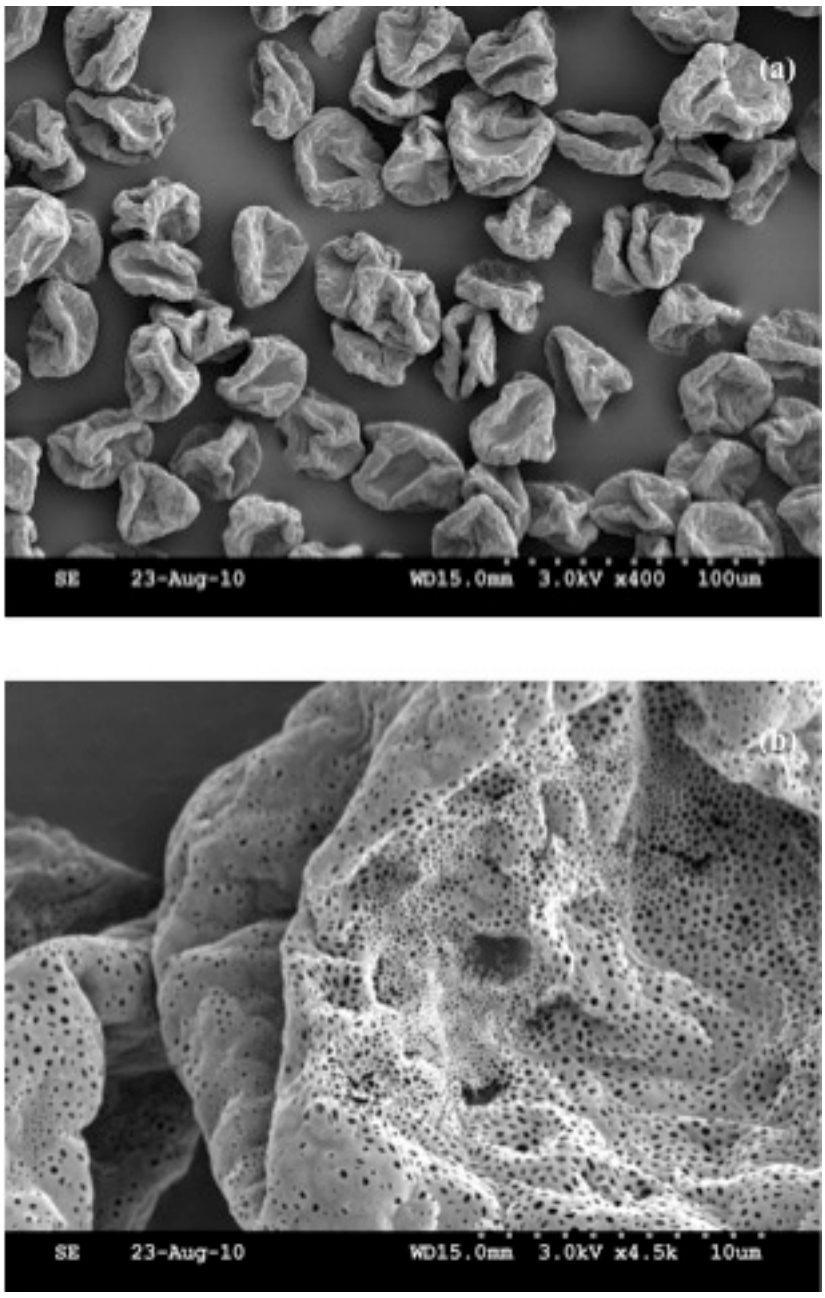

Figure 4.2: Effect of higher evaporation rate on particle morphology; Particles of PS-PMMA obtained from a 2wt% polymer solution in DCM using a 15 μm orifice (a) collapsed particles with large surface indentations. (b) surface perforations on the particles due to rapid evaporation of DCM.

Table 4-2: Vapor pressures of solvents used in the preparation of different polymer microparticles.

Solvent	Vapor pressure (mm Hg) @ 40 ^{0}C
Tetrahydrofuran (THF)	402
Dichloromethane (DCM)	750
Acetone	350
Ethanol (EtOH)	140

Hence, slow evaporation rate and immiscibility could lead to phase separation in the polymer blend system. The third system was a single polymer, PS, dissolved in acetone. The vapor pressures of all the three solvents are given in Table 4-2. Evaporation rate of the solvents are directly related to their vapor pressures and table 4-2 clearly shows that the solvent with the highest volatility is DCM. Figure 4.2 shows the scanning electron micrographs of microparticles of PS-PMMA generated from a 2wt% solution of polymers in DCM using a 15μm orifice. Equal ratio of both the polymers was used. The microparticles obtained had significant indentations as in the case of 2wt% PS-PVC-THF microparticles produced under the same experimental conditions but there were striking differences their external morphology. Figure 4.3 compares the SEM micrographs of both these microparticles. The microparticles prepared using DCM were highly porous. The pore diameters were in the range of 200-500 nm in size. Also, the shapes were far from spherical and had deflated balloon-like structures. This can be directly attributed to the very high volatility of DCM. As the DCM evaporated from the droplets rapidly, the skin forms at the surface almost immediately. Once the skin forms, the remaining DCM forces

itself out of the skin, which results in the formation of pores on the surface of the microparticles. Even though THF is highly volatile, when compared to DCM, its vapor pressure is about half that of DCM and hence there is sufficient time for the THF to escape slowly through the skin formed. The formation of pores can also be related to the softness or strength of the skin, which is a function of the nature of the polymers considered.

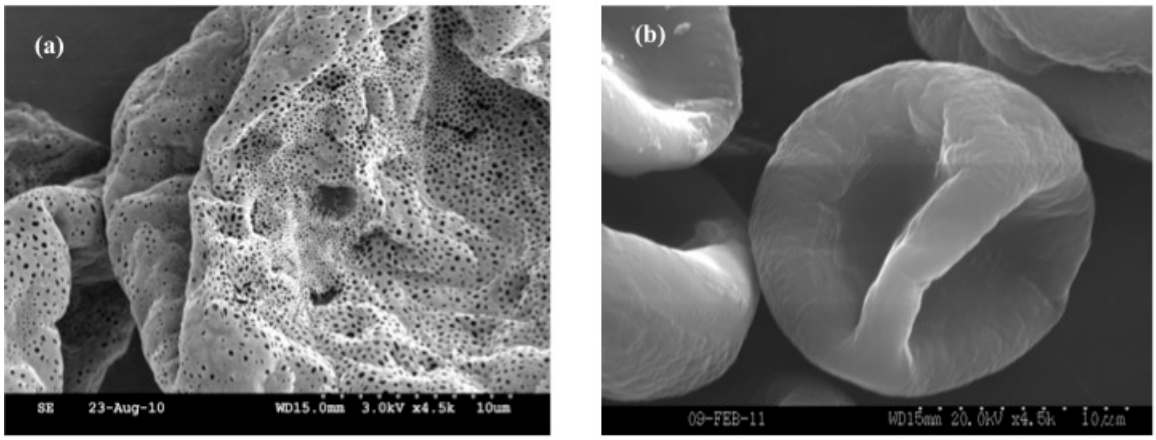

Figure 4.3: Comparison between microparticles of polymer blends produced using two different systems; (a) 2wt% PS-PMMA from DCM solution showing pores and (b) 2wt% PS-PVC in THF solution; both the microparticles were produced under same experimental conditions- 15 μm orifice, 1000 ml/min dispersion N_2 and 40 ^{0}C.

Figure 4.4 shows the SEM images of microparticles of PS in acetone. The PS concentration in acetone was 2wt%. Microdroplets of this solution were also generated using a 15μm. It was interesting to observe that the microparticles obtained from an acetone solution had some indentations but the surface was usually smooth and spherical as shown in figure 4.4 (a) and (c). The particle diameters obtained were also much smaller when compared to the case of 2wt% PS-PVC in THF as previously shown in

figure 4.1 (a). The average diameters obtained are about 10μm for the PS-Acetone microparticles. This can also be due to the fact that polystyrene is the only polymer interacting in this case whereas PVC might play a role during the evaporation of THF from the blend system. Also, acetone is a better solvent for PS than THF and hence the affinity and wettability of the polystyrene is more in the case of acetone than in THF.

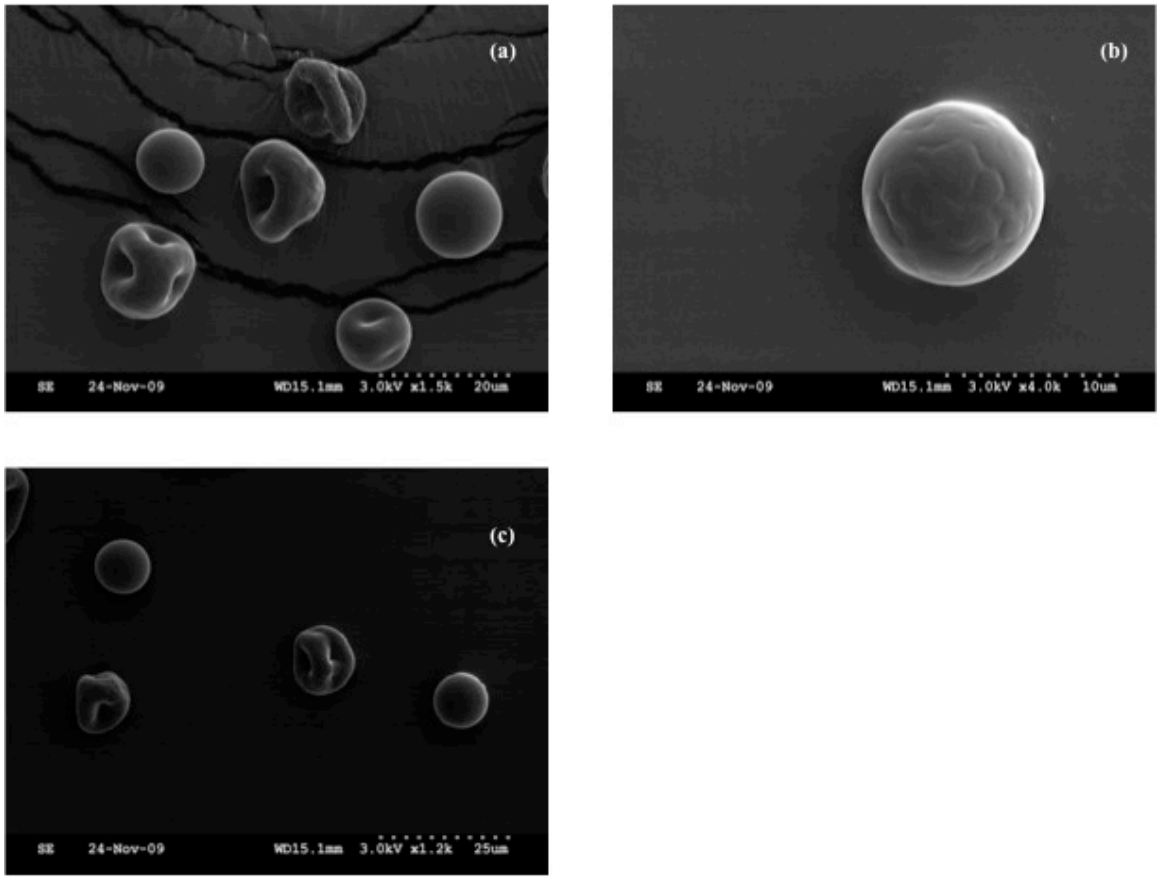

Figure 4.4: PS microparticles prepared using 2wt% polystyrene in acetone with dispersion flow (a) & (c) 1000 ml/min and (b) 1500 ml/min.

The micrographs in 4.4 (c) show that there are some particles which are not spherical. This we believe was due to the temperature difference inside the chamber. Near the walls the temperature was higher than at the center due to the large diameter of the chamber. This would have caused the drying of particles near the walls much faster than the particles at the center of the chamber. Some microparticles had golf-ball like features as shown in fig 4.4 (b). This was due to the dispersion N_2 that is introduced near the orifice and through a 1mm hole in the dispersion cap. The dispersion flow around the droplets for particles in figure 4.4 (a) and (c) was about 1000 ml/min (20m/s) whereas particles were formed using a higher dispersion flow of 1500 ml/min (30m/s). This high velocity around the droplet does not disrupt the shape of the droplets as such but the tangential force exerted on the surface of the droplets result in such wave-like profiles. These features were usually absent when low flow rates were used (figure (4.4(c)). Flow rates lower than 1000 ml/min resulted in incomplete drying of the droplets and wet particles were formed on the aluminum foil at the bottom of the chamber. Also, the dilute concentrations aid in formation of such morphologies. Since higher concentrations could not be studied, we cannot conclude the effect of concentration on such surface features but higher concentrations yield smoother surfaces as the force exerted on the surface of the droplet is balanced by the dense, thick skin formed.

Polystyrene and PVC do not dissolve in any other common solvent that has a lower volatility than THF but high enough for the droplets to completely dry and form microparticles. Ethanol dissolves in THF and hence a polymer blend system of 2wt% PS-PVC was prepared, with equal concentrations of both the polymers, in a THF-Ethanol solution. First a solution of polymers was prepared in THF and then ethanol was slowly

added to attain a homogenous solution. If the ethanol amount exceeded the limiting value slightly then the solution became turbid indicating the onset of phase separation. The limiting value was found to be 30% (by volume) in a THF-ethanol solution. A 75/25 volume ratio of THF/Ethanol was used to avoid near phase separation conditions and at the same time enough ethanol to study the effect of mixing such a non-solvent. Figure 4.5 shows the scanning electron micrographs of the polymer blend microparticles of PS-PVC prepared using a mixture of THF and ethanol.

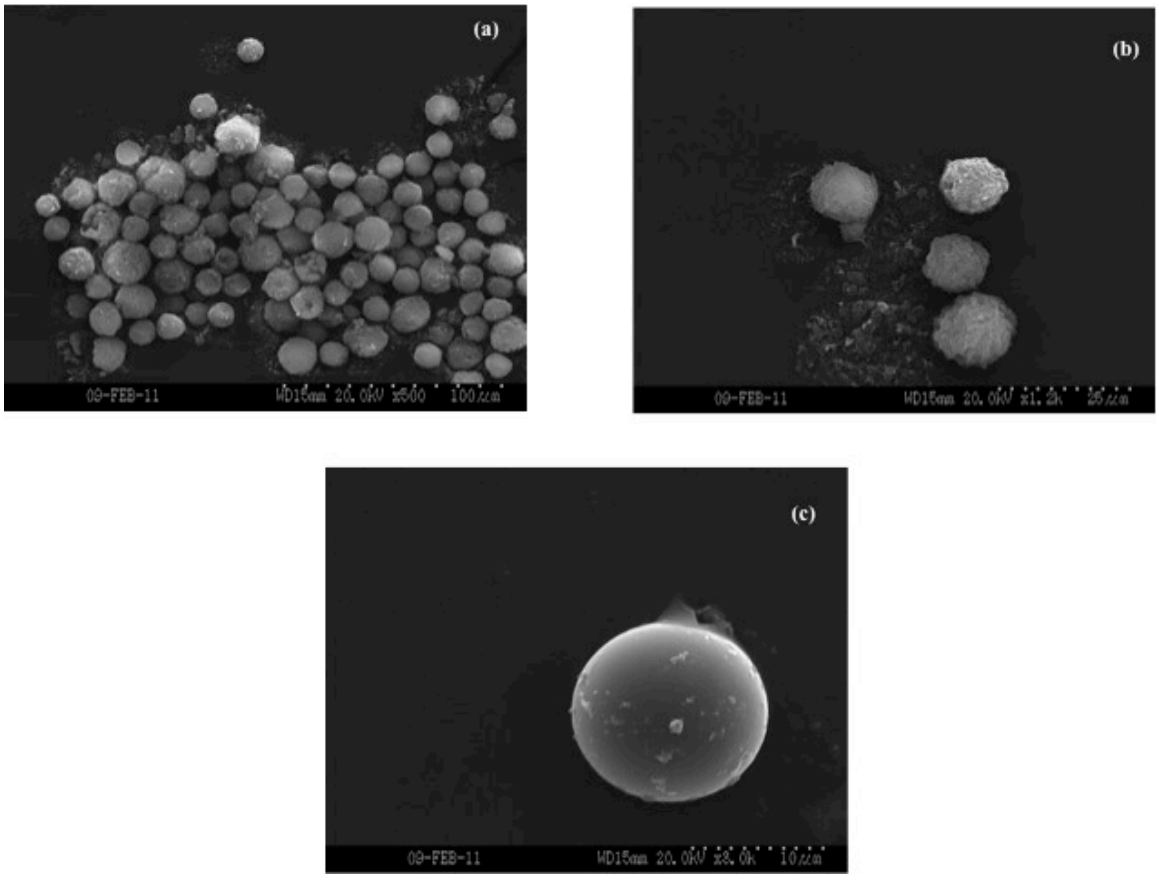

Figure 4.5: PS-PVC microparticles produced from a 2wt% polymer blend solution of PS- PVC in THF/Ethanol (75/25)

In figure 4.5 (a), one can clearly see that the polymer blend microparticles are more spherical and the average size of the particles is about 12.5μm. The sphericity directly depends on the drying time for ethanol (moderately slow) for solvent mixture when compared to particles obtained only with THF. Once the THF evaporates completely, the droplet/particle now consists of very fine chains of polymers dispersed in ethanol. Since ethanol is not a solvent for both the polymers, phase separation occurs and with evaporation of ethanol the phase separation becomes more pronounced. But due to the slow evaporation and increase in concentration of the polymers inside the droplet, there is a more uniform precipitation of the polymers and hence a thick-skinned spherical microparticle is formed as shown in figure 4.5 (b). Even though the particles have thick skins, most of the particles obtained are brittle (figure 4.5 (a) and (b)). One can clearly observe the flakes falling off of the surface of the blend microparticles shown in figure 4.5 (b). This is because of the very brittle nature of PVC in the blend. Very few microparticles had smooth spherical surfaces as shown in figure 4.5 (c). Even though the formation of such smooth surfaces cannot be explained with certainty, it is possible that a core-shell structure might have formed due to slow drying of some of the particles in the chamber. A large distribution in particle size was obtained with some of the particles almost double the size of the average particle diameters obtained. This may be due to the coalescence of the droplets near the mouth of the orifice. Another reason might be that the actual frequency of vibration may be lower from the input frequency due to the presence of particulate impurities on the surface of the orifice. Sometimes, a thin polymer film forms on the surface of the orifice and this can also result in lowering the frequency of vibration.

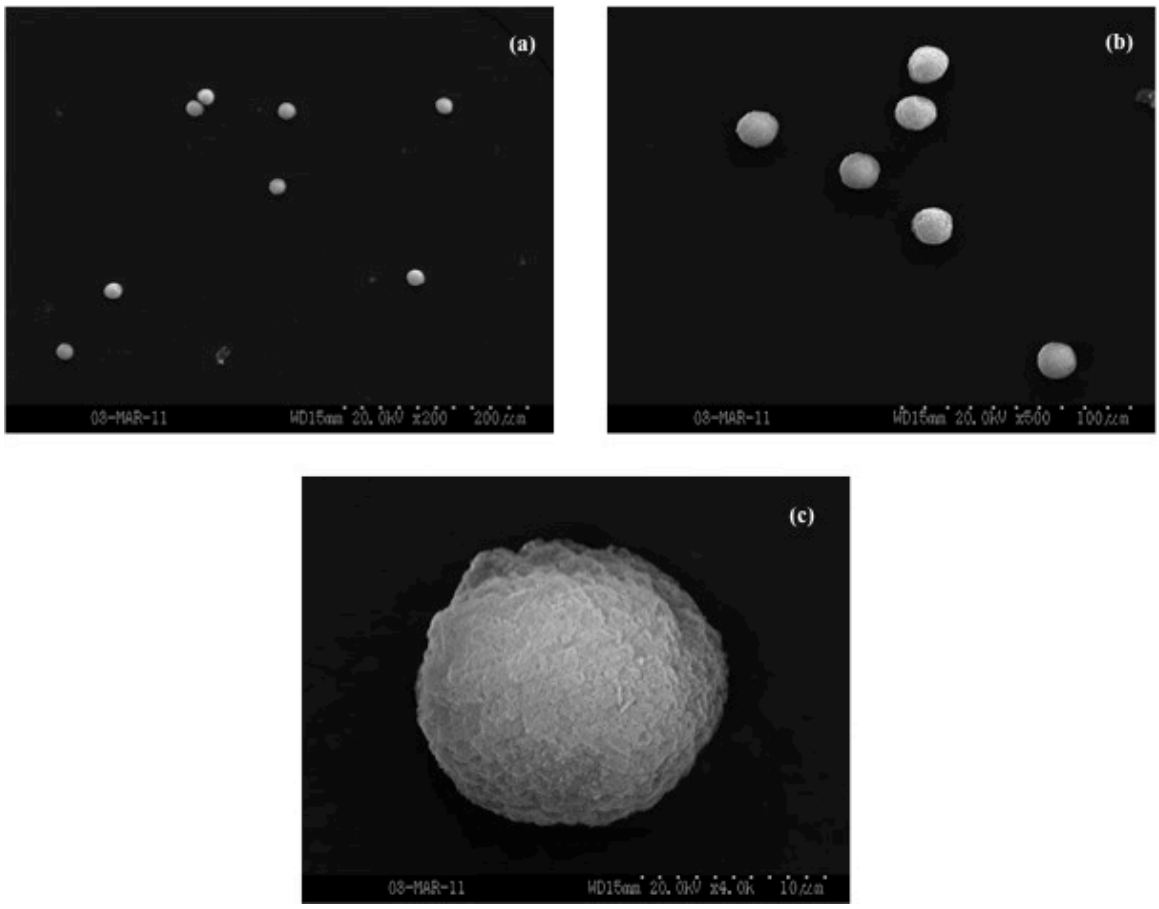

Figure 4.6: Highly monodispersed PS-PVC microparticles prepared from 2wt% polymer blend solution of PS-PVC in THF and Ethanol after rigorous cleaning of the orifice (f= 50 kHz, Q=0.146 ml/min) at different magnifications (a) 200x (b) 500x and (c) 4000x with surface irregularities

Rigorous cleaning of the orifice was done by flushing out the polymer solution from the drain several times to ensure that the orifice is not partially clogged and then the same polymer blend solution was used to generate the microparticles under the same operating conditions. A highly monodispersed microparticles of PS-PVC blend system was obtained as shown in figure 4.6. Figure 4.6 (a), (b) and (c) represent the same

microdroplets under different magnifications. The particles were still brittle with surface roughness and also no smooth surfaced particles were observed. This can be really important when tailored microparticles of two different polymers are to be prepared. Judicious combination of solvents can yield different morphologies ranging form core-shell to completely mixed particles.

4.2 Homogeneous Polymer Blend Microparticles

Section 4.1 dealt with the external morphology of the polymer blend microparticles prepared using the droplet evaporation technique. This section deals with studying internal distribution and also the thermal characteristics of the polymer blend microparticles prepared. Sectional images of the microparticles were observed under an SEM or a TEM and the thermal characterization of the blend system was done using a Differential Scanning Calorimeter (DSC). In all the studies, either pure polymer microparticles of PVC or PS or their blends, prepared by dissolving the polymer(s) in THF, were considered. Also, to use confocal microscopy as an effective tool for imaging the distribution of polymers in the blend, a self-fluorescing polymer, poly (vinyl carbazole) was used as one of the polymers in the blend system.

4.2.1 Internal morphology of polymer blend microparticles

The internal morphology of polymer blend microparticles was studied by mainly two techniques. The first was by using the micrographs obtained using TEM or SEM microscopes. This was done by dispersing the microparticles in a Spurr's resin in a beem capsule and then polymerizing the resin at 50 ^{0}C (and kept under vacuum for 48 hrs.) so that the resin hardens and particles are now embedded into the resin matrix. It should be noted here that the curing temperature of the resin must be lower than the glass transition temperature of either of the polymers. Ultra thin slices of this matrix were cut using a Reichert-Jung Ultracut E microtome. The thickness of the slices obtained was about 60 nm. The slices were mounted on copper grids and placed under an SEM or a TEM microscope for further study. First, internal morphology of a pure PVC microparticle sample was investigated by ultra-microtoming very thin slices of the microparticles. Figure 4.7 shows the micrograph of the ultra-microtomed slices of PVC. Due to a difference in contrast, PVC represents the darker areas in the image and the resin covers the bright white background. The first and the foremost observation is that the particles formed, as discussed in section 4.1 and thereafter, are hollow with a very thin skin of about 0.5μm. Secondly, the resin has diffused into the hollow core of the particles. Around the edges there are a few regions where the resin connects the core without any polymer film that separates them. These regions signify the presence of some very minute pore channels (not visible under an SEM though) on the surface of the microparticles but they are not distributed uniformly.

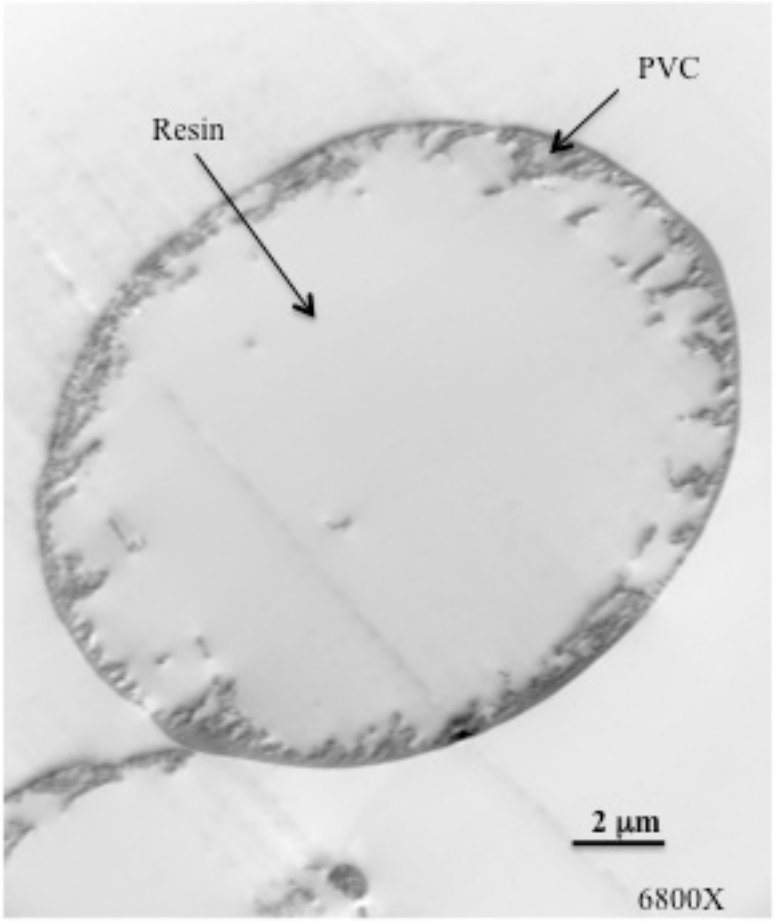

Figure 4.7: TEM micrograph of ultra-thin slice of pure PVC microparticles prepared from a 2wt% PVC-THF solution (15μm orifice with f=60 kHz, Q=0.1454ml/min). Dark regions represent PVC and the white region is the embedding resin used for ultramicrotoming the sample.

Although a good understanding of the internal morphology of the microparticles can be directly obtained from such a visual observation, to quantify the distribution an Energy dispersive X-ray analysis (EDAX) was performed on the films. It should be noted here that the elemental difference between PS and PVC is only the presence of chlorine. PVC contains about 55% of chlorine hence an equal ratio of PS-PVC blend would contain about 20% of chlorine. This prompted us to do an EDAX analysis on the microparticles

for the mapping of chlorine in the samples. Since ethanol is a non-solvent for both the polymers and since the evaporation is slow, we believed that during drying and formation of microparticles both the polymers will phase separate. TEM micrograph of an ultra thin slice of these particles is shown in figure 4.8 (a). An important observation from this micrograph was the internal structural morphology of these blend microparticles.

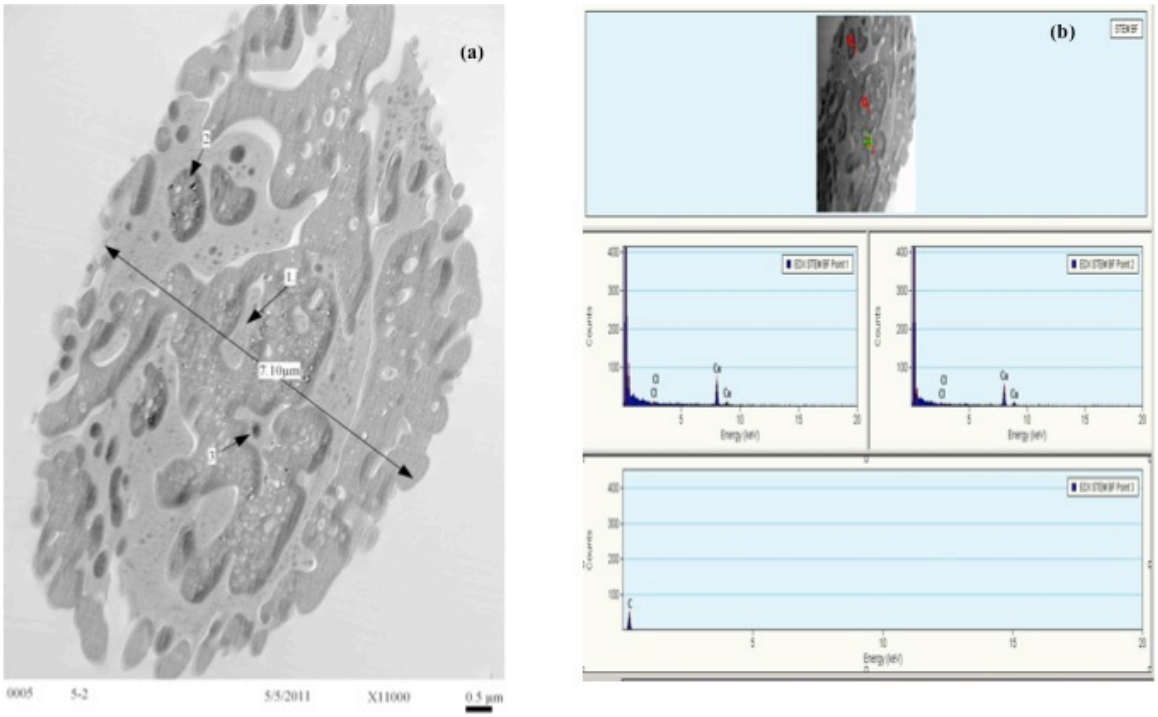

Figure 4.8: (a) TEM micrograph of a single ultra-microtomed slice of PS-PVC microparticle (length scale-0.5µm, mag-11000) (b) EDAX spectrum of the 3 points on the slice; microparticles are prepared from 2wt% polymer blend solution of PS and PVC in THF/EtOH.

Figure 4.8 (a) clearly shows domains of different contrast. Also, the contrast of the resin was different from the other contrasting domains observed inside the slice. This was a really good confirmation of phase separation in the polymer blend microparticles. Once the EDAX analysis was done at different cross-sections on the slice (points 1, 2 and 3) as shown in the figure 4.8 (b), there was absolutely no chlorine found in these slices. One reason could be the fact that the voltage used for the analysis in the TEM was about 100keV. As mentioned earlier, the thickness of the slice was about 60 nm. To get a higher count, one has to increase the voltages. The maximum voltages that can be achieved on this particular TEM were only 100 kV. Since the power was low another TEM was used with higher voltages in the range of 150-200kV but the thin slices burned when exposed to such voltages. Also, the TEM detector was not powerful enough for detection of traces of elemental chlorine. Even though SEM has a lower operating voltage than TEM, the EDAX was rated to be much more powerful on the SEM S-3200. This prompted the use of SEM instead of a TEM for further studies. Also, since chlorine was not observed in the spectrum observed from the slices, SEM-EDAX was first performed on the whole particles. All the particles showed consistent chlorine peaks in the X-ray spectrum. EDAX spectrum of one such particle is shown in figure 4.9. Several points were taken on the particle to check for chlorine. Each point corresponds to a $3x3\mu m^2$ area. The Chlorine counts for all the points except for point 4 (outside the particle) were almost 600 ± 100. Points 1, 6 and 7 showed amounts of chlorine slightly above average. These points and most of the corners do not have flat surfaces and are at an angle. This imparts a different hitting zone for the X-rays.

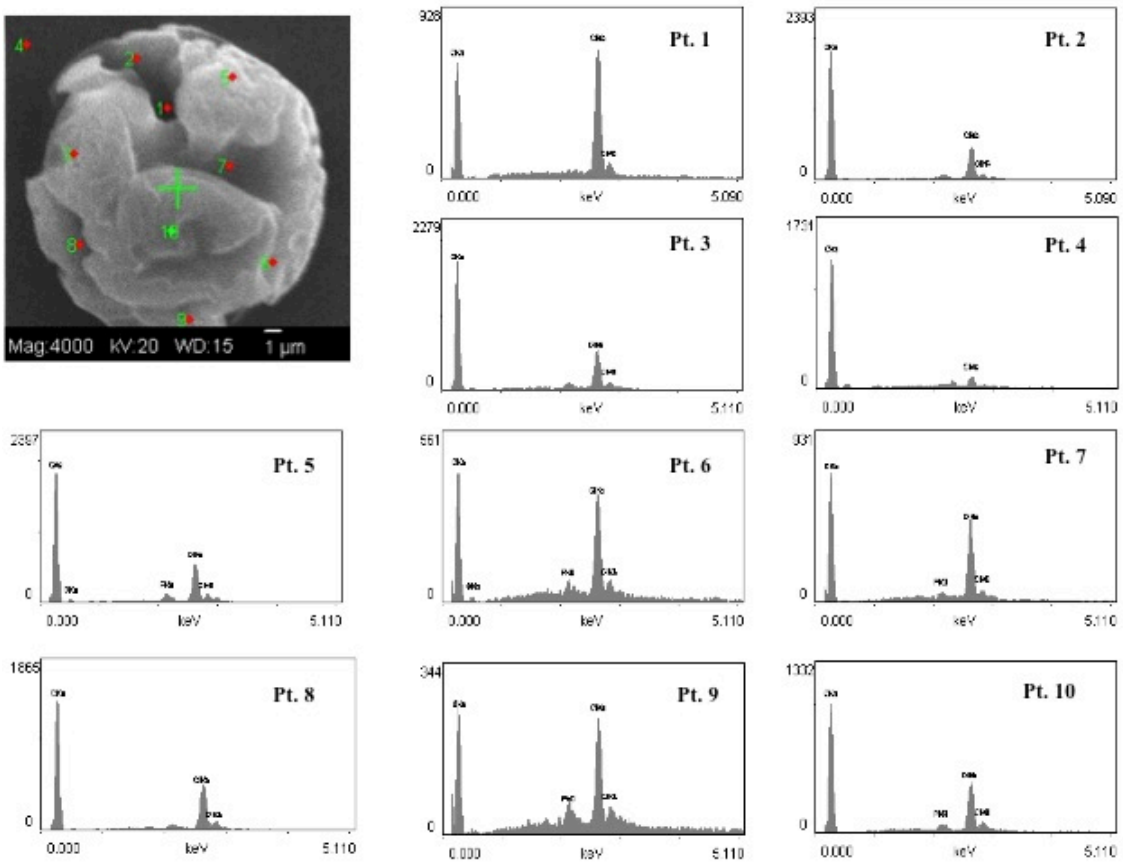

Figure 4.9: EDAX spectrum of a single PS-PVC microparticle prepared from 2wt% polymers in THF solution showing equal distribution of chlorine throughout the microparticle.

Hence, the curved surfaces of the particles can add to some error in the counts shown by the spectrum. Since the points (areas) are distributed throughout the particle surface, one can conclude that PVC is uniformly distributed on the surface. Once the chlorine was detected on the surface, the next step was to find chlorine on the slices. The biggest disadvantage of analyzing an ultra thin sample on an SEM-EDAX is the fact that there is a certain penetration depth of the X-rays. The X-rays can easily penetrate through the sample and the reading can comprise mostly of the carbon substrate on which the films

rest. Also, due to the presence of the copper grids and the delicate nature of the films, the contact and charging effect cannot be neglected.

To study the internal morphology of the polymer blend microparticles and whether there is any phase separation in the blends, two samples of PS-PVC microparticles were prepared under the same conditions, one only with THF and another one with THF-Ethanol mixture. Figure 4.10 shows the SEM micrographs of ultra thin samples of microparticles of PS-PVC prepared using both the solvents.

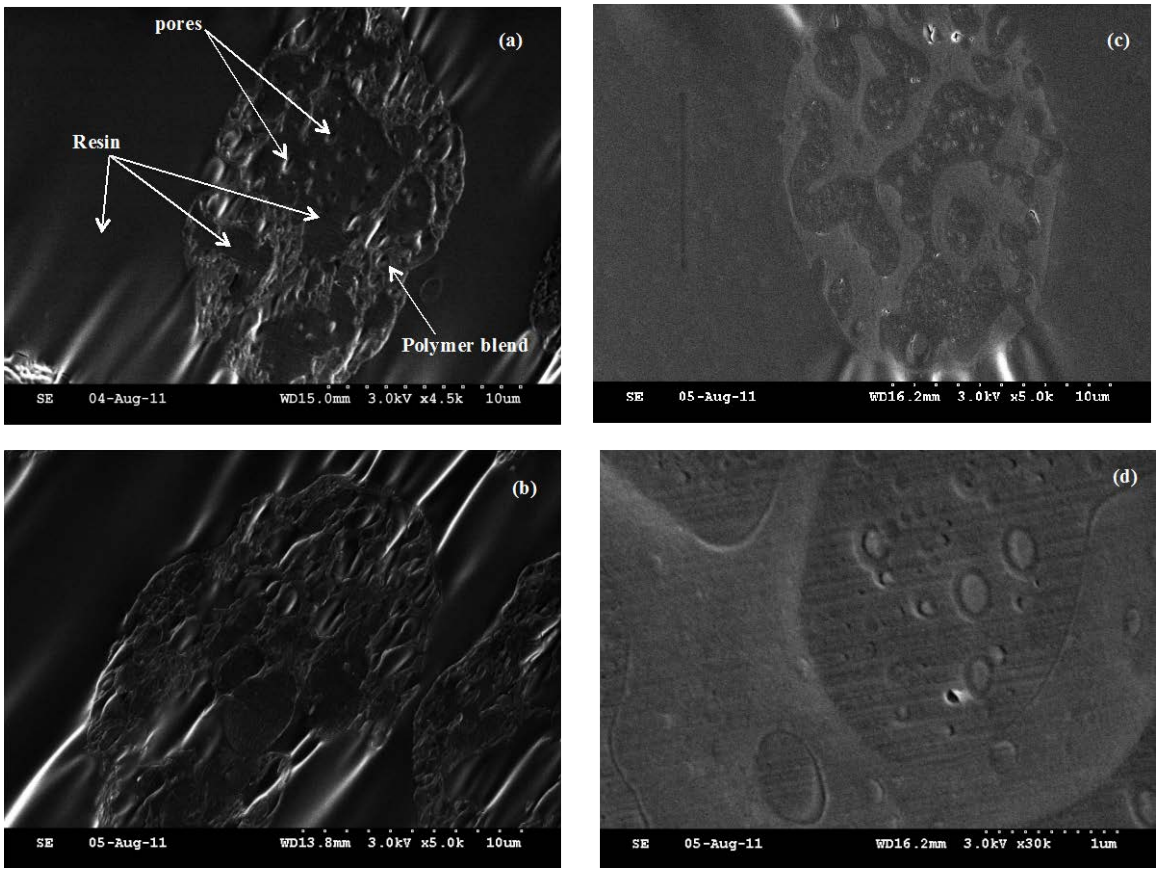

Figure 4.10: SEM micrographs of ultra thin slices of polymer blend microparticles of (a) 2wt% PS-PVC prepared in THF, (b) 3wt% PS-PVC prepared in THF, (c) &(d) 2wt% PS-PVC prepared using a 75/25 mixture of THF and ethanol.

Figure 4.10 compares the SEM micrographs of samples prepared using two different evaporation rates and for two different initial polymer concentrations (f = 50 kHz, Q = 0.15ml/min, Temp. = 40 ^{0}C and dispersion N_2 = 1000 ml/min). Figure 4.10 (a) shows the interpenetrating network of the polymer blend along with the pores created by the evaporation of THF. When the microparticles are dispersed in the liquid resin, before polymerization, the resin diffuses through the pores into the hollow regions of the microparticles and solidifies once the polymerization is completed. The cut slices show the same contrast as that of the resin material inside these regions as shown in the micrograph. To compare the effect of concentration a similar slice from a 3wt% polymers' concentration was used, the micrograph of which is shown in figure 4.10 (b). The interpenetrating network still existed but there are regions where one can distinguish the resin film clearly than the elliptical regions. The result can be interpreted in two ways. If the elliptical portion in the figure is the resin that has diffused through the pores then there is a chance that the solidified resin might have fallen off the film while cutting. The separations between the interpenetrating network and the ellipses can be seen clearly in the figure. There is a slight possibility that the polymer blend has phase separated and the elliptical structures are the domains of one of the polymers and the other polymer forms interpenetrating network. Figure 4.10 (c) and (d) are the micrographs obtained from the slices of microparticles of PVC-PS prepared by using a THF-ethanol solvent mixture. The thickness of the interpenetrating layers are more pronounced and smooth (figure 4.10 (c)) and if noticed carefully, at higher magnification, (figure 4.10 (d)) it is observed that there is phase separation of the polymers and a structure similar to nucleation and growth phenomena of phase separation can be observed.

Even though the TEM micrographs show a clear distinction in phases when a THF-ethanol solution was used, quantification of phase separation was an issue. The slices of the polymer blends were subjected to EDAX analysis and except in one such slice (as shown in figure 4.11), no slices showed the presence of chlorine. Even the slices that showed contrasting phases (figure 4.10 (d)) did not give any chlorine counts. This can only be attributed to the fact that the polymers' content in the slices is extremely low. The chlorine content throughout the sample might be significantly lower to excite significantly enough photons to be detected by the EDAX detector. EDAX analysis of the slice shown in figure 4.11 did show enough chlorine counts to conclude that chlorine, and hence, PVC is uniformly distributed in the polymer blend microparticle. Figure 4.11 (a) shows the slice on which the analysis was performed. The image of the slice was not clear due to the high voltage used and also due to the very high magnification. At low voltages (~3 kV), the images were much clearer as shown in previous micrographs in figure 4.10. The chlorine counts from the 3 chosen points were about 100. The counts were not enough to map the distribution of chlorine in the slice but the equal number of counts suggests that the distribution of chlorine might be uniform. Since, only one such slice was obtained wherein chlorine was detected, using this result alone we cannot conclude the uniform distribution of PVC and PS.

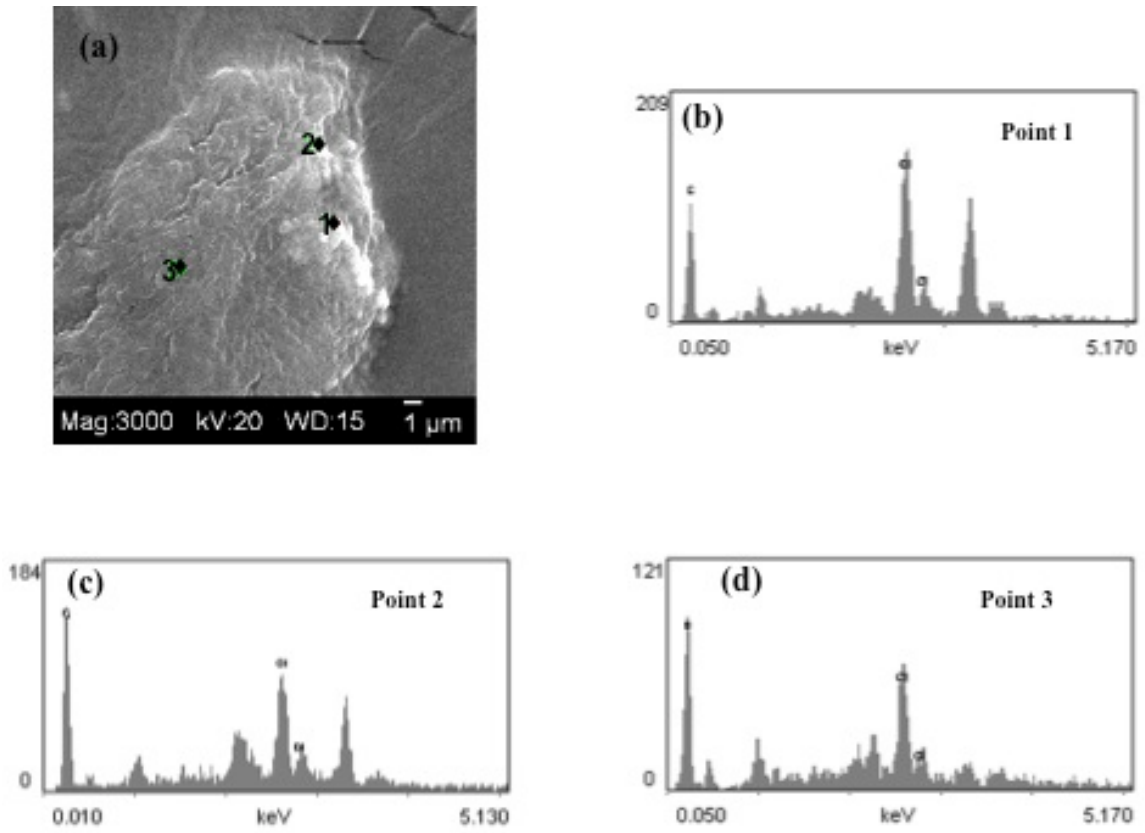

Figure 4.11: SEM-EDAX analysis of ultra thin slice of PS-PVC microparticle prepared from a 2wt% polymers' solution in THF showing the distribution of chlorine (PVC) in the slice.

4.2.1.1 Confocal Microscopy of polymer blend microparticles

Laser confocal microscopy involves visual sectioning of samples in any sectional plane and then obtaining information from the scattered light. A very powerful tool used in conjunction with such a process is fluorescence. While sectioning the samples, if fluorescent materials are present, then even with very little amounts of sample, fluorescence can be detected. For the present purposes, either one of the polymers can be functionalized with a material that can fluoresce. This method was very expensive and time consuming. To avoid such a process, and to check if the process yielded similar particle morphology, poly (vinyl carbazole) (PVK) was used instead of PVC to form PS-PVK microparticles. PVK is a self-fluorescing polymer whose fluorescence wavelength is somewhere around 350-370 nm in the ultra-violet range. The microparticles were prepared exactly in the similar fashion as that of PS-PVC blends. Before studying the blends under a confocal microscope, the particle morphology and the internal sectional morphology of the particles were observed under SEM. Figure 4.12 and 4.13 show the surface morphology and the internal morphology of the slices respectively.

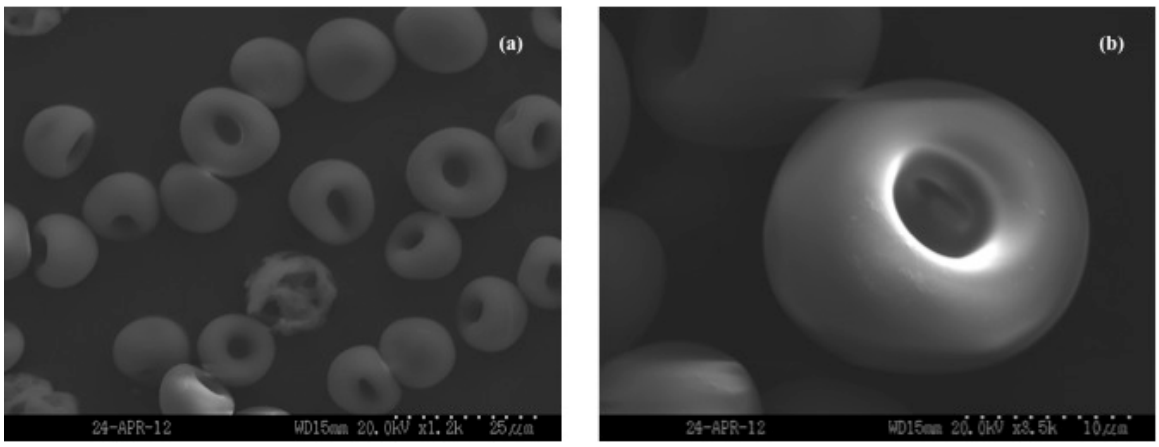

Figure 4.12: SEM micrographs of hollow PS-PVK microparticles prepared using a 2wt% polymers solution in THF (a) uniformly shaped (b) magnified one such microparticle showing the smooth surface and the hollow center.

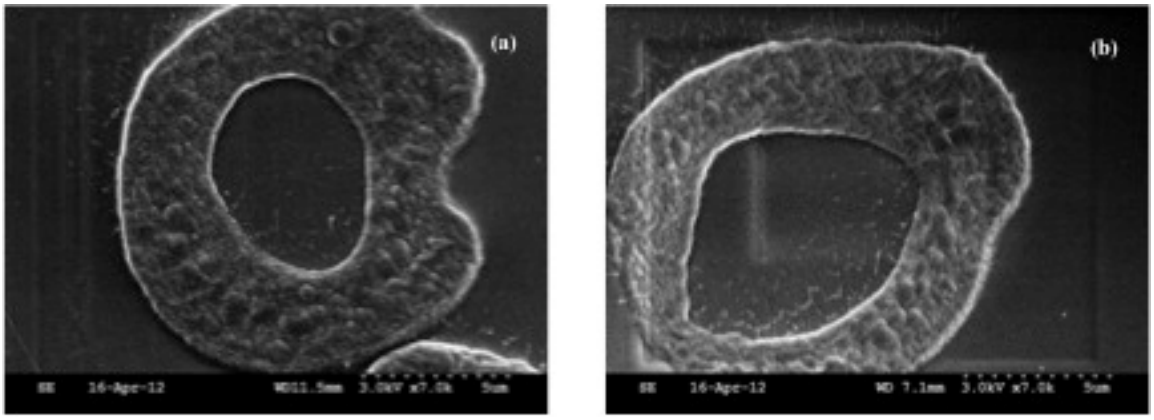

Figure 4.13: Ultra microtomed slices of PS-PVK microparticles shown in figure 4.12 (a) and (b) show two different slices both showing a similar hollow morphology.

Figure 4.12 shows that the particles of PS-PVK blend are much smoother. No wave-like features are formed on the surface of the particles. This was due to the rigidity of the PVK-PS skin formed during the evaporation and drying process. The thin sections of the blend microparticles in Figure 4.13 show that the particles are quite hollow. Also, there are no specific domains in the shell region. This also suggests that there is no phase separation in the microparticles.

To check for the fluorescence of PVK, a polymer blend film of PVK-PS was prepared by pouring a 10ml polymer blend solution, 2wt% PS-PVK (equal ratios) in THF, in a petri dish and evaporating the solvent at room temperature for about 3 days. The film was then peeled off and dried under vacuum for 48 hrs. before studying it under the confocal microscope. Bright field image of the film and also an overlay of the fluorescence image showed (figure 4.14 (a)) phase separation in the blend film with PS as the continuous phase and PVK as the dispersed phase. The dispersed and continuous phase formation mainly depends on the wettability of the solvent with the polymer and the substrate affinity of the polymers. PVK fluoresces and radiates a blue color as shown in figure 4.14 (b). This property was used to check for fluorescence in the polymer blend microparticles. Microparticles were directly transferred to a microscope glass slide and kept in the environmental chamber of a confocal microscope. A 350 nm wavelength laser illuminated the microparticles and visual sections, each section of about 500 nm thickness, were cut horizontally and the images were recorded.

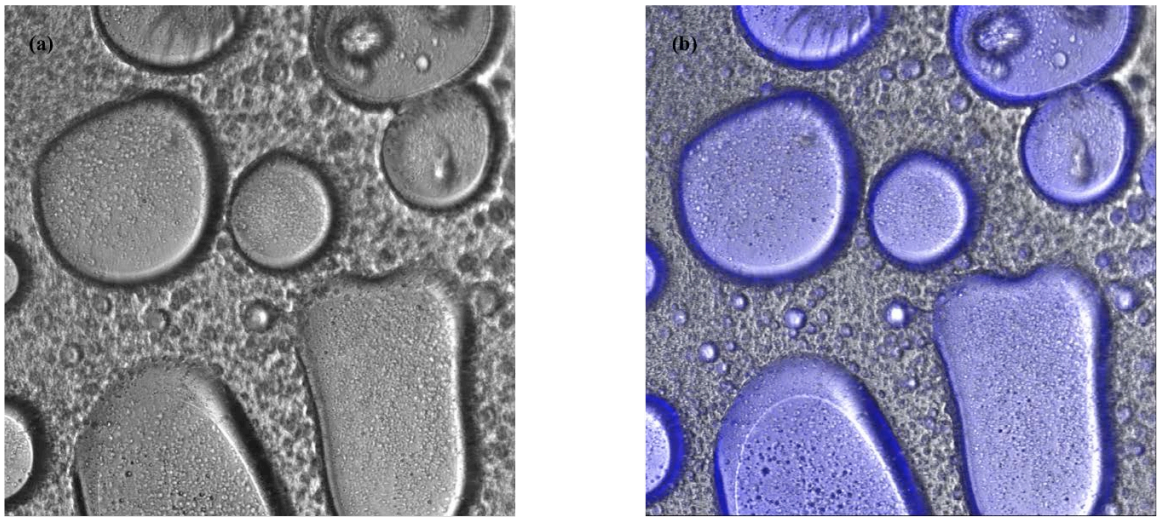

Figure 4.14: Confocal microscope images of polymer blend film of PVK-PS prepared using THF as solvent by evaporating a 10 ml solution in a petridish.

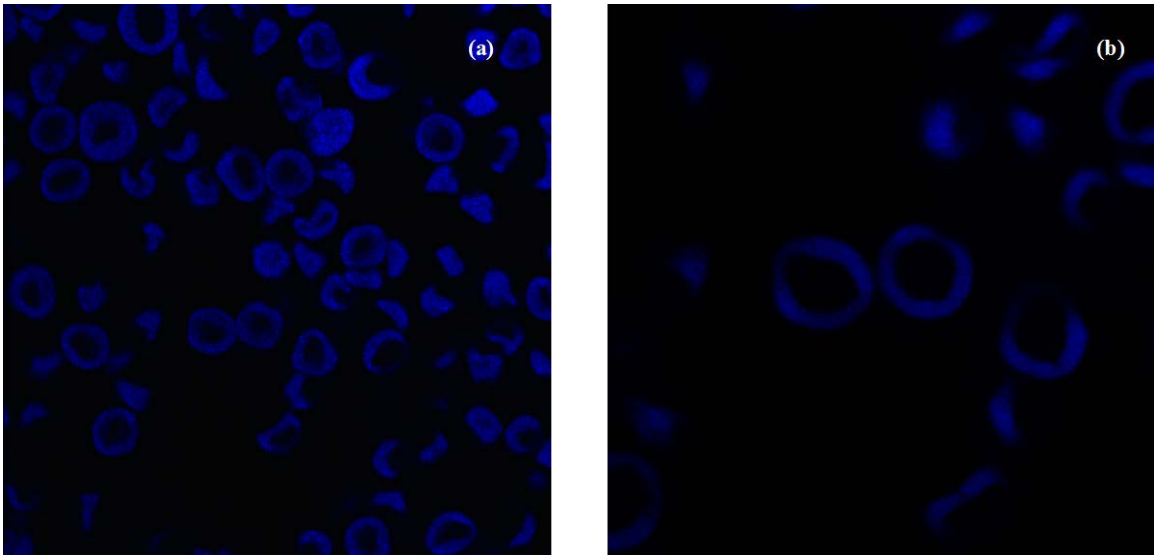

Figure 4.15: Optical cross-sectional fluorescence image of two sections of PS-PVK polymer blend microparticles from confocal microscope. (a) 2μm depth from top (b) magnified portion of the same cross-section.

Figure 4.15 (a) and (b) show that the outer skin of the microparticles fluoresces and the center regions of the microparticles have no fluorescence. This can be either due to a formation of a core-shell microparticle with PS core or if the particles are hollow. It has already been shown that the particles are hollow as shown in figure 4.13. Since polystyrene has to be present in the skin along with PVK and there does not seem to be a distinction in fluorescence in the skin, this further corroborates the fact that the microparticles formed are homogeneous polymer blend microparticles.

4.2.2 Differential Scanning Calorimetry (DSC)

A common method used as a proof of miscibility in polymer blends is through measurement of the glass transition temperature, T_g, of the blend. A miscible polymer blend is expected to exhibit a single glass transition temperature whereas an immiscible blend exhibits more than one glass transition temperature. Two equations that are commonly used when a single T_g is observed are the Fox equation and Woods equation given as follows,

$$\frac{1}{T_g} = \frac{w_1}{T_{g_1}} + \frac{w_2}{T_{g_2}} \tag{4.2}$$

$$T_g = w_1 T_{g_1} + w_2 T_{g_2} \tag{4.3}$$

where, T_g is the expected glass transition temperature of the miscible blend, T_{g_1} and T_{g_2} are the glass transition temperature of the pure polymers and w_1 and w_2 are the weight fractions of the respective polymers in the blend.

In a typical DSC experiment, the difference in the heat required for maintaining or increasing the temperature of the sample and the reference is recorded as a function of temperature. Both the reference and the sample are maintained at nearly the same temperature. The temperatures of the samples are usually increased linearly with time. A typical DSC curve shows the variation of the net heat flux (exothermic or endothermic) with temperature.

In the present work, microparticles of pure polymers and a polymer blend of PS and PVC, with equal wt% of both the polymers have been prepared. All the blend microparticles prepared had a 2wt% of the total polymer concentration in THF. A sample of 7-10 mg of the sample was loaded on the aluminum pan and sealed off using an aluminum lid. The aluminum pan was placed into the DSC equipment for further study. Heating rate plays a major role in determination of the glass transition temperature. Low heating rates can lead to thermal relaxations in the polymer blend that may lead to inaccurate determination of the transformations involved. There is also a possibility that the polymer blends might phase separate during the slow heating process. Here, a heating rate of 20 ^{0}C/min was used to determine the glass transition temperature. The system was equilibrated at 25 ^{0}C for 5 min and then the heating ramp was started. Figure 4.16 shows the DSC curve for a pure polystyrene microparticles prepared 2wt% PS-THF solution using the droplet evaporation technique. The T_g of as-bought PS was 100 ^{0}C. The glass transition temperature measured using the DSC curve yielded a value of 89 ^{0}C. In very dilute solutions, polymer chains are expanded and elongated. During rapid evaporation and drying of the solvent from the solution droplets, these chains immobilize almost instantaneously. The polymer microparticles prepared by such a process is in a highly

non-equilibrium state. Since, the polymer is already in an elongated state, the amount of energy required by the polymer to go from a solid to a glassy state lowers and hence the glass transition temperature is lower than that of the as-bought sample.

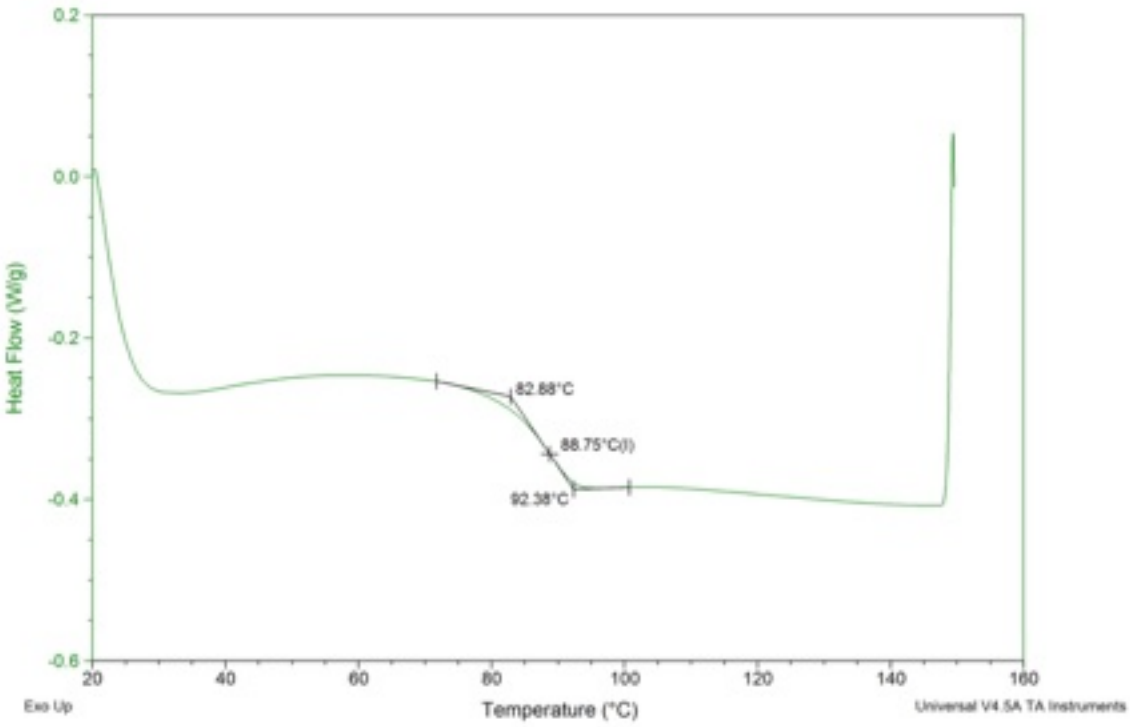

Figure 4.16: DSC curve of polystyrene microparticles prepared from a 2wt% PS solution in THF. Heating rate of 20 ^{0}C/min was used (first heating cycle).

Next, thermal analysis of 2wt% polymer blend microparticles of PS and PVC, with equal percentages of both the polymers, was done to measure the glass transition temperature. Since the polymers are in a highly non-equilibrium states, once the first DSC scan is finished, the polymers tend to relax and move from the non-equilibrium state to the more preferred conformation. This is a major limitation of a DSC while studying the phase separation or miscibility of polymer blend microparticles. Nevertheless, the DSC analysis was performed on the blend microparticles with 20 ^{0}C/min heating rate and the DSC plot obtained from the first heating scan is shown below in figure 4.17 (a). The DSC curve

exhibits a single transformation, which confirms the homogeneity of the blended microparticles. As discussed above, in case of just one polymer, the chains just elongate but in case of polymer blends, in dilute solutions, the elongated chains of one polymer are completely mixed with the elongated chains of the other polymer. Once the evaporation proceeds, the elongated chains do not shrink but instead entangle themselves and the mobility of both the polymers are now interdependent with each other due to the entanglement effect. Once the blended microparticles are heated and cooled several times, both the polymers undergo conformational changes relating to their chain length and an equilibrium state of phase separation is achieved. This is clearly shown in the fourth heating scan for the same polymer blend sample in figure 4.17 (b).

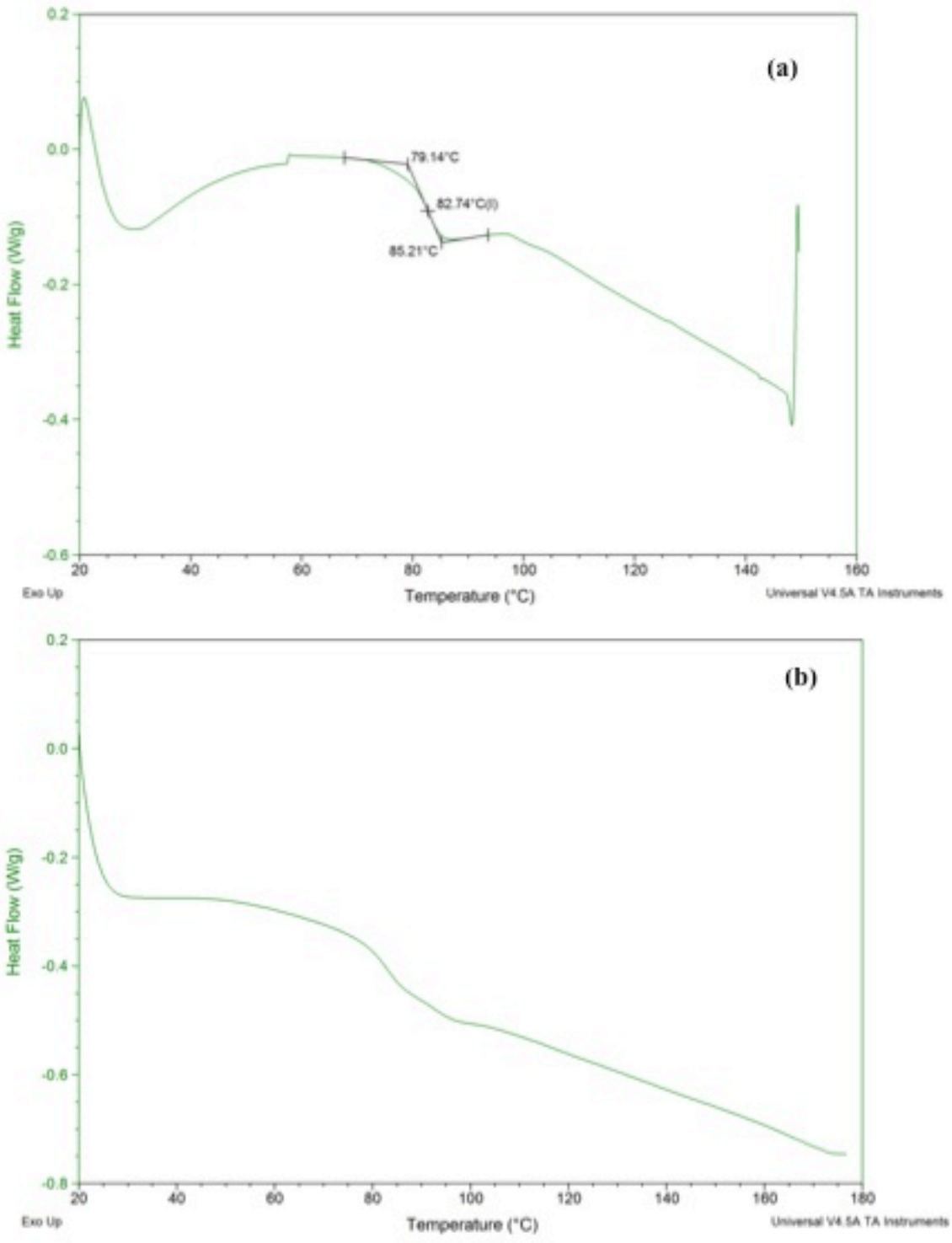

Figure 4.17: DSC curve of PS-PVC blend microparticles prepared using the droplet evaporation technique (a) first heating scan (b) fourth heating scan.

4.3 Conclusions

Polymer blend microparticles of different initial concentrations were successfully prepared in our laboratory using microdroplet evaporation technique. The method involves preparation of dilute polymer solutions in a highly volatile solvent, atomization of the solution (using a VOAG) into micro-sized droplets and finally drying of the microdroplets in a drying chamber to obtain polymer blend microparticles. Operating parameters such as initial concentration, temperature and orifice size were varied to optimize the operating parameters for the successful generation of the microparticles based on the morphology of the microparticles obtained.

The microparticles were characterized for their shape and size using SEM. It was shown that the size of the microparticles obtained was dependent on the initial concentration of the microdroplets. Higher temperatures were not studied due to the several problems associated with the chamber. A new chamber was built to prevent such problems but future studies would be required to optimize the new drying chamber for different operating conditions. We believe that the collection efficiencies can be increased substantially by incorporating such a chamber. Also, the dispersion air used to prevent coalescence of the droplets affect the patterns (golf-like) formed on surface of the particles.

The effect of solvent evaporation rate on the morphology of the polymer/polymer blend microparticles was demonstrated by using solvents such as THF, DCM and acetone to produce PS-PVC, PS-PMMA and PS microparticles respectively. Particles were either spherical or close to spherical for a lower volatile solvent, in this case acetone. Also, very high volatility solvent, when used, perforated the skin formed. Usually, with high

evaporating rates it was observed that the particles formed were crippled and internally collapsed due to their ultra low densities. To show the effect of low evaporation rates, a solvent mixture of ethanol and THF was used for the preparation of PS-PVC microparticles. The morphologies obtained with ethanol were highly monodisperse and spherical.

To show the distribution of each polymer in the blend, several ultra microtomed sections were studied under an SEM and TEM microscope. The sectional films did not show any contrast between phases for a 2wt% polymer blend microparticle whereas it showed a slight contrast when a 3wt% microparticle was studied. The sectional films also showed interpenetrating networks of the phases with a highly porous structure. This can be due to phase separation of the polymers. TEM micrographs of microparticle slices prepared by using mixture of a solvent and a non-solvent (ethanol) revealed spinodal decomposition-like formation of phases.

EDAX spectrum of different polymeric phases in the blend was also tried to quantify the distribution of phases. Equal distribution of chlorine was found out in the PS-PVC blend microparticles but when a slice was studied for the same, no chlorine was detected by the instrument. This was attributed to the trace amount of chlorine in the ultra-thin sections.

Confocal fluorescence microscopy coupled with fluorescence was used to differentiate the polymer phases when one of the phases was self-fluorescing. In this case, PS-PVK blends were used. The PS-PVK blends showed uniform blue fluorescence in the skin regions of the blend microparticles. This coupled with the fact that the

particles obtained were hollow forced us to conclude that the polymer blend microparticles formed are indeed homogeneous.

Differential scanning calorimetry is the most commonly used technique to measure glass transition temperature and a single glass transition temperature usually means miscible blends. DSC plots of pure polymer microparticles revealed that the glass transition temperature was lower when microparticles are formed by the droplet evaporation technique. A single glass transition temperature was obtained for the blend microparticles of PS-PVC from the first heating scan. Subsequent heating and cooling cycles resulted in phase separation in the blend as the curve started to broaden and two distinguished curves can be clearly observed at the end of the fourth heating scan. This represents existence of two separate phases.

Even though the methods used above have been simple yet effective to prove the homogeneity of the polymer blend microparticles, ideally, phase separation in polymer blends should be defined based on the length scales of phase separation. Sophisticated techniques such as 2-D solid state Nuclear Magnetic Resonance (NMR) can reveal more details about the homogeneity of the blend with respect to appropriate length scales. Fluorescence spectroscopy can further be used by covalently attaching fluorescent materials to one of the polymers. This is rather expensive and time-consuming method but might yield insightful information about the distribution of polymers in the blend.

CHAPTER 5

5. MODELING EVAPORATION OF A SOLUTION DROPLET WITH CONVECTION

5.1 Introduction

Evaporation and drying of microdroplet solutions to form microparticles find wide range of application in the field of pharmaceutical technology, food industries, ceramics production and production of many other polymeric microspheres of specialty chemicals. The techniques used to manufacture these products include spray drying, spray freeze-drying, spray pyrolysis, and fluidized bed drying. In these methods, solution droplets of precursor solutions are generated and subsequent drying of the solution droplets result in formation of particles. Different morphologies of particles are obtained based on the nature of the solute and solvent, their mutual solubility limit, the initial size of the droplet, the initial concentration, extent of supersaturation, drying gas temperature, solvent volatility, etc. To predict or understand these processes, it is important to understand the drying of a single solution droplet. Liquid solutions are atomized by various means to form droplets. Once the droplets are formed, they are introduced into a stream of dry gas. The evaporation and evolution of droplet/particles can be understood by following the temperature versus time and solvent content versus time plots shown in figure 5.1 (a) and 5.1 (b) respectively. Solvent evaporation takes place at the droplet surface. Initially, there is an unsteady steep increase or decrease in temperature (points A or A' to B). This is due to the fact that the net heat gained or lost by the drop depends on extent of solvent evaporation or sensible heat gained by the drop from surrounding air respectively. After this, the droplet temperature remains constant till it reaches point C.

During this period the evaporation rate is also constant and is called the constant rate period. This is depicted in figure 5.1 as the region between points B and C. The evaporation process also increases the concentration of the solute at the surface. When this concentration reaches a critical value a very thin layer of the solute is formed on the surface. This layer is either called a crust or skin depending on the nature of the layer formed. This layer can either be impermeable or permeable. Permeable shells usually form a solid crust due to crystallization and nucleation & growth whereas usually an impermeable shell results in direct precipitation and skin formation. Once a crust is formed, the droplet consists of an inner solution droplet core and an outer shell that is made up of the solute. The evaporation rate changes because of the resistance to mass transfer from the shell. The thickness of the crust increases due to further loss of solvent and when all the solvent is evaporated or, in case of water, when the particle reaches its equilibrium moisture content, the evaporation stops (point D). Once this condition is reached, the droplet (now referred to as a particle) just gains heat and then reaches the surrounding gas temperature (points E-F). The process can either result in a solid or hollow microparticle formation. Sometimes during hollow microparticle formation, there is a possibility of vapor of the gas being trapped inside the shell. If the shell is rigid enough, the gas cannot escape the shell and hence with increase in temperature, there is a pressure build-up inside the shell. This may cause rupturing or breaking up of the shell in some cases. In other cases, crippled, shriveled or donut shaped particles are formed when there is no vapor inside and the skin is soft enough for negative pressure drop inside the shell. The various morphologies that can result during the process of drying is shown in figure 5.2 below. Figure 5.2 shows the effect that evaporation rate and concentration of

the solute in the solution droplet has on the final morphology of the microparticles obtained. A rapid evaporation takes less time to form a skin and if the concentration is dilute enough then vapor may get trapped inside the particles. These particles collapse and form shriveled particles once the remaining solvent vapors evaporate. A thin skin is formed from such a process and the particles obtained are comparatively larger. The results obtained and discussed in section 4.1.1 further corroborate the effect of rapid evaporation and dilute concentrations on final particle morphologies.

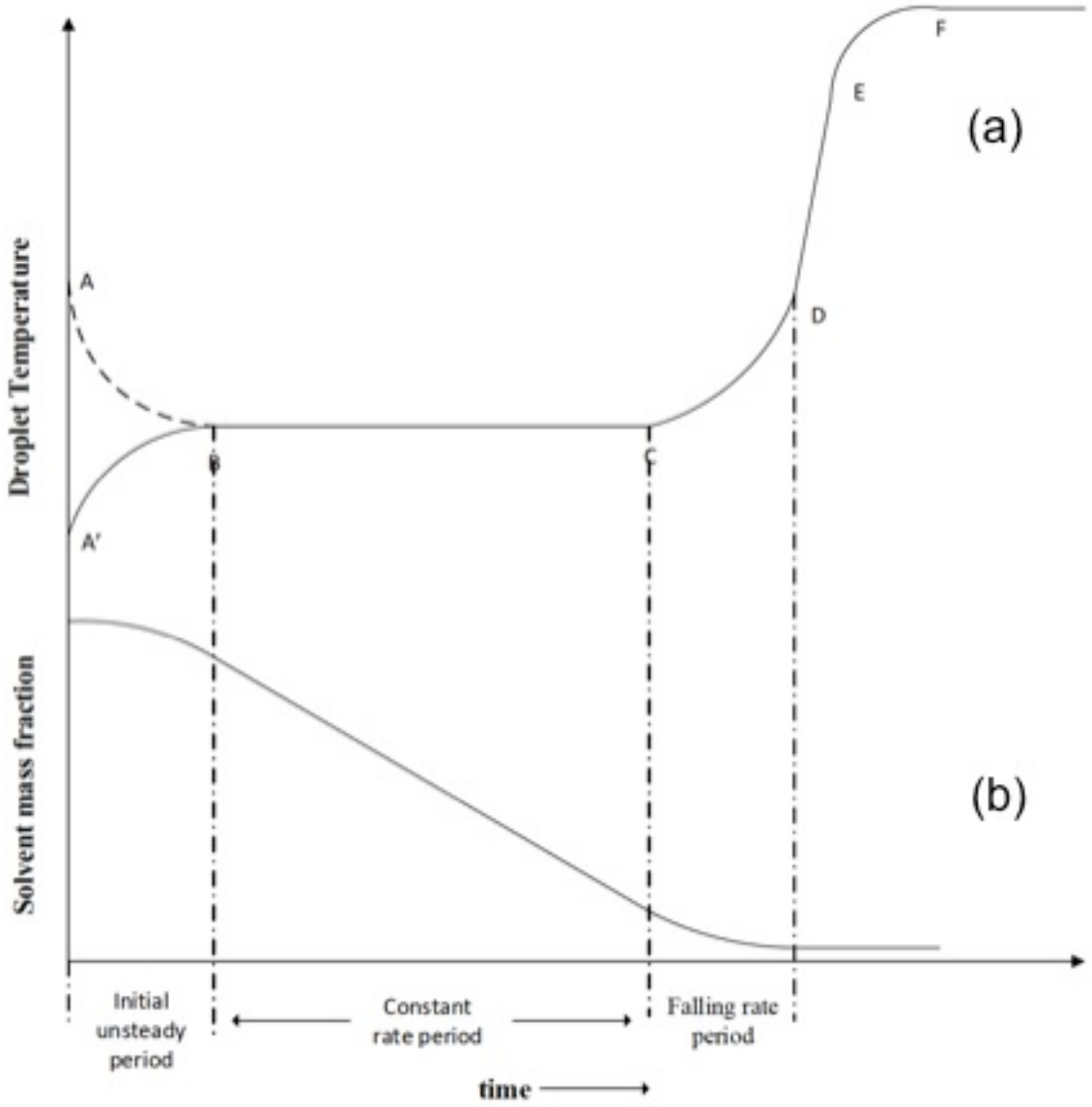

Figure 5.1: Different stages of evolution of (a) droplet temperature and (b) droplet solvent content as the drying proceeds

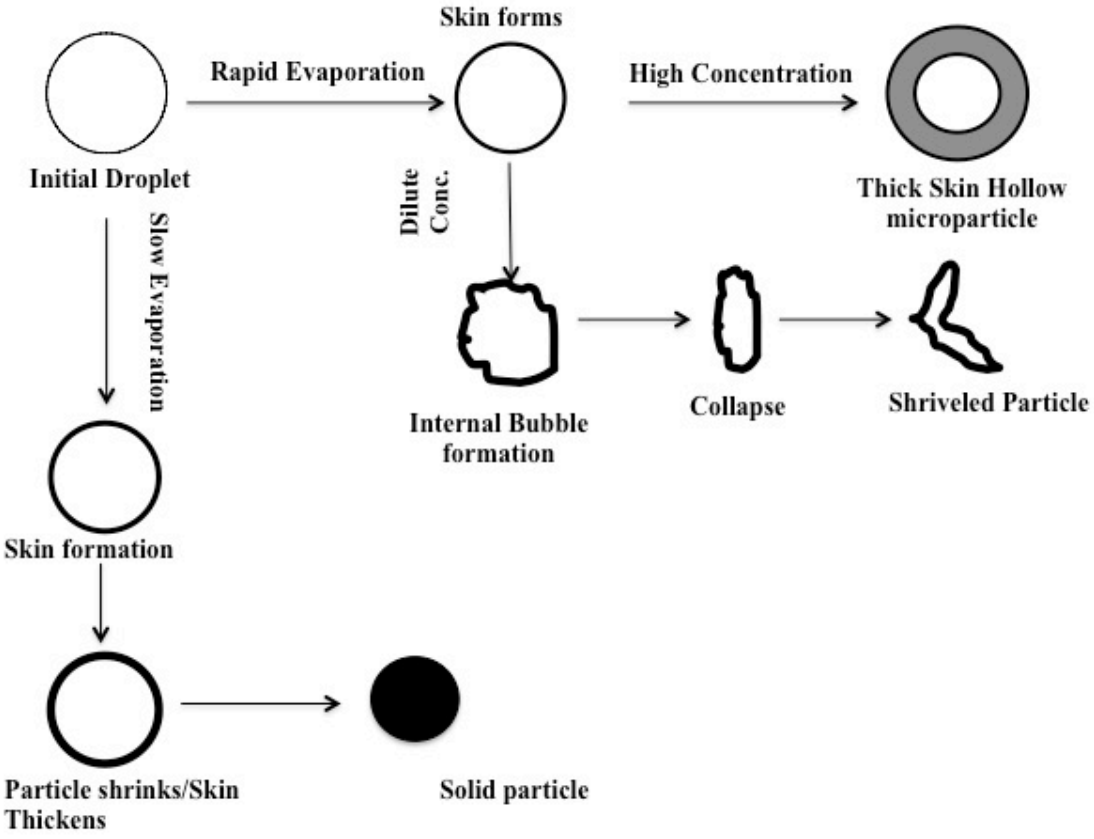

Figure 5.2: Effect of evaporation rate and solution concentrations on the evolution and final morphology of microparticles obtained

Numerous theoretical models have been developed to study different stages of droplet evaporation and drying. These can be broadly divided into either semi-empirical models, based on actual measurements of temperature and moisture content of the droplet, or, transport phenomena models, based on diffusion and evaporation inside the droplets, and models based on reactions engineering approach. These models can also be further classified based on whether the solute is dissolved in the solvent or if they are suspension/ colloids (slurry droplet) in the solvent medium. Chen and Li (2005**)** give a

brief classification where they classify the models as (i) transport phenomena approach, (ii) characteristic drying curve approach and (iii) reaction engineering approach.

Section 5.2 discusses the available literature in the subject relating to theoretical models developed and used to understand the physics of drying of binary microdroplets containing solids. The objective of the present work is stated in section 5.3.

Section 5.4 gives a detailed description of the model developed and used in the present work along with the solution methodology in section 5.5. Section 5.6 lists the various model parameters and their respective values used to solve and predict the variables in the present model. Section 5.7 presents the predicted results obtained by solving the model and discusses the effect of several key parameters such as initial polymer concentration, initial droplet size and ambient temperature on the time to skin formation and concentration profile inside the droplet at this time.

Section 5.8 concludes the chapter along with some future suggestions for the proposed model.

5.2 Previous models

One of the first theoretical considerations for evaporation and drying of droplets containing a non-volatile solute was given by Charlesworth and Marshall (Charlesworth and Marshall 1960). A simple diffusion model, as in the case of pure droplets was developed but the droplet size was assumed to be constant to avoid the moving boundary complication. Further assumption was made that the evaporation rate of the droplet was same as that of the pure water droplet of same size and using the d^2-law an expression for the constant rate drying of the droplet obtained. Using the equations developed, an analytical expression was obtained for the concentration profile inside the droplet with time. They also performed experimental investigations on droplets of aqueous ammonium sulfate, ammonium chloride, sodium chloride, potassium nitrate, lithium hypochlorite, sucrose, dispersion blue dye, fresh whole milk and polyvinyl acetate dispersion in water. One of the major limitations of the model was obviously the consideration of a constant size that can lead to erroneous predictions of the concentration profiles. Also, the temperature variation inside the droplet was not considered even though the initial size of the droplets was quite large to start with. Also, although, a time-dependent analytical expression was obtained, but the initial unsteady behavior of the drying droplets was not taken into account.

A simplified transport phenomena model was developed by Nesic and Vodnik (1991) for the drying of solution droplets. Their model assumed five stages of drying namely, initial heating and evaporation, quasi-equilibrium evaporation, crust formation and growth, boiling and porous particle drying. They assumed that the same laws govern all these five stages and hence a single set of equations can be used to predict the

behavior in each stage. A formulation for evaporation rate based on the resistance offered by both the gas boundary layer and the through the crust was assumed. A similar equation was developed for the energy balance and a diffusion equation was used to define the concentration profile of water inside the droplet. An expression for shell thickness was developed by conserving the solids inside the droplet. The diffusion coefficient in the shell was determined as a function of the local moisture concentration. Experimental studies were performed on droplets of sodium sulphate, colloidal silica and skimmed milk and the data agreed well with the model predictions. There were some minor discrepancies in the temperatures predicted though. They concluded from experiments that the sodium sulphate solution formed the most rigid crust and skimmed milk formed the most porous one. This reflected in their values of the crust diffusion coefficient.

Jayanthi et. al. (1993) developed unsteady state model of evaporation of water by spray pyrolysis. The model consisted of a diffusion equation representing the concentration profile inside the droplet and since the droplet temperature was assumed to be uniform, the temperature variation with time was given by the heat balance equation. They modeled the evaporation stage of a droplet, at different drying gas temperatures, till the on-set of precipitation of solids on the droplet surface. The concentration difference was used as a reference to understand the formation of either solid or hollow microparticles. To explain this, a model system of Zirconium hydroxychloride (ZHC) and water (experimentally studied by them for spray thermolysis) was used. The initial droplet temperature was kept constant at 50^0C for all the simulations. The effect of initial solute concentration (varied between 0.5 to 5.7 mol/L) and the drying gas temperatures (30^0C -150^0C) was shown and compared to their experimental results. They showed that

the equilibrium and critical supersaturation values of the solute was one of the major contributors towards a volume precipitation and solids formation. They concluded that high initial concentrations and low gas temperatures generally results in solid particles but there was some discrepancy at low initial solids concentrations when compared to their experimental results. They attributed this to the fact that the effect of temperature on the critical and equilibrium saturation was not taken into account in their model. Their model did predict the qualitative behavior of droplet evaporation when crystalline salts are taken into account but no simulations were performed for skin forming substances. Also, initial and final diameters were >1μm so Knudsen diffusion was not taken into account.

Farid (2003) proposed a mathematical model for drying of solution droplets based on a temperature profile inside the droplets. He showed that the Biot number does not decrease proportionately with the droplet size and that the temperature is not uniform. A single equation was given for the crust-wet core region for the temperature distribution. The model predicted the temperature distribution and compared well with the experiments of Nesic and Vodnik (1991) but during the second stage, the evaporation rate does not depend on the resistance offered by the crust, which should not be the case. Also, average properties of the solution inside the core and shell were used for calculations and also the void fraction of the crust was not taken into account in the droplet mass balance equation. This also might add to some discrepancy in the representing the physics of the solution.

Brenn et. al. (2001) used a one dimensional diffusion equation to represent the variation of mass fraction of the liquid component inside the droplet. It was assumed that

the temperature inside the droplet was uniform. The initial unsteady behavior of the droplet evaporation was neglected and it was assumed that the evaporation followed d^2-law. Also, non-dimensionless equations yielded a characteristic morphological parameter G that is inversely proportional to the Sherwood number. A threshold value for this parameter was obtained as 3.3. This value was reached by comparing various experimental observations from literature and from their own experiments from an acoustic levitator and a commercial spray dryer. They concluded that when G was less than the threshold value a hollow particle would form whereas a value greater than the threshold resulted in solid particles.

Brenn (2004) extended the above model in the other two dimensions as well for determining the concentration profile inside the droplet. The temperature of the droplet was assumed not to change with space inside the droplet. The model only accounted for the drying and evaporation of the droplet until the onset of precipitation. The droplet evaporation rate was assumed to follow the d^2-law and an analytical solution was formulated using the method of separation of variables. A model system of sodium chloride in water was used to simulate the model.

Sloth et. al. 2006 developed a diffusion model for predicting the concentration profile inside a drying droplet that forms dense, solid particles. The temperature inside the droplet was also modeled using he heat diffusion equation but with mass averaged values of the heat capacity and thermal conductivity. The change in Sherwood number was related to the changing radius of the drop. Two different compounds, maltodextrix DE15 and trehalose in water were taken as model systems for predicting the concentration and temperature inside the drying droplet. The same solution drops were

studied in an ultrasonic levitator to obtain experimental values of droplet size. The comparison between the experimental and model predicted values of size reduction corresponded well with the experimental data but the temperature and water content profiles were not compared to any experimental data. It was shown that the water mass fraction reached a value close to zero at the onset of skin formation. This suggests a formation of dry skin instead of a wet skin at the surface as shown in cases involving salts and other crystalline solids. Also, since the ambient temperatures taken are low, no predictive results were shown for high evaporation rates.

Recently, Eslamian et. al. (2006) have extended the model developed by Jayanthi et. al.(1993) for droplets smaller than 1μm in diameter to account for the Knudsen diffusion. The model was also corrected for droplet evaporation under reduced pressures. An expression for the evaporation rate of the droplet was derived from the kinetic theory to account for the Knudsen diffusion in very small sizes. The initial droplet sizes were 0.5, 0.05 and 5 μm under drying gas temperatures of 100, 200 and 300^0C. The model was used to show three zones of droplet drying, an initial rapid heat-up or cool down zone, a constant drying zone and a ramp-up zone due to increase in solute concentration. The experimental results compared well with the model and the values obtained were further regressed to obtain two semi-empirical correlations for final particle size and thickness of the crust formed respectively. They were shown to depend upon the temperature, pressure and initial solution concentration. It was also shown that the particle size and thickness are weak functions of pressure when the initial droplet size is in the range of 1 to 10 μm. They also found by their experimental investigations that the final particle size is slightly smaller than the model predicted. Thus, they further extended their model (Eslamian et.

al. 2009) to account for this discrepancy by introducing an “induction period” just after the onset of precipitation. An expression was given for the induction time based on the activation energy of the process. This was one of the limitations, as the values of activation energy must be calculated experimentally for each process. They assumed that during this period the droplet continued to shrink and the outer solid layer thickens. The solid layer is assumed to be a combination of the solution (solute+solvent inside the layer) and the solid itself. Once a rigid crust was formed, the shrinkage stopped and the constant diameter period was assumed during which the remaining solvent evaporated from the droplet. The shell thickens further as the remaining solute precipitates at its inner wall. Assuming that there is no void volume, they ended up getting a straightforward expression for the final thickness of the shell in terms of inside and outside diameter of the particle. An overall energy and material balance across the length of the reactor was coupled with the droplet evaporation model for predicting the temperature and size across the reactor length. Their experimental results generally agreed well with their predicted results except in the case of highly crystalline materials such as sodium chloride. Also, they did not mention how amorphous skin forming materials would behave during evaporation and shell formation.

Shabde et. al. (2006) have proposed a spray drying model to produce hollow polymer microparticles. They used a simple unsteady diffusion equation for concentration profile and temperature inside the droplet but they assumed that the droplet surface reaches the boiling point of the solvent. This might not be true in cases, as even at high drying gas temperatures, the surface temperature does not reach the boiling point. They used a gradient weighted finite element method to solve the system of equations.

Since there were no comparisons made with the experimental results, they studied the effect of changes in heat and mass transfer rates on the polymer concentration profiles inside the droplet and also predicted the time at which the crust/skin forms. Also, it was shown that the skin formation occurred when the surface concentration of the solute reached close to zero as discussed by several other researchers. They also showed that the time taken to skin formation increases when the ambient gas temperature increases.

An effective diffusion model was developed for skin forming substances such as maltodextrin DE5 (Werner et. al. 2008). The radius of the droplet does not cease at the onset of the skin formation but the droplet continues to shrink until a critical temperature differene ($T-T_g$) is reached, where T_g is the glass transition temperature of the substance. The model was developed to simulate and understand the formation of dense skin porous particles and collapsed particles.

Most of the experimental research in the area of spray drying has water as a solvent and the solute that crystallizes and follows the nucleation and growth principles. Next few paragraphs will review the models based on such assumptions.

Mezhericher et. al. (2007), in their model, introduced the concept of a wet particle in the second drying stage (i.e. after the onset of precipitation). They assumed that the liquid core is surrounded by a porous crust. They also assumed that the diameter of wet particle did not change once the crust is formed. Hence, the model was called a receding interface model. During this stage, they assumed that the temperature of the crust and the wet core are significantly different and hence defined separate energy balance equations for each. Knudsen diffusion was assumed to be negligible. Their model assumed that the crust is made up of cylindrical pores through which the solvent would escape and this

was related to the porosity of the crust formed. They further extended their model to breaking of particles during drying (Mezhericher et. al. 2009). Thermal and mechanical stresses inside and around the sphere was calculated. From this model, they concluded that mechanical stresses play an important role during initial formation of the crust but when the crust is fully formed, the thermal stresses are predominant and play a major role in the break-up of the particles. It was also found out that the total tangential stress on the crust of silica particle was about five times greater than the radial components. No experimental validation of the model was shown during their analysis. Also, the initial diameter of the silica colloidal particles was very large and to achieve faster drying, very high temperatures were assumed. This can largely affect the stress on the crust formed.

A new droplet drying framework was proposed by Seydel et. al. (2004) for the solids formation at spray drying. They assumed that a porous, permeable shell is formed at the surface of the droplet and this porous shell consists of many single particles. The evaporation rate was modeled based on the resistance offered by both the gas phase and the shell, similar to Nesic and Vodnik. A population balance approach was used to model the concentration and temperature profiles inside the droplet. An extra term for the phase transformation of the solution to small particles was introduced in the equations. Extra equations for the population growth of solid particles and the porosity of the shell were developed. They studied the results based on the particle number density. No concentration or temperature profiles were reported. Their discussions on formation of solid or hollow particles were purely based on the small particles' formation in the shell.

A more detailed description of the above model was given in Seydel et. al. (2006). Sodium chloride solution was assumed to be the model system for studying the simulated

results. Even though a permeable shell was assumed, it was shown that the outer droplet radius was constant once the precipitation and crystallization started. The temperature predictions agreed well with the usual drying temperature curves. Since the model is based on population balances, the skin formation of shells cannot be explained using this model.

Handscomb and Kraft (2010) used a similar population balance approach similar to that of Seydel et. al. They modeled the droplet evaporation as consisting of a continuous phase and a discrete solids phase. Once the surface shell was formed, the model was divided into different sub-model cases namely, thickening shell model, dry-shell sub-model, wet-shell sub-model and slow boiling sub-model. Usage of the appropriate sub-model was determined by calculating the pressure drop across the surface of the droplet at the onset of precipitation. The strength of the surface was determined by calculating the buckling pressure. The results of the model were compared to experimental results obtained by Nesic and Vodnik for drying of colloidal silica droplets until the onset of precipitation. They concluded that the size of the suspended colloidal particles influences the drying modes and hence the final morphology of the dried solids. Colloidal particles with sizes >1μm bypass the wet shell regime and form solid particles wheres particles with sizes in the range 50-1000 nm go through the wet drying stage and form hollow particles.

Some researchers used artificial introduction of bubbles inside the spray droplets (aeration) to obtain foam-like particles and to enhance drying rate without the loss of solvents. Drying of these particles was modeled using an assumption of bubbles inside the droplets. Few of the models are discussed here. Frey and King (1986) developed the model for formation of foam particles. The model was developed for constant rate drying period and assumed that the foamed droplet contains very small internal bubbles. They concluded that the drying rates did increase due to the introduction of the bubles inside the droplets. Hecht and King (2000) developed two models for predicting the particle morphology and retention of the volatile component, in their case, water. The first model is a set of simple ordinary differential equations for predicting the droplet temperature and evaporation rate. The rate of change of temperature was not taken into account. An expression is obtained for change in temperature versus rate of change of solvent with time. This was compared to the experimental data and a correction factor for heat transfer is introduced. The second model assumed a bubble inside the droplet that changes its size depending on the temperature and water activity. Taking a ternary system of SF_6/sucrose/water, they tried to show the effect of selective diffusivity on the evaporation rate and stated that if the liquid inside the drops is well mixed without the bursting of the bubbles then the drying rate can be enhanced substantially without additional loss of the volatile component.

5.3 Objective

All the theoretical models discussed above are primarily based on the definition of transport equations inside and outside an evaporating droplet. Even though these models closely resemble the process at hand but their formulations are highly complex and result in computational difficulties more so after the formation of the crust/skin.

The major limitations of these models are two fold. The first limitation comes from the fact that most of the models are validated against experimental results involving aqueous solution droplets. Most of the aqueous solution droplets have a certain characteristic critical saturation concentration at which the precipitation begins. But, in case of polymers and other skin forming materials, this is not always true. Secondly, the evaporation rates associated with all the above models are either slow or temperature dependent. Invariably, the temperature at the surface of the droplet is raised to the solvent boiling temperatures and once this temperature is reached it is assumed that the temperature remains constant till the onset of skin formation. In case of low glass transition polymers, high temperatures degradation of the polymers may occur. Also, the rate of evaporation is very high in case of high volatile solvents and hence the surface temperature never reaches the boiling point of the solvent. Instead there is an initial cool down zone. This has not been dealt with in the above models. Also, at such high evaporation rates there is an inherent convection inside the droplet that needs to be considered which is not dealt with in most of the previous models discussed.

In the present work, a solution droplet evaporation model for rapid drying of a skin forming polymer solution (in a highly volatile solvent such as THF) is developed with and without convection. The model was compared with the size obtained using

experimental results obtained in chapter 4. Also, the onset of skin formation is discussed qualitatively by showing how the variation in the operating parameters such as ambient temperature, initial solute concentration and initial droplet size affect the formation of the skin.

5.4 Model Description

Consider a droplet of initial radius a_0 containing a dissolved solute (B) in a highly volatile solvent (A). The droplet is evaporating in a gas (air) phase (C). The gas phase is assumed to be very large when compared to the size of the droplet and the amount of solvent vapor in the gas phase is negligible. Following assumptions were made during the formulation of the model:

(i) the droplet size is small enough that the temperature inside the droplet is uniform and is only a function of time.

(ii) the droplet is spherically symmetric at all times. In most cases this assumption is valid throughout the lifetime of the droplet. In some cases where the resulting density of the particle is very low, the particle loses its sphericity depending on the nature of the skin formed.

(iii) Kelvin effect on the equilibrium vapor pressure is negligible as the initial and final droplet sizes are greater than 1μm.

(iv) Ideal solution behavior is assumed with no change in volume.

(v) We also assume that the diffusivity of the solvent in the polymer is independent of the temperature and composition of the polymer.

With the above assumptions, the following partial differential equations that govern the evaporation of solvent from the solution droplet is presented as follows.

Species balance of solvent,

$$\frac{\partial \rho_A}{\partial t} = \frac{1}{r^2}\frac{\partial}{\partial r}\left(r^2 \rho D_{AB}\frac{\partial w_A}{\partial r}\right) - \frac{1}{r^2}\frac{\partial}{\partial r}(r^2 v_r \rho_A) \tag{5.1}$$

where, ρ_A is the mass concentration of the solute in the droplet, D_{AB} is the solute-solvent binary diffusion co-efficient that is assumed to be independent of concentration of the solute, v_r is the convective velocity inside the solution droplet and w_A is the mass fraction of the solute inside the droplet.

Since the density of the solution is also changing with time due to the convection inside the droplet, the overall continuity equation is given by,

$$\frac{\partial \rho}{\partial t} = -\frac{1}{r^2}\frac{\partial}{\partial r}(r^2 \rho v_r) \tag{5.2}$$

The boundary and initial condition pertaining to the above system of partial differential equations are presented below.

At the center of the droplet, there is no accumulation and hence the total flux is equal to zero, i.e., at r = 0,

$$\rho D_{AB}\frac{\partial w_A}{\partial r} - \rho_A v_r = 0 \tag{5.3}$$

At the surface, r=a(t),

$$\rho_A \frac{da}{dt} + \rho D_{AB}\frac{\partial w_A}{\partial r} - \rho_A v_r = \frac{dm}{dt} \tag{5.4}$$

$$\rho \frac{da}{dt} - \rho v_r = \frac{1}{4\pi a^2}\frac{dm}{dt} \tag{5.5}$$

The initial conditions for the above formulation are

At t = 0,

$$a(0) = a_0$$

$$w_B(r,0) = w_{B0} \tag{5.6}$$

$$\rho(r,0) = \rho_0$$

where, a_0, w_{B0} and ρ_0 are the initial radius of the droplet, initial mass fraction of the solute and the initial density of the solution.

The evaporation rate (change in mass of the droplet) and the change in temperature of the droplet can be obtained by a mass and energy balance at the droplet-air interface. Change in mass of the droplet is due to the evaporation of the solvent from the droplet surface due to convection. It is given by,

$$\frac{dm}{dt} = -2\pi a N_{sh} D_{AC} M_A (C_{As} - C_{A\infty}) \tag{5.7}$$

where $C_{A\infty}$ is the concentration of the solvent far away from the droplet. It depends on the solvent concentration in the gas phase. C_{As} is the surface concentration of the solvent which is given by the vapor pressure of the solvent at the interface.

$$C_{As} = \frac{P^{sat}(T_d)}{RT_d} \tag{5.8}$$

where R is the universal gas constant and T_d is the droplet temperature. The presence of solute lowers the vapor pressure of the solvent and in case of polymer solutions Raoults

law is not applicable. According to Flory-Huggins theory, the lowering of vapor pressure of the solvent in a polymer-solvent solution is given by equation 3.9.

$$P(T_d) = P^{sat}(T_d) \exp[\ln(\varphi) + (1-\varphi) + \chi(1-\varphi)^2] \tag{5.9}$$

where, φ is the volume fraction of the solvent and χ is the polymer-solvent interaction parameter. It should be noted here that the interaction parameter is assumed to be a constant in the present study as THF is a very good solvent for polystyrene. For poor solvents, the interaction parameter is a function of polymer concentration. In the present work, a value of $\chi = 0.41$ is chosen from the work of Emerson et. al. (2013).

When the droplet evaporates, loss of solvent results in a loss of latent heat due to which the droplet temperature reduces. At the same time the droplet gains temperature from the surrounding gas temperature. Thus, the energy balance is given by,

$$mC_{pL}\frac{dT_d}{dt} = 2\pi a k_g N_{Nu}(T_\infty - T_d) - \Delta H_{vap}\frac{dm}{dt} \tag{5.10}$$

where C_{pL} is the specific heat capacity of the solution, k_g is the thermal conductivity of the gas phase and ΔH_{vap} is the heat of vaporization of the droplet.

Equations (5.1-5.10), cannot be solved as such because of the extra variable v_r. We know that ρ_A and ρ_B are functions of w_A and using this equation (5.1) and (5.2) can be re-written as

$$\frac{d\rho_A}{dw_A}\frac{\partial w_A}{\partial t} = \frac{1}{r^2}\frac{\partial}{\partial r}\left(r^2\rho D_{AB}\frac{\partial w_A}{\partial r}\right) - \frac{1}{r^2}\frac{\partial}{\partial r}(r^2 v_r \rho_A)$$

$$\frac{d\rho}{dw_A}\frac{\partial w_A}{\partial t} = -\frac{\rho}{r^2}\frac{\partial}{\partial r}(r^2 v_r) - v_r\frac{d\rho}{dw_A}\frac{\partial w_A}{\partial r}$$

Now using the relation, $w_A = \frac{\rho_A}{\rho}$, we get,

$$\rho\frac{d\rho_A}{dw_A} - \rho_A\frac{d\rho}{dw_A} = \rho^2$$

Using this equation and equating the above equations we get,

$$\frac{\partial}{\partial r}(r^2 v_r) = -\frac{1}{\rho^2}\frac{d\rho}{dw_A}\frac{\partial}{\partial r}\left(r^2\rho D_{AB}\frac{\partial w_A}{\partial r}\right)$$

Now to solve the obtained velocity expression, an expression for the overall density of the droplet is required. If an ideal mixing is assumed then one can write the overall density, ρ, in terms of the pure component densities and the mass fraction of A, i.e.

$$\rho = \frac{\overline{\rho_B}}{1 - (1 - \overline{\rho_B}/\overline{\rho_A})w_A}$$

where $\overline{\rho_B}$ and $\overline{\rho_A}$ are pure component densities of solute and solvent respectively.

This expression is used to obtain $\frac{d\rho}{dw_A}$ and then substituting in equation (), we get,

$$r^2 v_r = -r^2\frac{D_{AB}}{\rho}\frac{\partial w_A}{\partial r} + f(t)$$

where $f(t)$is a function of integration. At the center of the droplet, the velocity and density have finite values and therefore, $f(t)$ must be equal to zero. Therefore,

$$v_r = -\frac{D_{AB}}{\rho}\frac{\partial w_A}{\partial r} \qquad (5.11)$$

This is the required expression for velocity in terms of the mass fraction. Substituting this expression in equation (5.2) we get,

$$\frac{\partial \rho}{\partial t} = \frac{D_{AB}}{r^2}\frac{\partial}{\partial r}\left(r^2 \frac{\partial \rho}{\partial r}\right) \tag{5.12}$$

Equation (5.12) describes the variation of density of the solution droplet with time and radius. To solve the above partial differential equation a new set of boundary conditions is required. Using the relationship $\frac{d\rho}{dw_A}$ obtained above in equation (5.3) we get,

at r = 0,

$$\frac{\partial \rho}{\partial r} = 0 \tag{5.13}$$

To obtain an expression for boundary condition at surface, multiplying both sides of equation (5.12) by $4\pi r^2$and integrating w.r.t. r, we get,

$$\int_0^{a(t)} \frac{\partial \rho}{\partial t} 4\pi r^2 dr = \left(4\pi r^2 D_{AB} \frac{\partial \rho}{\partial r}\right)_{r=a} \tag{5.14}$$

Also, applying Leibnitz rule to LHS of equation (5.14) and keeping in mind the fact that the rate of change of droplet mass is only equal to the rate of change of mass of the solvent,

$$\frac{dm}{dt} = \frac{dm_A}{dt} = \int_0^{a(t)} \frac{\partial \rho}{\partial t} 4\pi r^2 dr = \frac{\partial}{\partial t}\int_0^{a(t)} \rho 4\pi r^2 dr - \rho 4\pi r^2 \frac{da}{dt} \tag{5.15}$$

Also,

$$\Delta m = m_0 - m = \frac{4}{3}\pi a_0^3 \rho_0 - \frac{4}{3}\pi a^3 \rho$$

$$\Delta V = \frac{\Delta m}{\overline{\rho_A}} = \frac{4}{3}\pi a_0^3 - \frac{4}{3}\pi a^3$$

$$m = \frac{4}{3}\pi a_0^3 \rho_0 - \frac{4}{3}\pi a_0^3 \overline{\rho_A} + \frac{4}{3}\pi a^3 \overline{\rho_A}$$

$$\frac{dm_A}{dt} = 4\pi a^2 \overline{\rho_A} \frac{da}{dt}$$

Substituting this in equation (5.15) and using equation (5.14), we get the boundary condition

$$D_{AB} \frac{\partial \rho}{\partial r} = (\overline{\rho_A} - \rho) \frac{da}{dt} \tag{5.16}$$

Equation (5.12) along with the initial and boundary conditions given by equations (5.13) and (5.16), along with equations that defines the rate of change of size and temperature with time (equations 5.7 and 5.10 respectively) describe the system under consideration. The system of equations in its present form has a moving boundary at *r = a(t)*. The equations can be transformed to fix the boundary using the following dimensionless variables,

$$Y = \frac{r}{a_0} \frac{(\rho - \overline{\rho_A})}{\overline{\rho_A}}, \qquad \bar{T} = \frac{(T_d - T_\infty)}{T_\infty}$$

$$z = \frac{r}{a(t)}, \qquad \tau = \frac{D_{AB} t}{a_0^2}, \qquad A = \frac{a}{a_0}$$

Using these variables, equations (5.12) is transformed as,

$$\frac{\partial Y}{\partial \tau} = \frac{1}{A^2} \left[\frac{\partial^2 Y}{\partial z^2} + zA \frac{dA}{dt} \frac{\partial Y}{\partial z} \right] \tag{5.17}$$

along with the dimensionless initial and boundary conditions,

$$Y(z, 0) = \left(\frac{\rho_0 - \overline{\rho_A}}{\overline{\rho_A}} \right) z$$

$$Y(0, \tau) = 0 \tag{5.18}$$

$$\frac{\partial Y}{\partial z} = Y(1, \tau)(1 - A \frac{dA}{dt})$$

and equations (5.7) and (5.10) are transformed as

$$A\frac{dA}{d\tau} = -\frac{N_{Sh}D_{AC}M_A P_A^0(T_\infty)}{2D_{AB}\rho_0 RT_\infty}\left\{\frac{\gamma_{As}x_{As}}{(1+\bar{T}}\exp\left[\frac{\Delta H_{vap}}{RT_\infty}\left(\frac{\bar{T}}{1+\bar{T}}\right)\right] - S_{Ag}\right\} \quad (5.19)$$

where $S_{Ag} = P_A^\infty / P_A^0(T_\infty)$

$$\alpha\left(\frac{\rho_0 - \overline{\rho_A}}{\overline{\rho_A}A} + A^2\right)\frac{d\bar{T}}{d\tau} = A\frac{dA}{d\tau} - \beta\bar{T} \quad (5.20)$$

where $\alpha = \frac{C_P T_\infty}{3\Delta H_{vap}}$ and $\beta = \frac{k_g N_{Nu} T_\infty}{2\rho_0 \Delta H_{vap} D_{AB}}$

5.5 Solution Methodology

The coupled system of partial differential equations (pde's) and ordinary differential equations (ode's) is numerically solved using finite difference method of lines. Here, the space derivatives in the pde's are replaced by approximate algebraic expressions, i.e. finite differences. The spacial derivatives are now implicit and are independent of the spacial variable. This turns the pde's into a system of ode's that approximate the original pde's with only one independent variable, time. Hence, the resulting systems of equations are a system of initial value ode problems. Careful approximation of the ode's is necessary to approach the solution of the problem.

Discretization

This step involves dividing the spacial domain into very small grids of size, nz. It follows that the number of grid points including the boundaries 0 and 1 will be equal to nz+1. Now, a central difference formula is used for discretization of the first and second derivative of Y w.r.t. z given by,

$$\frac{\partial^2 Y}{\partial z^2} = \frac{Y_{j-1} - 2Y_j + Y_{j+1}}{(\Delta z)^2}$$

$$\frac{\partial Y}{\partial z} = \frac{Y_{j+1} - Y_{j-1}}{2\Delta z}$$

Using the above difference formulas in equation (3.17) yields,

$$\frac{dY_i}{d\tau} = \frac{1}{A_i^2}\left(\frac{Y_{j-1}-2Y_j+Y_{j+1}}{(\Delta z)^2} + z_i A_i \frac{dA}{d\tau}\left(\frac{Y_{j+1}-Y_{j-1}}{2\Delta z}\right)\right) \tag{5.21}$$

where, i is the index representing the time and j is the spacial index designated to a particular grid point. Equation (5.21) represents a system of nz+1 equations with nz+1 variables that represent the values of Y at each grid point. It should be noted here that when j=1, Y1=0, therefore, we need to solve the system of equations from j=2 to nz+1 only. Also, using the boundary condition at z=1 (nz+1 grid point), we get the value of an arbitrary Y_{nz+2} and substitute it back in equation (5.21) at j=nz+1.Equation (5.21) along with equations (5.19) and (5.20) was then integrated using the stiff integration ode function ode15s in Matlab to solve for the concentration profile, temperature and size with time. Number of grids were chosen to be about nz = 121 for predicting the concentration profiles. A time step of $1e^{-4}$ s was chosen to integrate the ode's.

5.6 Model Parameters

The model description in section 5.4 contains many physical and chemical parameters. For effective prediction of the droplet drying kinetics, appropriate definitions and relations has to be given. Most of the parameters are dependent on either temperature or composition of the droplet or both. The properties of THF and PS and the gas phase properties are iterated in Table 5.1 below. It should be noted here that the diffusion co-efficient of the polymer in solvent is actually a strong function of composition but due to lack of experimental values in the literature for our system and the fact that dilute polymer concentration is used, the value is assumed constant. Under stagnant gas conditions, the Sherwood and Nusselt number values are equal to 2, however, when the droplet is falling, the evaporation rate is significantly enhanced and the Sherwood number is calculated from the correlation given by equation 5.22 below.

$$Sh = 2 + 0.6Re^{1/2}Sc^{1/3} \tag{5.22}$$

where *Re* and *Sc* are the Reynolds and Schmidt number respectively.

Devarakonda and Ray (2003) have discussed the effect of inter particle interactions when droplets are generated using a vibrating orifice aerosol generator and also gave a formula for an effectiveness factor that is based on the inter-particle distance and droplet diameter. In the present model, this could not be incorporated as the experimental values of inter-particle distance for the system under consideration was not available.

Table 5-1:Properties of solvent, solute and air used for predicting the evaporation of binary solution droplets

Density of pure solvent (THF), $\overline{\rho_A}$ (kg/m^3)	889.2
Density of polystyrene (PS), $\overline{\rho_B}$ (kg/m^3)	1050
Mol. wt. of THF, M_a (kg/mol)	0.0721
Initial mass fraction of THF, w_{A0}	0.98, 0.93 or 0.88
Initial droplet temperature, T_{d0} (K)	298
Diffusion coefficient of PS-THF, D_{AB} (m^2/s)	5.6e^{-10}
Diffusion coefficient of Air-THF, D_{AC} (m^2/s)	0.0936e^{-4}
Heat of vaporization, ΔH_{vap} (J/kg)	443000
Vapor pressure of THF at 313 K (mm Hg)	350
Specific heat capacity of THF, C_{pL} (J/kg-K)	1970
Thermal conductivity of air, k_g (W/m-K)	0.0271

5.7 Results and Discussion

The mathematical model predicts the concentration profile inside the droplet at any time, *t*. Two model systems are chosen to show the effect of solvent on the convection of the evaporating solution droplet. First, a very high evaporating solvent (THF) and solute (polystyrene) in solution is chosen as the model system. The values of the parameters used in simulating the above mathematical model were close to the experimental conditions used for preparing polymer microparticles. Effect of initial droplet size, initial solute concentration and gas phase temperature along with the effect of convection has been studied. The model predicts the change in temperature with time along with the radius of the droplet.

5.7.1 Model Validation

The model was validated by comparing the results of Jayanthi et. al. (1993) for an inorganic aqueous solution. In their model, an aqueous evaporating droplet is considered with no convection present inside the droplets. The equilibrium saturation (solubility limit) and critical supersaturation (concentration at which the solute crystallizes) is well defined for inorganic solutes in water. The model developed in this work predicts the evaporation of an aqueous solution microdroplet even when convection is taken into account and compares very closely to result obtained by Jayanthi et. al. Figure (5.3) shows the plot of concentration profile inside the droplet at two different time instances. Crust forms at the surface of the droplet at about 0.05s when the surface concentration reaches the critical supersaturation of the solute. The concentration profiles obtained are not steep enough as in the case of rapid evaporating droplets. The difference in concentration between the center and the surface of the droplet at the onset of

precipitation is about 0.12. Even at such small time scales, the concentration difference is not steep and hence volume precipitation prevails in such conditions and a solid particle is formed at the end of the drying process.

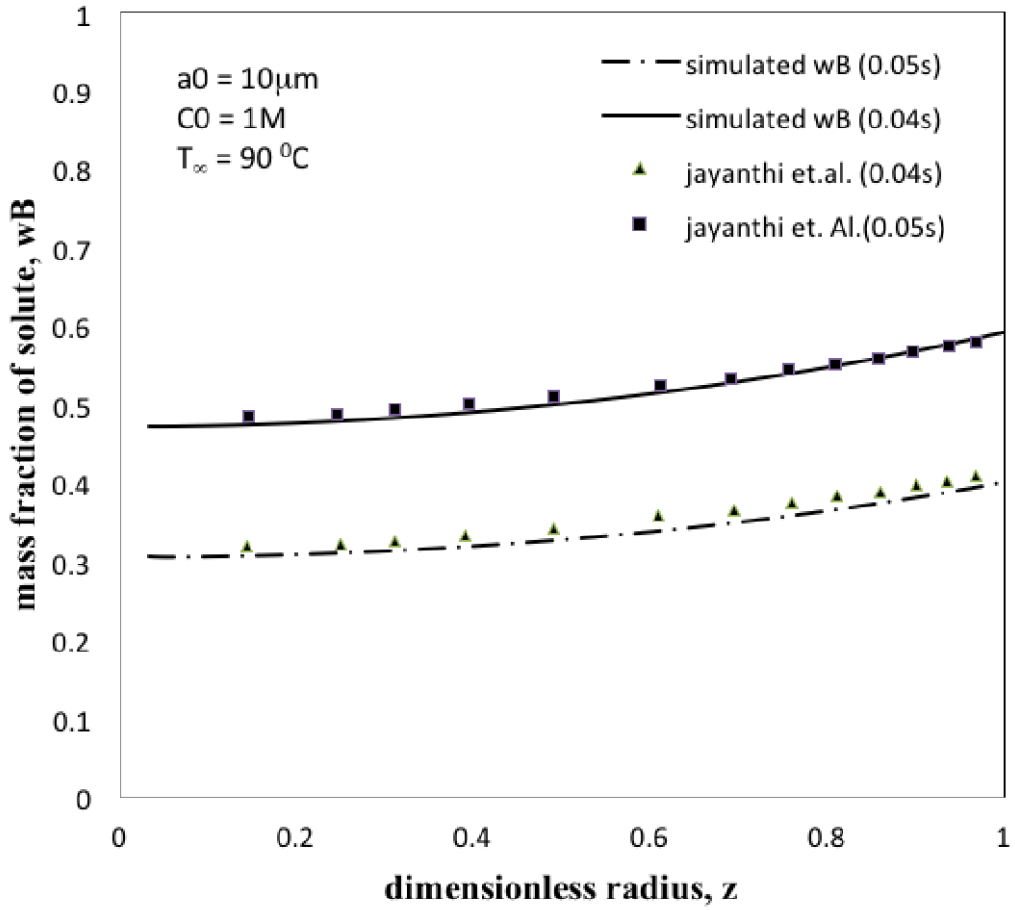

Figure 5.3: Comparison of predicted concentration profile with the data obtained by Jayanthi et.al. at different time instances for a 10 μm droplet. 0.05s denote the time at which the skin/crust forms at the surface of the drop.

5.7.2 Model Results

When a binary solution droplet evaporates rapidly such as in the case of very dilute (2 wt%) PS-THF solution, the surface/size of the droplet recedes rapidly due to the high vapor pressure of the solvent. This in turn gives rise to convection inside the droplet and hence the concentration profile is steeper than the case when no convection is assumed while modeling the system under consideration. The concentration values predicted are much lower than that predicted when no convection is assumed. A typical plot of change in temperature with time for an evaporating droplet of PS-THF solution is shown in Figure 5.4.

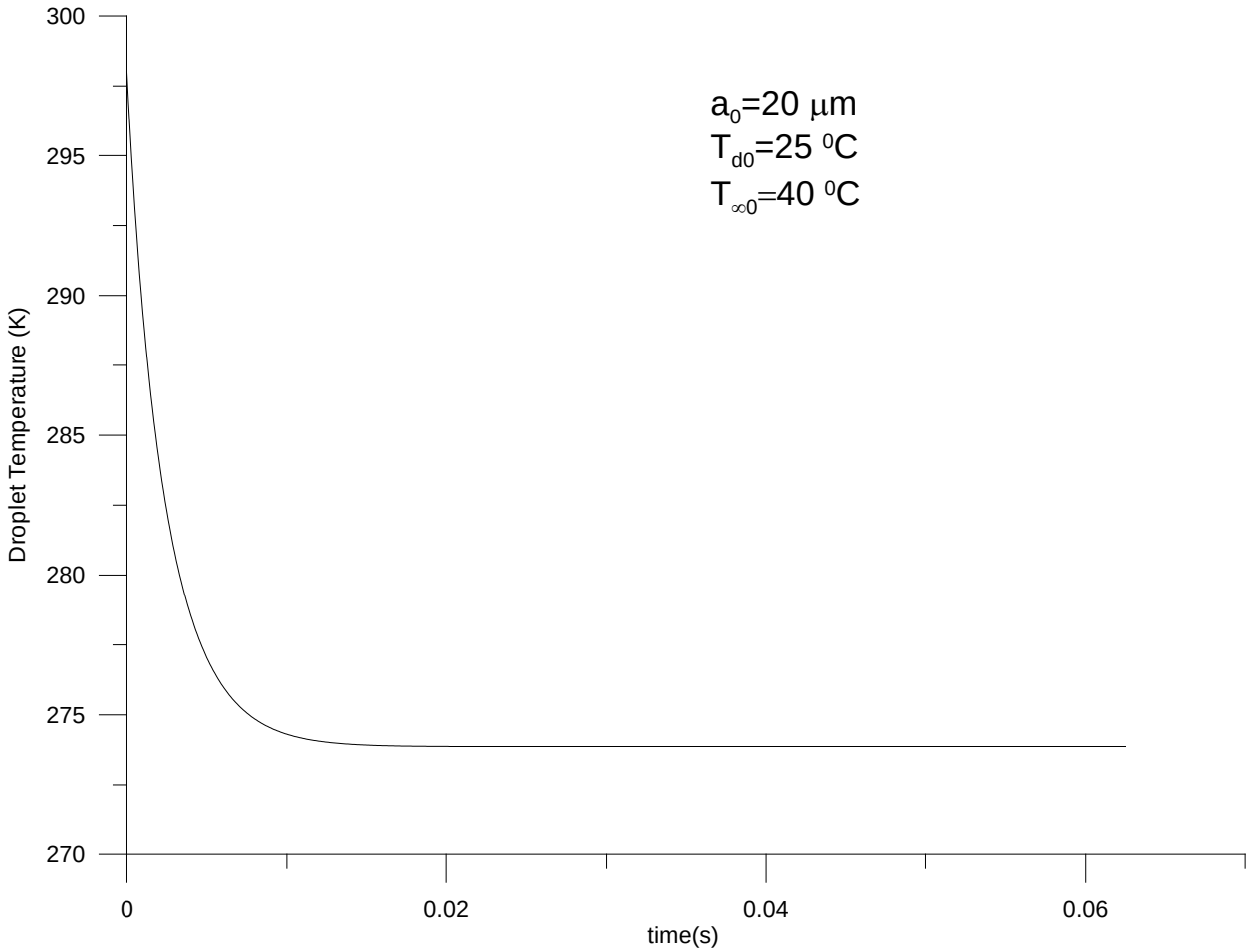

Figure 5.4: A typical plot of evolution of droplet temperature

The droplet temperature decreases from the initial temperature to a steady state value of about 273.86 K. The net droplet temperature decreases as a result of expense of the latent heat to the surrounding gas due to evaporation. Once the steady state is reached, even though the size of the droplet reduces the square of the radius of the droplet remains constant during the constant drying period. This can be shown from the plot of square of radius with time in figure 5.5.

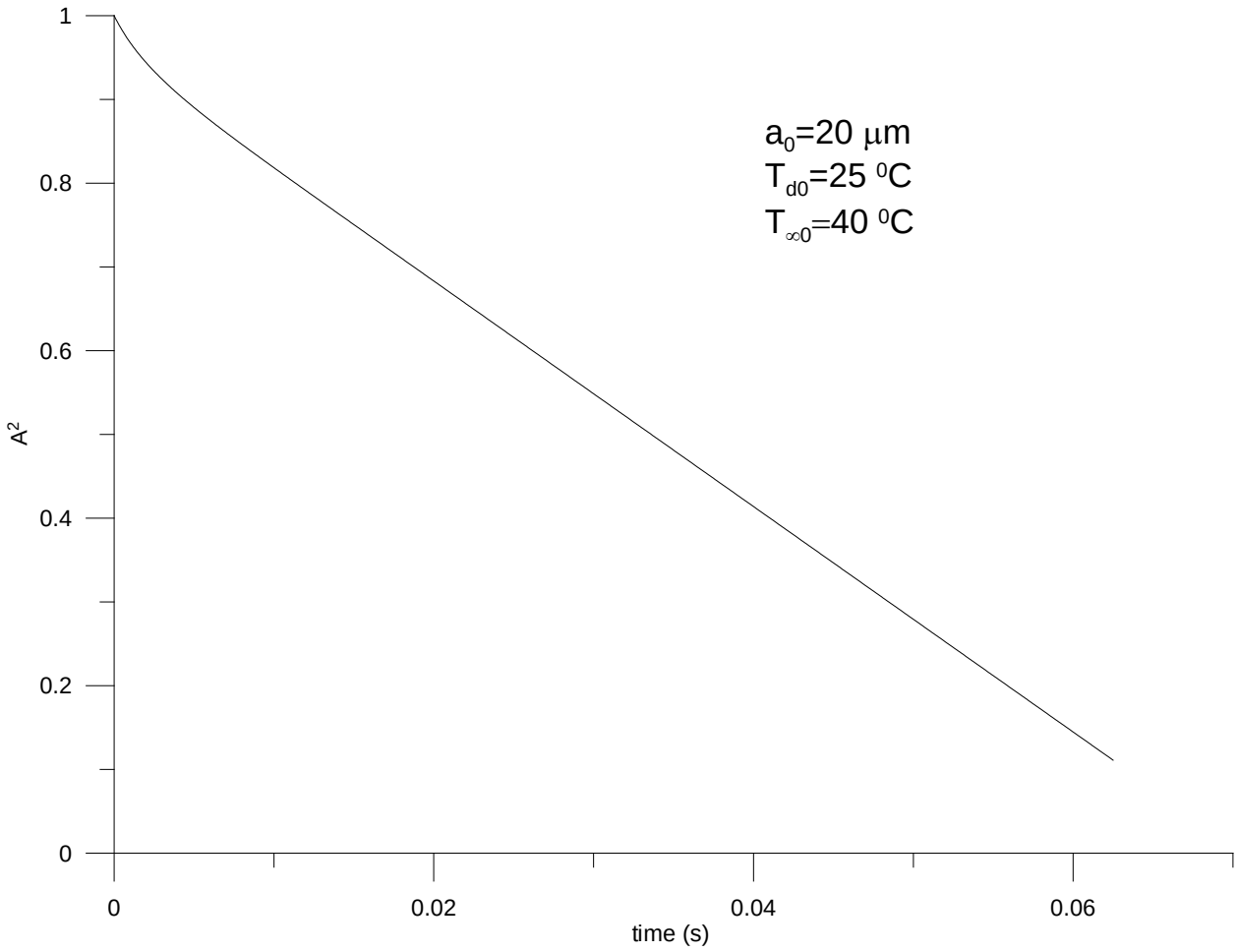

Figure 5.5: A typical plot of square of the radius with time obtained from model

Due to the unsteady evaporation of the droplet there is an initial steep decrease in the rate but after about 2.5ms the evaporation of the droplet reaches a steady state. The quasi steady-state evaporation of the droplet which when compared to the d^2-law yields the value of the evaporation rate constant. The solute concentration profile inside the droplet plays a major role in determining the morphology of the particles obtained. The concentration profile inside the droplet is shown in figure 5.6 below. Initially it is assumed that the solution is well mixed, i.e. the concentration of the solute is uniform inside the droplet (w_B=0.02). Once the evaporation starts, the surface concentration increases rapidly but the concentration near the center of the droplet remains at a much lower temperature. It is this difference that plays a major role in determining the morphology of the particles. At about 63 ms, the concentration of the solute at the surface reaches close to unity, which results in the formation of a very thin skin of the polymer. Also, the final particle size obtained from the vibrating orifice aerosol generator for a polymer blend microparticle was similar to the droplet size obtained at the onset of precipitation, i.e. when the concentration reaches 1. The value of the particle diameters predicted from the model is about 14μm and that from the VOAG is about 15 μm. From this we can conclude that the skin formed from dilute polymer solution results in a soft impermeable shell of polymer that undergoes no/very little size reduction.

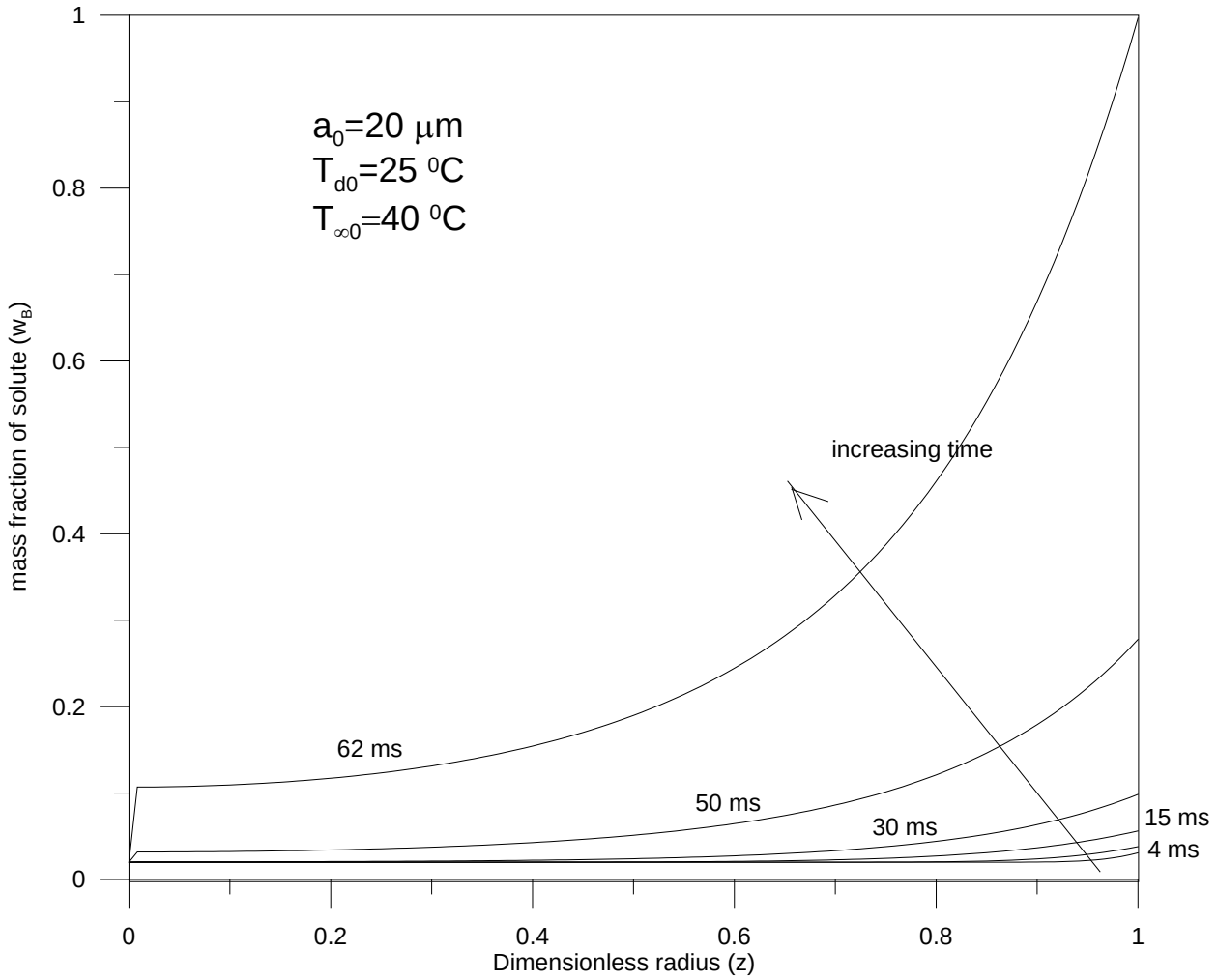

Figure 5.6: Plot of mass fraction of polymer vs size at different time instances showing the steep concentration gradient near the surface

Once the skin is formed, the temperature of the droplet starts to climb due to the increase in the heat of precipitation. Due to the large difference in the solute concentration at center and at the surface, a hollow particle is formed. Depending on the nature of the surface of the thin film formed and the wettability of the solvent and the polymer, the size of the polymer either becomes a constant and all the remaining solvent evaporates or the size reduces with simultaneous evaporation. Another important observation from the

values predicted is that the density of the solution at the surface of skin formation is about the same as that of the polymer. If we follow that there is no size change after the formation of the skin, then, once all the solvent evaporates, the final density of the particle as a whole is given by ratio of mass of the particle to its volume. Since, the mass of the polymer is equal to the mass of the particle (polymer does not leave the drop) and the volume of the particle can be calculated from the size, we get an overall particle density of approximately 400 kg/m^3. This is very much lower than the actual polymer density (1050kg/m^3). Hence this shows that low particle densities are achieved when very dilute polymer solutions are rapidly evaporated using droplet evaporation. One can control the properties of the polymer particles obtained by tuning the initial parameters, for various applications, such as aerosol delivery of drugs, by controlling the density of the prepared polymer microparticles. Several researchers have produced low-density pharmaceutical particles with similar density values. For example, Lucas et. al. (1999) have produced spray dried leucine particles with a density of 400 kg/m^3. They used a lower initial concentration of about 1wt%. In the next sections we will study the effect of initial solute concentration, initial size and gas phase temperature on initial skin formation.

5.7.3 Effect of droplet conditions and ambient temperature

The initial conditions of the droplet such as size, concentration of the solute and the operating ambient temperature affect the final particle size or the rate at which the skin forms at the droplet surface. The initial droplet size affects the surface to volume ratio of the droplet and hence the evaporation rate. The coming sections will discuss the variations of these initial and operating conditions on the final particle size obtained and also on the concentration profile inside the droplet at the onset of skin formation.

5.7.3.1 Effect of initial droplet radius

The effect of initial droplet size was studied by varying the initial droplet size from 20 μm to 10 μm. It can be clearly seen from the evaporation rate plot in Figure 5.7 that the time required for the surface concentration to reach close to unity reduces by approximately 4 times. This is due to the fact that the surface area per unit volume is about 4 times as that of a 20μm drop. In other words, if a smaller drop of polymer solution is used then the skin forms much quicker (about 16ms). When dealing with polymer blend solutions this can be highly advantageous as the diffusion process of phase separation is much slower that these time scales. The final particle size obtained from a 10 μm droplet was about half when compared to the initial droplet radius of 20 μm. This implies that the initial size of the droplet significantly affects the onset of skin formation during evaporation and can also affect the thickness of the film formed, as the concentration gradient can be much steeper. This effect can also be seen from the plot of change in temperature with time (Figure (5.8)). The sudden increase in the temperature of the 10μm is attributed to the heat of precipitation.

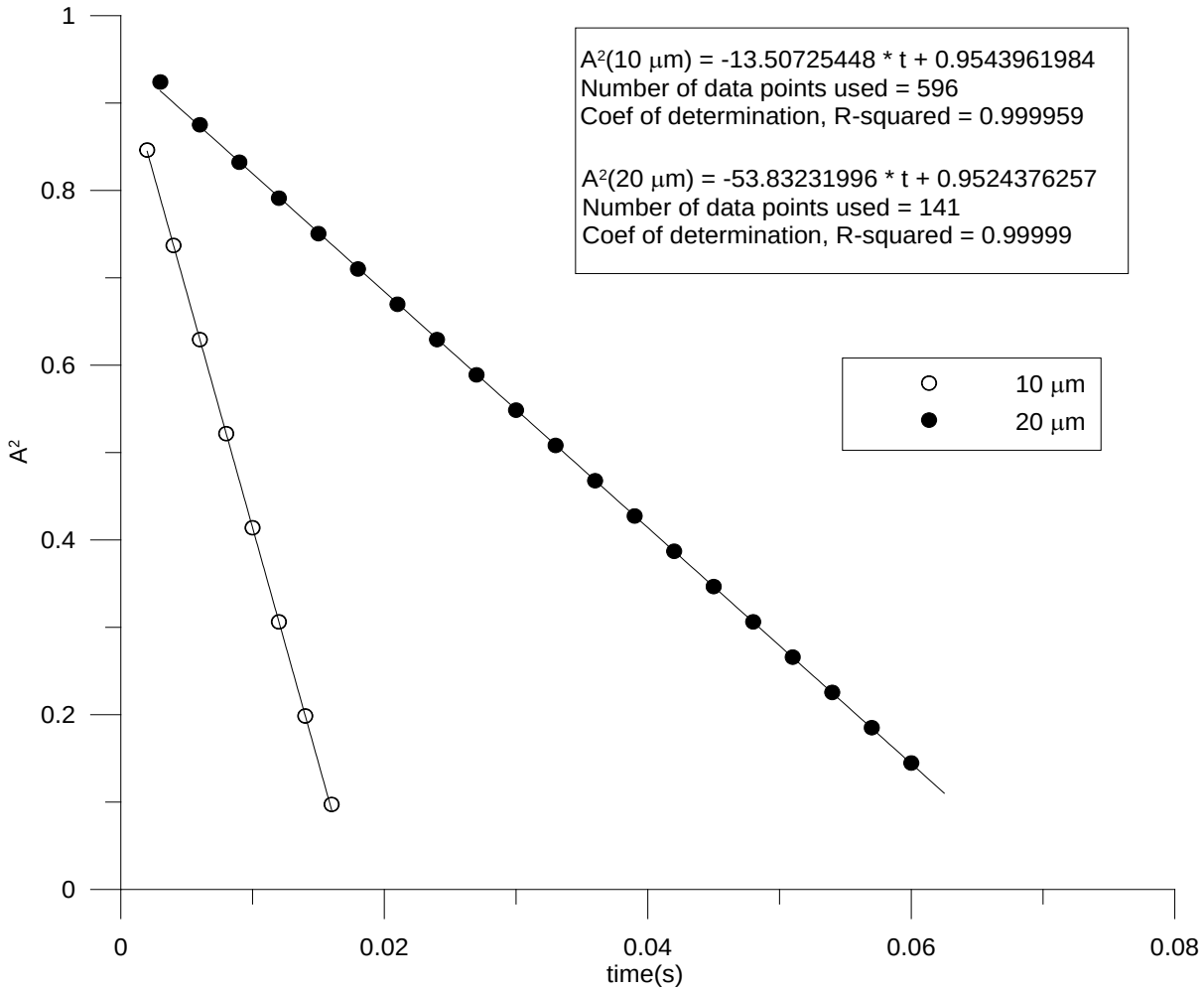

Figure 5.7: Effect of change in initial droplet size of PS-THF solution with initial droplet temperature 25 ^{0}C and gas phase temperature of 40 ^{0}C.

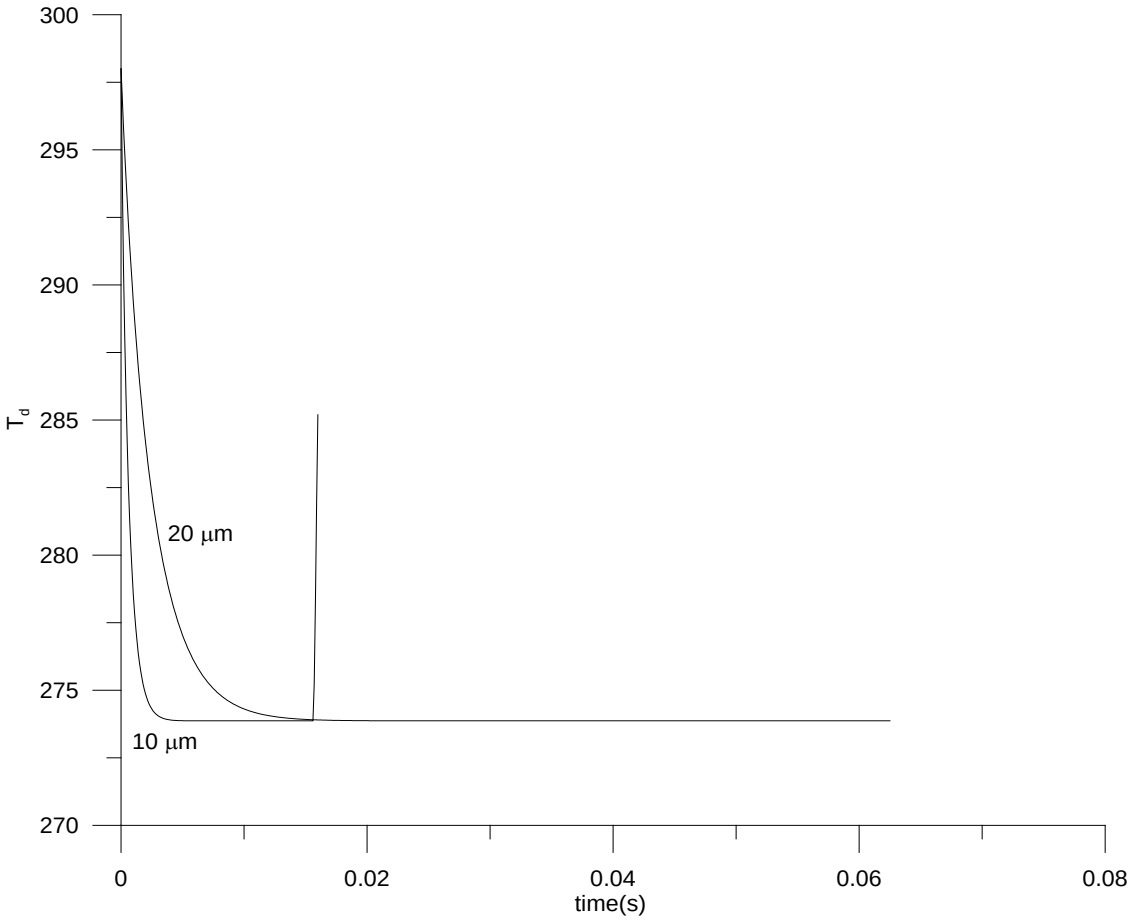

Figure 5.8: Plot of droplet temperature with time for droplets with initial radius 10 and 20 μm. T_{d0}=25 ^{0}C and T_∞=40 ^{0}C.

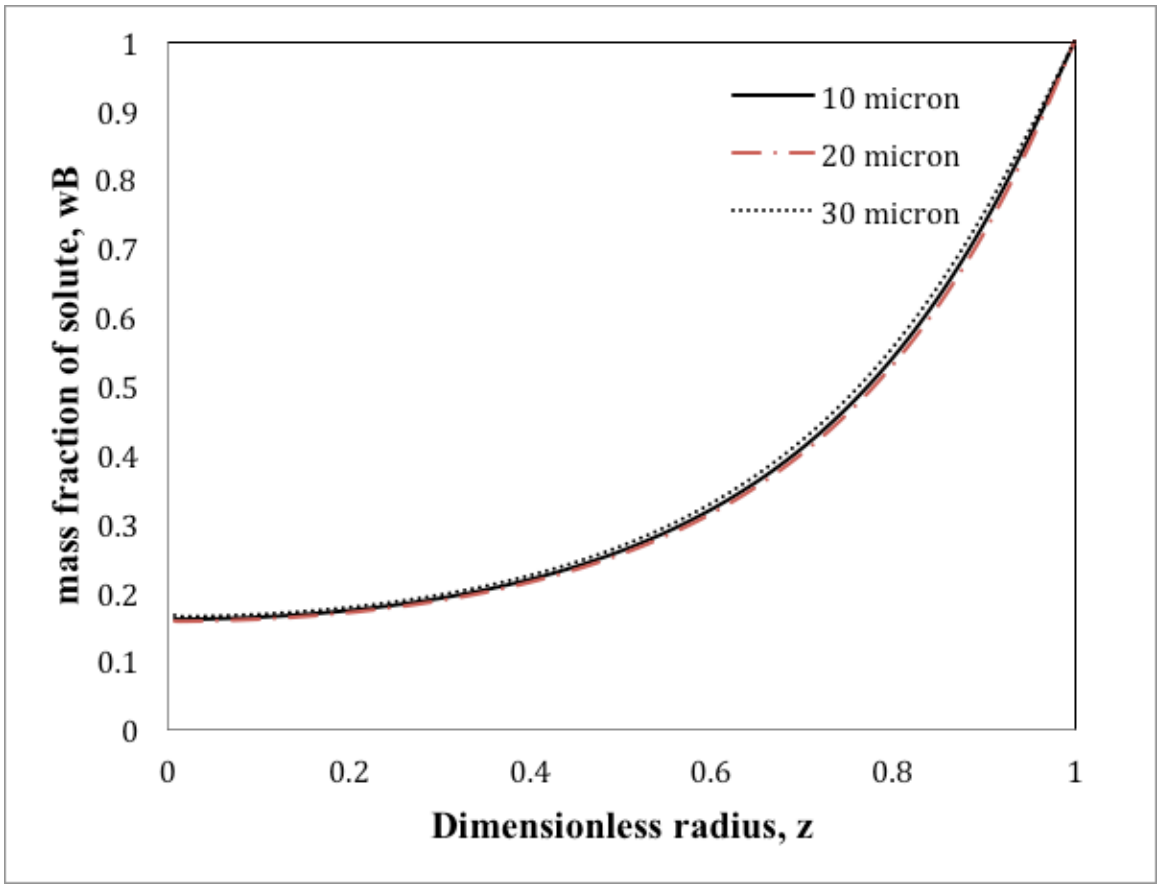

Figure 5.9: Concentration profile inside the droplet at onset of skin formation for different initial droplet sizes (T_∞=40^{0}C).

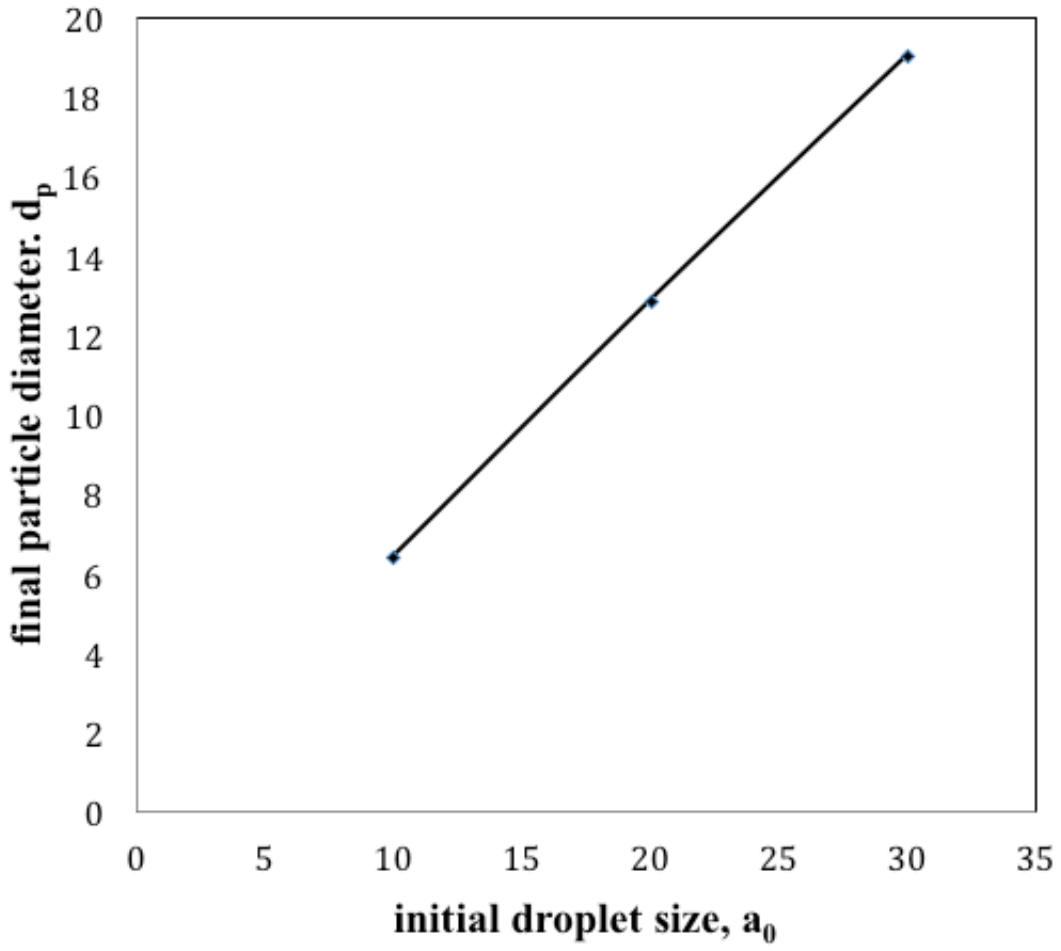

Figure 5.10: Variation of final particle size with initial droplet size. (T_∞ = 40 ^{0}C, w_{B0} = 2wt% and T_{d0} = 25 ^{0}C).

It was expected that the concentration profile at the onset of skin formation would be much steeper for smaller droplets as the evaporation rates are significantly higher for small droplets as shown in figure 5.7. Keeping this in mind, concentration profiles at the onset of skin formation starting with different initial concentration of the polymer were plotted as shown in figure 5.9. Interestingly, the concentration profile inside the droplet at the onset of skin formation was independent of the initial droplet size. This can be

verified by the fact that the concentration profiles depend directly on the rate of diffusion and evaporation. Even though they are different but their relative change is similar due to their dependence on the square of the radius. Therefore, if everything else is constant then change in radius should not affect the concentration profile inside the droplet. Even though the concentration profiles were nearly identical, the final particle size obtained increased with increasing initial size of the droplets as shown in figure 5.10. Also, with higher concentrations, the skin formed would be much thicker and hence, the drying characteristics would be quite different once the skins are formed which will have a significant effect on the final particle morphology obtained.

5.7.3.2 Effect of initial polymer concentration

This section attempts to study the effect of initial polymer concentration on the size of final particle size. To do the same, two different polymer concentrations 7wt% (+5%) and 12wt% (+10%) were used to predict the behavior of the evaporating solution droplet till the point of skin formation. For an initial polymer concentration of 0.07 (wt%), the time taken for the polymer skin to form is lower. It is even lower for an initial polymer concentration of 0.12. The plot of polymer surface concentration with time is shown in figure 5.11. The size obtained at the onset of skin formation was also higher when a higher initial polymer concentration was used as shown in figure 5.12. Also, the difference between the surface concentration and the center of the drop was estimated to be 0.84 even for a drop with initial polymer concentration 12wt% showing that even at slightly higher concentrations hollow microparticles are obtained.

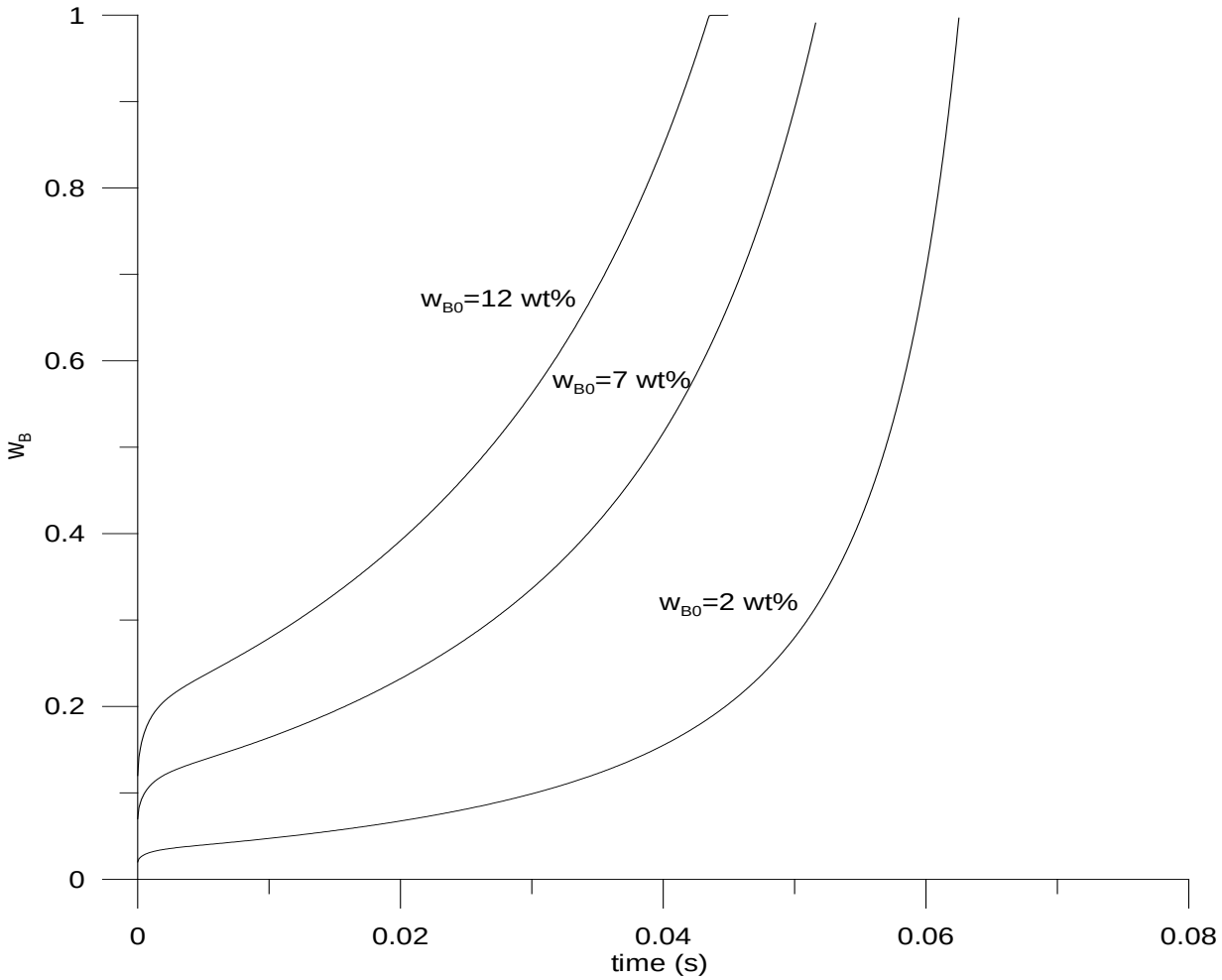

Figure 5.11: Plot of polymer surface concentration with time for different initial polymer concentrations of 2wt%, 7wt% (+5%) and 12wt% (+10%){T_{d0}=25 ^{0}C & T_∞ = 40 ^{0}C}.

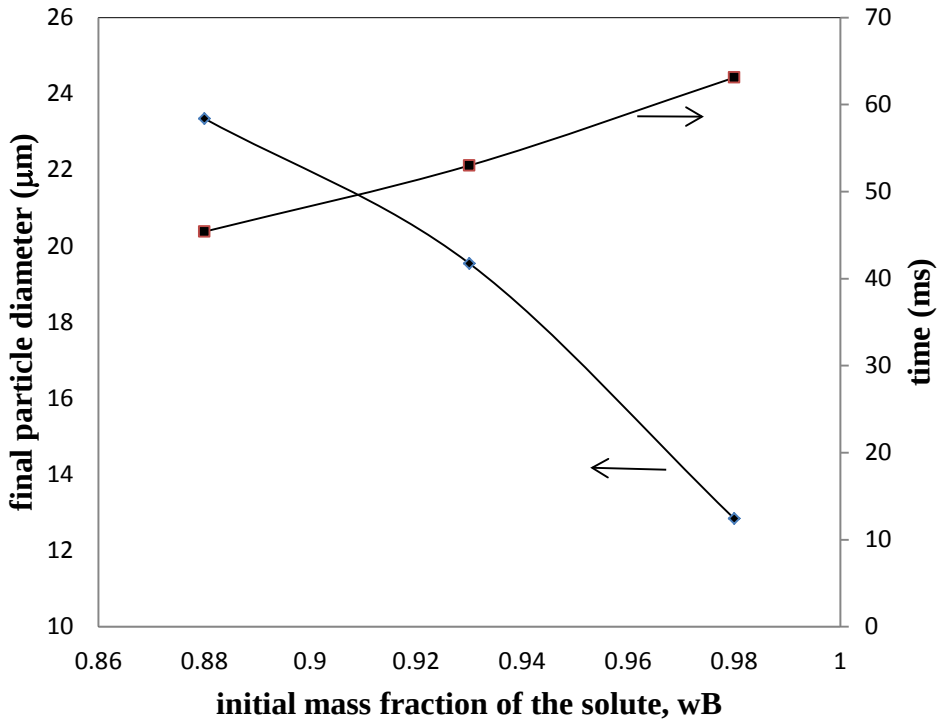

Figure 5.12: Variation of final particle size and the time taken to skin formation with initial polymer concentration at the onset of skin formation.

5.7.3.3 Effect of ambient gas temperature

The effect of gas phase temperature on the concentration profile inside the droplet plays a major role in determining the nature of the final particle morphology. With the increase in gas phase temperature the vapor pressure of the solvent at the surface of the droplet increases and hence the evaporation rate is higher than at lower temperatures. The concentration profile inside the droplet at the onset of skin formation with different ambient temperatures is shown below in figure 5.13.

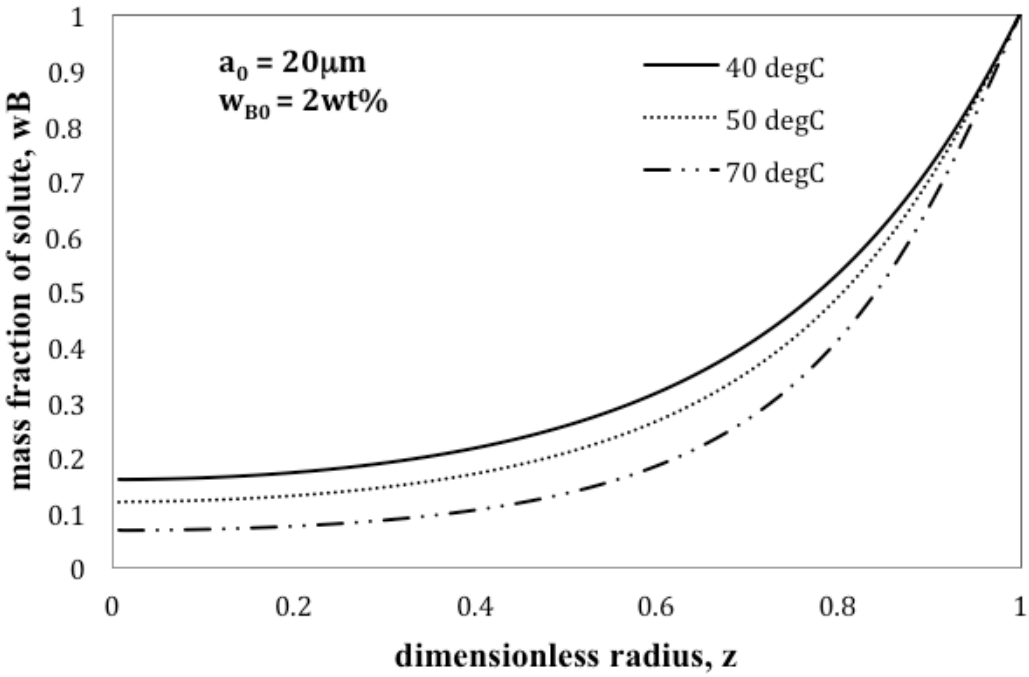

Figure 5.13: Effect of ambient gas temperature on polymer concentration profile inside the droplet at the time of skin formation.

The concentration gradient inside the droplet at a higher temperature is slightly steep. The skin forms even faster in such cases. At an ambient temperature of 40 ^{0}C (experimental conditions), the time to skin formation is 63.1ms whereas when the temperature is raised to 70 ^{0}C the time reduced to 41ms. Even though we do not have experimental results to back up the hypothesis but we believe that the faster the time it takes to skin formation, if the initial concentration of polymer is same, then the skin formed will be thinner. Also, the sizes obtained at the onset of skin formation are slightly higher at higher temperatures as shown in figure 5.14. This is again due to the fact that the skin forms much faster due to higher evaporation rates. The change in final particle diameter predicted from the model is from 12.8μm to 13.7μm, which is only about 6.5% when compared to a

significant change in size (from 12 to 24 μm) when the initial concentration of the solute was varied.

5.8 Conclusions

The model developed in the present work predicts the heat and mass transfer in a dilute polymer solution droplet with the effect of convection. The model (keeping convection terms intact) was validated for the case of no convection. Effect of various parameters such as initial droplet size, ambient temperature and initial polymer mass fraction on the final particle morphology was discussed qualitatively. The steep concentration gradients achieved during the evaporation and drying of a highly volatile solvent was predicted.

For a given initial concentration and size of the droplet, a steep polymer concentration gradient exists near the surface of the drop and a large difference in concentration between the center and surface is obtained. The skin forms when the polymer concentration at the surface reaches close to 1. This results in a hollow microparticle formation. Also, the sizes compared well with the experimental sizes obtained in Chapter 4 using a vibrating orifice aerosol generator. With the increase in initial concentration, the times at which the skin forms decreases and the difference in the concentrations between the center and the surface decrease only slightly. The final particle size, however, increases significantly with the increase in the initial concentration. Experimental investigations in Chapter 4 involved dilute polymer blend solutions rather than a single polymer in solvent. It was discussed that the time scales of evaporation will play a major role in inhibiting the phase separation in such systems. From the model for a single polymer in solution, the time scale of evaporation was

predicted to be about 63ms. Even for a polymer blend system, at such high evaporation rates, the polymer-polymer mobility would be substantially reduced and the time scales of evaporations might as well be close to a single polymer solution.

Increase in ambient temperature results in increased evaporation rates and larger particle sizes are obtained. Also, the concentration gradients are much more in the case of higher temperatures that lead to faster skin formation. One has to keep in mind that if the temperature of the surroundings is higher than the boiling point of the solvent, then once the skin forms, the vapors may be trapped inside the thin skin and depending on the nature of the skin (porous, hard, etc.), eventually lead to the rupturing of the skin. Also, at temperatures above the boiling point of the solvent, voids may form inside the droplet and the obtained microparticles may have voids instead of strictly hollow microparticles.

The initial radius of the microdroplet was also varied to predict the effect of surface evaporation. The evaporation of the microdroplet increased significantly by 4 times when the initial droplet size was reduced from 20μm to 10μm. Also, the final particle sizes obtained were significantly lower. It is interesting to note that the concentration profile of the polymer inside the droplet was similar for different initial sized droplets. All these predictions can be used to better control the morphology of the final particles obtained form experiments.

Even though the model predicts the final particle size obtained from evaporation of a highly volatile solvent from a dilute polymer solution, the assumption of constant solvent-polymer diffusion coefficient is not a practical one. As the solvent evaporates, the concentration at the surface increases. Hence, the diffusion of the solvent through to the surface is reduced by about 10 times. This can significantly reduce the evaporation rates

and the time to skin formation. A suitable relationship for the diffusion co-efficient as a function of polymer concentration should be incorporated in the model for understanding the onset of skin formation and final particle morphologies. Also, once the skin is formed there is a significant resistance offered to diffusion of the solvent through the skin to the external surface. This resistance increases as the skin thickens. Also, if one can track the pressure inside the droplet once the skin forms and the stresses exerted on the skin, a better understanding of the formation of different morphologies can be achieved. Above all, for polymer blend systems, the microscopic interactions between the two polymers and the solvents also need to be taken into account. All these points need to be considered and a rigorous model should be developed for better predicting the morphology of the microparticles formed from such processes.

APPENDIX: CHARGE LIMITS ON DROPLETS WITH DISPERSED POLYMER ADDITIVE

A1.1 Introduction

Charged droplets are encountered in many atmospheric phenomena and industrial applications such as spray painting, electrospray ionization, ink-jet printing and nanoparticle production. All these processes involve evaporation of charged droplets and their explosions.

When a charged droplet evaporates, the surface charge density increases and the electrostatic repulsive force increases. When the charge on the droplet reaches a certain value, the repulsive forces overcome the surface tension forces in the drop and the drop becomes unstable. The drop then explodes to form a stable parent drop and other satellite droplets. The criterion of instability of droplet explosion is given by Lord Rayleigh as,

$$q_R = 8\pi\sqrt{\varepsilon_0 \gamma a^3} \tag{A1.1}$$

where, q_R, is the charge on the droplet, ε_0 is the permittivity of free space, γ is the surface tension of the drop and a is the radius of the droplet.

Several researchers have since tried to validate the theoretical Rayleigh limit using experiments. In particular, Electrodynamic Balance coupled with light scattering apparatus have been extensively used to study charge and mass losses during droplet break-ups. Typically, a single charged droplet is suspended in an electric field depending on the charge-to-mass ratio of the drop. Size of the drop is estimated by measuring the light scattering intensity with time and comparing with Mie Theory and the charge on the

droplet at the instance of droplet break-up is determined which can then be compared to the theoretical charge obtained from equation A1.1.

Charge limits on pure droplets have been extensively studied. Richardson et. al. (1989) studied dielectric droplets and reported that the charge losses are about 10-20% at fission. Also, for conductive droplets, negligible mass loss (<0.1%) and significantly higher charge losses up to about 50%. This result was qualitatively in agreement to the experimental results of Li et. al. (2005) who studied droplets of various pure liquids having different electrical conductivity. They showed that even though the Rayleigh charge limit is closely satisfied ($\pm$4%) for all the droplets studied but the charge losses from a higher conductivity material is higher than low conductivity material along with lower charge losses. Taflin et. al. (1988) measured charges at droplet explosion for water droplets containing SDS. They showed that the charge loss at explosion was 17.7% whereas the mass loss from droplet was 3.9%. Taflin et. al. (1989) studied heptadecane and dodecanol droplet fissions in radioactively contaminated gaseous medium. They reported that in an ionized gaseous medium the charge losses were much higher (70-80%) when compared to the non-ionized case (10-20%). They concluded that all the droplets exploded below the Rayleigh limit (at about 80%). Davis and Bridges (1994) studied charge limits on droplets of 1-dodecanol and aqueous solution droplets containing sodium dodecyl sulphate (SDS). They found that both 1-dodecanol and water droplets exploded 90% of Rayleigh limit. SDS reduces the surface tension of water and the electrostatic charge required to overcome the surface tension barrier reduces, therefore reducing the charge limits on such droplets.

Duft et. al. (2002) studied ethylene glycol droplets suspended in a quadrupole trap. They used a technique independent of droplet size and charge measurement and found that the charge instabilities and fission occur above 95% of Rayleigh limit. For the same droplets, the charge limits calculated from the size and charge measurements yielded a value of 70% of Rayleigh limit. They attributed this disparity in results to the lowering of surface tension due to droplet shrinkage and surface contaminants.

Charge limits on droplets containing either dissolved salts or colloids have also been recently studied. Most of the previous studies involved determination of charge limits lower than the theoretical Rayleigh limit. But recently few researchers have used ionic solutes such sodium and lithium chloride and other ionic surfactants to understand the mechanism of charge droplet breakup and the effect of thermal conductivity on such phenomena. Smith et. al (2002) studied various compounds containing NaCl explode at a higher value than the postulated Rayleigh limit. Li and Ray (2005) have shown that for DEG and TEG droplets containing LiCl explode significantly higher than the Rayleigh limit. They also measured the charge limits on droplets containing suspended polystyrene nanoparticles in these glycols and concluded that the presence of such particles again raises the charge limit upto 3 times higher than Rayleigh limt and also the size of the nanoparticles and their concentration effect the charge at which droplets explode. To understand the role of ions and to characterize the progeny droplets produced during the columbic fission, Hunter and Ray (2009). They concluded that presence of ions at the surface does not affect the charge limit of the drops but increase in ion concentrations increases the charge losses.

In the present study, the work of Li and Ray (2005) is extended to predict charge limits on droplets containing a colloidal suspension of a polymer solute. The following sections briefly describe the theory and experimental methods used to predict the charge limits of droplets.

Section A1.2 describes the electrodynamic balance required to suspend the droplet along with the diffusion chamber and light scattering set-up for controlling the ambient conditions of the drop and acquiring the light scattering data from the drop respectively.

In Section A1.3 the method for analysis of the acquired light scattering data along with the voltage versus time data during our experiments have been presented by taking an example of a pure DEG droplet.

The charge on the droplets of DEG doped with PEG are obtained in section A1.4 along with the comparison of these values with the Rayleigh limit of pure DEG droplet. Section A1.5 concludes the work briefly.

A1.2 Experimental

In the present work, an electrodynamic balance (EDB) is used to study the effect of more than one component on the stability and explosion of charged droplets. The electrodynamic balance incorporated in the present study is the same used by Tu (2001) and Hunter (2010). The most salient features of the balance are discussed here. The top view of the experimental set-up along with the electrical and optical components are shown in figure A1.1. The electrodynamic balance used in the present study for suspension of charged droplets consists of three major parts namely, (i) the charged droplet generation, (ii) droplet levitation or Electrodynamic Balance (EDB), (iii) the cloud chamber and the optical system. Each one is discussed briefly in the next sections. The EDB is housed inside the cloud chamber.

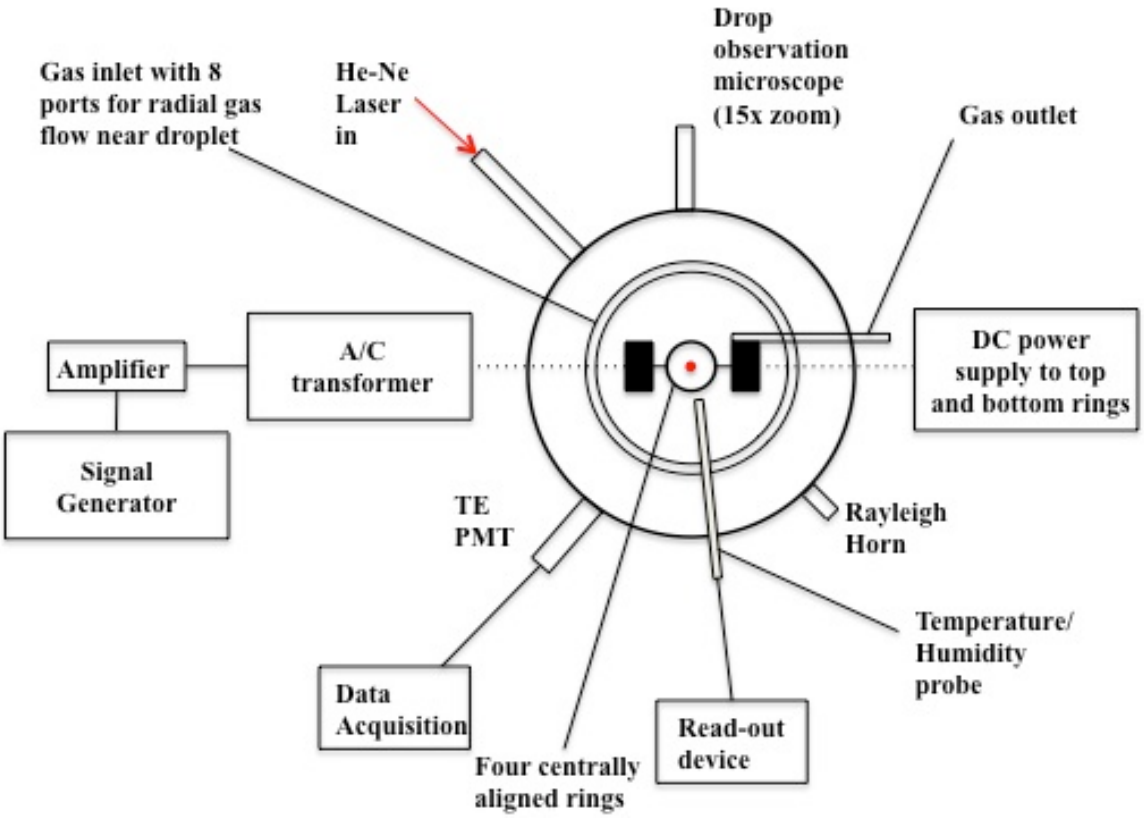

Figure A1.0.1: Schematic top view representation of the Electrodynamic balance and the diffusion cloud chamber along with electrical and optical components.

Figure 4.11 (a) shows the slice on which the analysis was performed. The image of the slice was not clear due to the high voltage used and also due to the very high magnification. At low voltages (~3 kV), the images were much clearer as shown in previous micrographs in figure 4.10. The chlorine counts from the 3 chosen points were about 100. The counts were not enough to map the distribution of chlorine in the slice but the equal number of counts suggests that the distribution of chlorine might be uniform. Since, only one such slice was obtained wherein chlorine was detected, using this result alone we cannot conclude the uniform distribution of PVC and PS.

A1.2.1 Charged droplet generation

A stainless steel hypodermic needle with a flat tip is filled with the liquid under study. A couple of drops of the liquid is enough to generate and suspend a single charged droplet. The needle is connected to a high voltage DC power supply (HP 6525A) and the electrical circuit is designed such that a negative voltage is supplied to the needle. Also, the voltage supplied is regulated to provide a pulsed voltage only when triggered. The needle is mounted on top of the diffusion cloud chamber along the central axis and when given a high voltage pulse, the liquid at the tip of the needle spray into highly charged droplets. These droplets pass through the top plate and enter the EDB. The electrodynamic balance is discussed in section A1.2.2. The EDB captures a single droplet with a suitable charge-to-mass ratio. Once a stable droplet is suspended, the needle holder is removed and the opening is closed by mounting a photomultiplier tube (PMT) on top of the cloud chamber for collecting the light scattering from the droplet.

A1.2.2. Electrodynamic Balance

In the present study, a four-ring electrodynamic balance is used for suspending a charged droplet. A schematic representation is shown in figure A1.2. The center-to-center distance between the four rings is equally spaced, 3/16” apart. All the four rings are symmetrically aligned and the geometrical center of the aligned rings is called the null point. If the rings are aligned precisely then the charged droplet is suspended exactly at the null-point of the EDB. The rings are supported on two mica blocks. An ac potential of about 1200 V and frequency 200-500 Hz is imposed on the central electrodes using a circuit consisting of a signal generator (Dynascan 3010 function generator), an audio amplifier (Realistic SA-150) and a high voltage ac transformer. The top and bottom

electrodes impart a dc voltage, which is controlled appropriately to set the droplet exactly at the null point.

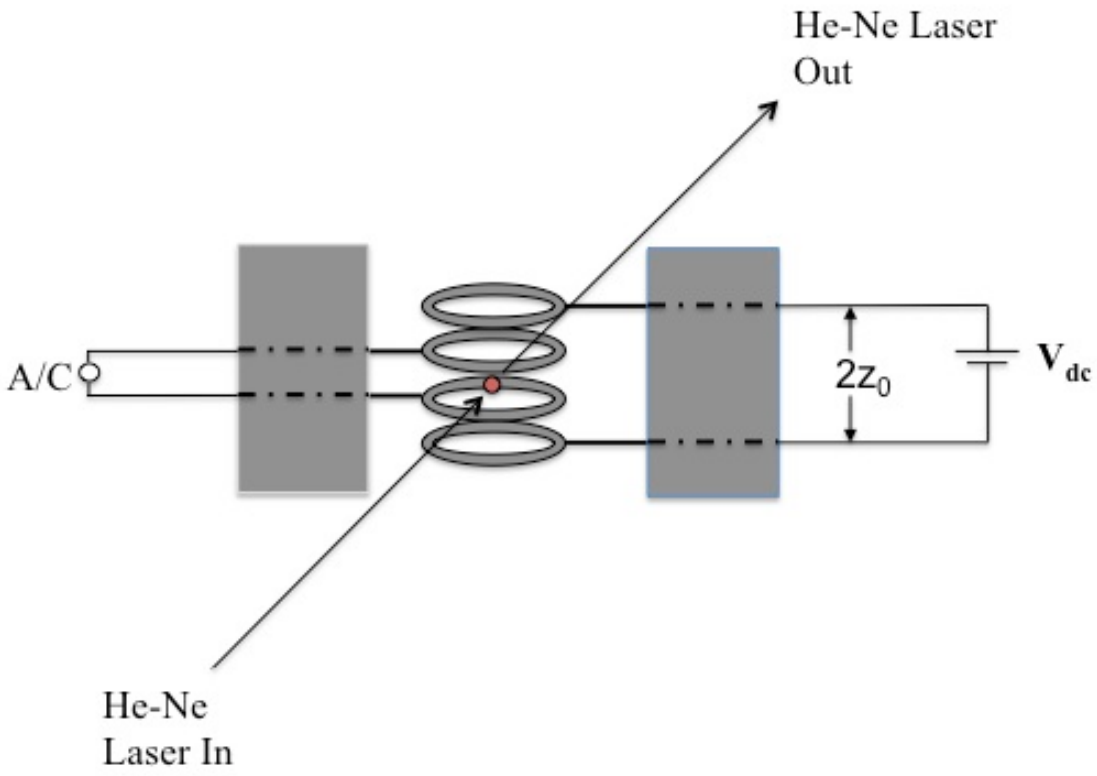

Figure A1.0.2: Schematic of the Electrodynamic Balance (EDB) consisting of 4 rings with central rings connected to a high voltage a/c signal and the top and bottom electrodes with +ve and –ve dc potentials respectively.

A1.2.3. Diffusion Cloud Chamber and Optical System

The chamber used in the study consists of a central stainless steel plate that supports the EDB at the center. Two similar hollow stainless steel plates are used on top and bottom of the central plate and a coolant (water) is circulated through the hollow plates for maintaining the temperature inside the central plate. The temperature of the chamber is maintained within $\pm 1^0$C. The lower and the middle plate are fixed and the upper plate is detachable allowing cleaning and other activities prior to the start of experiments. As shown in figure A1.1, the middle cylindrical section consists of several port-holes for measurement of temperature, humidity and light scattering spectrum. The temperature and humidity of the chamber are measured using a traceable hygrometer (ThermoFisher 11-661-7B) with its probe placed about 2 inches from the center of the droplet. The humidity in the chamber was controlled by passing dry nitrogen gas from one of the port-holes. The flow of the nitrogen gas was controlled using an MKS (1259B-01000SV) flow controller.

Optical system and Data Aquisition

Once the droplet is suspended, a 20mW He-Ne laser (vertically polarized) illuminates the droplet. The droplet scatters light from the laser and the scattering is detected by PMT's along the two perpendicular planes. The scattering light along the horizontal plane corresponds to transverse electric (TE) mode and one along the vertical plane corresponds to transverse magnetic (TM) mode. The illuminated droplet is observed through a 15x optical microscope.

The low voltage output signals from the PMT's are amplified and the data is saved onto a PC using a data acquisition card from Measurement Computing (PCI-DAS1602/16). A

visual basic program is used as a user interface for passing proper parameters for data collection. The parameters used for data acquisition are the rate at which data need to be collected (Rate), number of sampling points (Counts).

A1.2.4 Experimental Procedure

The diffusion cloud chamber is cleaned thoroughly and then sealed and isolated from the ambient atmosphere. Prior to closing the chamber, all the rings are coated with a black conductive ink (Ted Pella, Colloidal Graphite) and the supports are coated with a non-conductive liquid insulation tape to eliminate unnecessary scattering. Circulation of the coolant is started along with the passage of the dry gas through the chamber (500 ml/min to 1000 ml/min) and sufficient time is allowed for achieving the required chamber conditions. For all the experiments, the chamber was operated under atmospheric pressure, and a constant temperature of 25.3 ^{0}C with 0% relative humidity (RH). The temperature and RH were monitored continuously using a Thermo Fisher Traceable temperature/ humidity/dew point probe (11661-B). The droplet was illuminated using a He-Ne laser. The hypodermic needle filled with couple of drops of the liquid under study is placed on top of the chamber and the high voltage impulse is triggered. A mist of microdroplets with different mass to charge ratios is generated into the EDB. Several droplets with suitable mass to charge ratio are trapped inside the EDB. With proper adjustment of the frequency and voltage of the ac field, a single droplet is trapped at the center of the EDB. The position of the droplet is adjusted using the dc voltage across the top and bottom ring electrodes to bring the droplet to the null point of the balance. When a charged droplet is balanced at the null point of an electrodynamic balance, under no other external force other than gravity, the gravitational force acting on the droplet is

balanced by the electrostatic force from the dc voltage across the electrodes. By balancing both these forces, we get

$$mg = -C_0 q V_{dc}/2z_0 \quad \text{(A1.2)}$$

where, m is the mass of the droplet, q, the charge on the droplet, $V_{dc}$is the dc voltage measured across the top and bottom electrodes and $2z_0$ is the distance between the top and bottom dc electrodes. C_0 is the geometrical constant of the electrodynamic balance. For the electrodynamic balance under study, C_0 was determined using the marginal stability analysis procedure as explained by Davis (1985). The marginal stability curve is a plot of field strength parameter, $\eta = 8gV_{ac}/(4\pi^2 C_0 z_0 V_{dc} f^2)$ and drag parameter, $\delta = 9\mu/(4\pi a^2 \rho f)$ where f is he frequency of the ac signal, V_{ac} the high voltage a.c. applied to the central rings of the EDB, μ and ρ are the viscosity and density of the droplet under consideration. During an experiment, keeping all other parameters in the above expressions for field strength and drag parameter constant, the signal frequency is varied such that the droplet just elongates. This point is called the marginal stability point for the droplet at a particular size. Corresponding size and dc voltages are recorded and the several of such readings are repeated during the course of the evaporation experiment. The data is fitted to the marginal stability curve given by Davis (1985) from which C_0 is evaluated. For the particular electrodynamic balance under study C_0 was found to be 0.43.

Once a stable droplet is bought to its null point, the light scattering data is acquired at time, t=0. Simultaneously, as the droplet evaporates, it loses mass and hence the dc voltages are lowered to bring the droplet back to the null point. Both the time and corresponding voltages are recorded, as they are required for calculating the charge limits

on the droplets under consideration. Even though low flow rates of dry gas is used, it should be noted here that, to avoid any drag in the calculations, the flow of the gas is switched off before setting the null point of the drop and taking the voltage reading. At a certain moment during the experiment, the voltage suddenly increases to a higher value and then reduces again periodically as before. This point indicates a droplet explosion and there is a discontinuity in the droplet light scattering spectrum. When the experimental spectrum is matched to the theoretical spectrum obtained from Mie theory, the exact size and time of the break-up can be obtained.

A1.3 Data Analysis

A1.3.1 Evaporation and Light scattering from a single homogeneous droplet

As soon as the droplet is formed it begins to evaporate. Evaporation rate of the drop varies depending on the vapor pressure of the drop, which in turn depends on its surface temperature. For a single component, spherical, isolated microdroplet evaporating under a steady state, the size of the drop varies with time as,

$$a^2 = a_0^2 - \frac{2D_{Ag}M_A P_A^0(T_{ds})}{\rho_A R T_{ds}}\left(1 - \frac{P_{A\infty}(T_\infty)}{P_A^0(T_{ds})}\right)t \qquad \text{(A1.3)}$$

where, a is radius of the droplet at any time t, a_0 is the initial radius at the start of the experiment ($t=0$), M_A is the molar mass of the component, ρ is the density of the component, P_A^0, is the saturation vapor pressure of the drop at its surface temperature T_{ds} and $P_{A\infty}$is the partial pressure of the component in the gas phase at gas phase temperature T_∞. From equation A1.3 it can be concluded that, under quasi-steady state assumptions, the square of the droplet radius varies linearly with time. This variation of size with time is referred commonly as the d^2-law. A dimensionless size, called the size parameter, is usually used to normalize the size obtained in evaporating droplets and is defined by $x = 2\pi a/\lambda$, where, a is the radius of the spherical droplet and λ is the wavelength of incident monochromatic laser beam. Equation 4.3 can be re-written as,

$$x^2 = x_0^2 - \alpha t \qquad \text{(A1.4)}$$

where α is a constant given by $\alpha = \frac{8\pi^2 M_A P_A^0(T_{ds})}{\rho_A R T_{ds}\lambda^2}\left(1 - \frac{P_{A\infty}(T_\infty)}{P_A^0(T_{ds})}\right)$.

According to Lorenz-Mie theory, when a highly polarized beam (vertically polarized in the present case) of light having a fixed wavelength, λ, illuminates a homogeneous spherical droplet or particle, the intensity of scattered light in the horizontal plane (TE) and vertical plane TM are given by,

$$I_1 = \frac{I_i \lambda^2}{4\pi^2 r^2}\left\{\sum_{n=1}^{\infty} \frac{2n+1}{n(n+1)}\left[a_n \frac{P_n^1 cos\theta}{sin\theta} + b_n \frac{d}{d\theta} P_n^1 cos\theta\right]\right\}^2 \quad \text{(A1.5)}$$

$$I_2 = \frac{I_i \lambda^2}{4\pi^2 r^2}\left\{\sum_{n=1}^{\infty} \frac{2n+1}{n(n+1)}\left[b_n \frac{P_n^1 cos\theta}{sin\theta} + a_n \frac{d}{d\theta} P_n^1 cos\theta\right]\right\}^2 \quad \text{(A1.6)}$$

where, θ is the angle between the incident beam and scattering direction and $a_n$and b_n are the scattering coefficients for the TE and TM mode respectively. For a homogeneous sphere, the scattering coefficients depend only on the refractive index, m and size parameter, x and are given by,

$$a_n = \frac{A_n(x,m)}{A_n(x,m)+i\, C_n(x,m)} \quad \text{(A1.7)}$$

$$b_n = \frac{B_n(x,m)}{B_n(x,m)+i\, D_n(x,m)} \quad \text{(A1.8)}$$

where A_n, B_n, C_n and D_n are related to the Ricatti-Bessel function of first and second kinds. For a fixed scattering angle, the scattering intensity spectrum shows sharp peaks. These sharp peaks are called morphology dependent resonances (MDR). In figure A1.4 (b) a plot of intensity versus size parameter for a given refractive index (pure DEG drop)

and scattering angle is generated using Mie theory. In this particular spectrum only peaks are observed between the time intervals shown in the figure but the resonances can either occur as peaks or troughs. We will refer to both peaks and trough as peaks in the rest of thesis. These resonances occur when the incident light is totally, internally reflected within the sphere. From a theoretical standpoint, these resonances occur when the imaginary terms in the coefficients of $a_n$and $b_n$equals zero. **Tu (2000)** has shown that for a given refractive index and scattering angle the shape of the intensity spectrum is unique and that each resonance peak repeats itself every Δx distance where Δx is approximately a function of refractive index, m and is given by,

$$\Delta x = \frac{tan^{-1}\left(\sqrt{m^2-1}\right)}{\sqrt{m^2-1}} \tag{A1.9}$$

A1.3.2 Analysis of Droplet Break-up

As the drop evaporates, the voltage required for bringing the drop back to the null point reduces. This voltage and the corresponding times are recorded during evaporation of a single drop. The rate at which the voltages are recorded depends upon the rate of evaporation of the drop.

Once the light scattering data and the voltage versus time readings are recorded, the next step is to analyze the data for size and charge on the droplets. The TE mode light scattering data and the ${V_{dc}}^{2/3}$ versus time data from a typical experimental run of an evaporating pure single diethylene glycol (DEG) droplet are shown in Figure A1.3 below. From the ${V_{dc}}^{2/3}$ vs time data in figure A1.3, three discontinuities are observed. Each discontinuity marks an explosion of the droplet somewhere in between those discontinuous time intervals. When droplet break-up occurs at a certain size, there is a

charge loss associated with the droplet. At a particular size, the charge on the droplet is inversely proportional to the voltage and hence due to charge loss during explosion the voltage required to balance the droplet increases steeply.

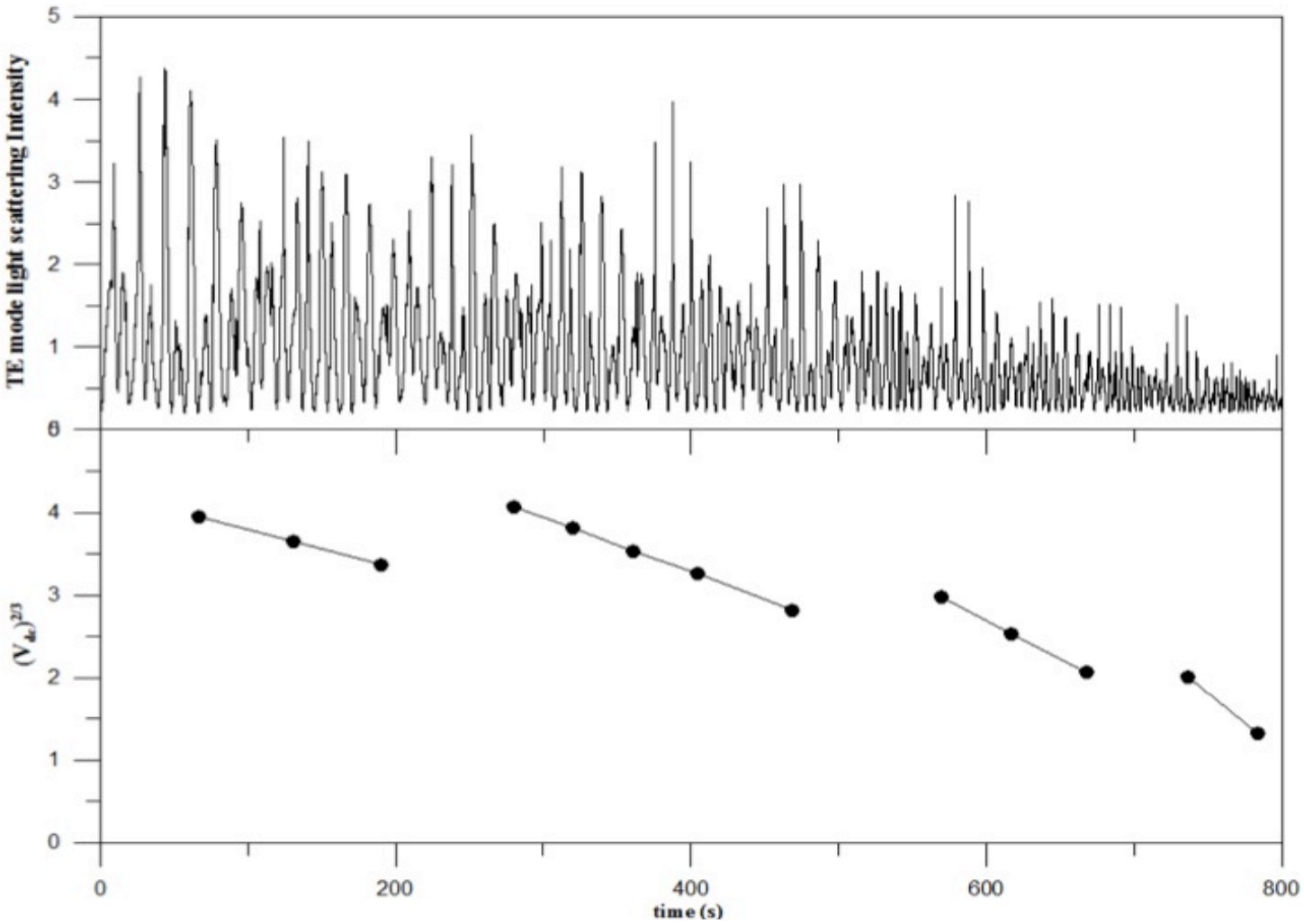

Figure A1.3: Balancing DC voltage and observed TE mode light scattering intensity as a function of time for a pure DEG droplet at 25.3 ^{0}C

It should be noted here that care must be taken to track both the voltage and intensity w.r.t. the same real time. Once the experimental spectrum is obtained, using Mie theory for light scattering, the theoretical scattering spectrum is generated for a given refractive index (for a pure DEG drop, refractive index, m= 1.443 at 25.3 ^{0}C) by varying the scattering angles. For each scattering angle the theoretical spectrum is compared with the experimental spectrum until a perfect match is obtained for a particular scattering angle. This is shown in figure A1.4 (b). It can be observed clearly that the two spectrums are identical with the theoretical spectrum having more pronounced peaks than the experimental spectrum. It should be noted that in figure A1.4 (b) theoretical intensity is plotted versus decreasing square of the size parameter, x ($x = 2\pi a/\lambda$), instead of the size parameter itself due to the fact that the square of the radius decreases linearly with time.

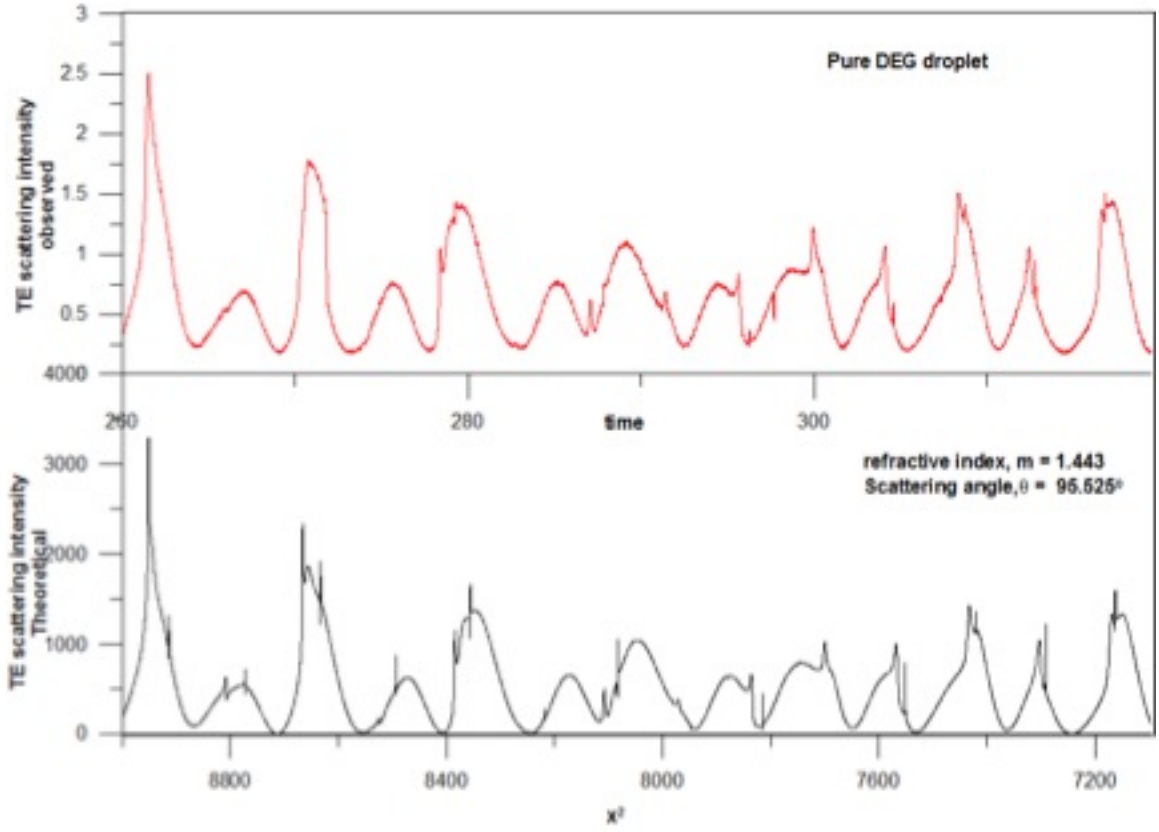

Figure A1.4: Visual matching and comparison of the experimental and theoretical spectrum for a pure DEG droplet for a given refractive index and scattering angle. (x is the size parameter)

Once the visual matching of the spectrum is done, occurrence times of resonance peaks of the same order are tabulated and numbered from 1 to N. Mass of the droplet is related to the radius and radius can be written in terms of the size parameter, *x*, and therefore, equation A1.2 can be re-written as equation A1.10.

$$V_{dc} = \left(\frac{\rho g z \lambda^3}{3\pi^2 q C_0}\right) x^3 \tag{A1.10}$$

If, during evaporation of the droplet, there is no charge loss, then equation A1.10 can be written as,

$$x = k\, V_{dc}^{1/3} \tag{A1.11}$$

where $k = \left(\frac{3\pi^2 q C_0}{\rho g z_0 \lambda^3}\right)^{1/3}$

Similarly, equation 4.3 can be re-written as,

$$\left(\frac{3C_0 q}{8\pi\rho g z_0}\right)^{2/3} {V_{dc}}^{2/3} = a_0^2 - \left[\frac{2D_{Ag} M_A P_A^0(T_{ds})}{\rho_A}\left(1 - \frac{P_{A\infty}(T_\infty)}{P_A^0(T_{ds})}\right)\right] t \tag{A1.12}$$

or,

$${V_{dc}}^{2/3} = {V_{dc,0}}^{2/3} - \beta t \tag{A1.13}$$

where V_{dc} is the dc voltage applied across the top and bottom electrodes and β is a constant if the charge on the droplet remains constant during the time period between break-ups. As mentioned earlier, at time t=0, recording of the light scattering spectrum is started and it is in reference to this time that the voltage versus time data for the droplet

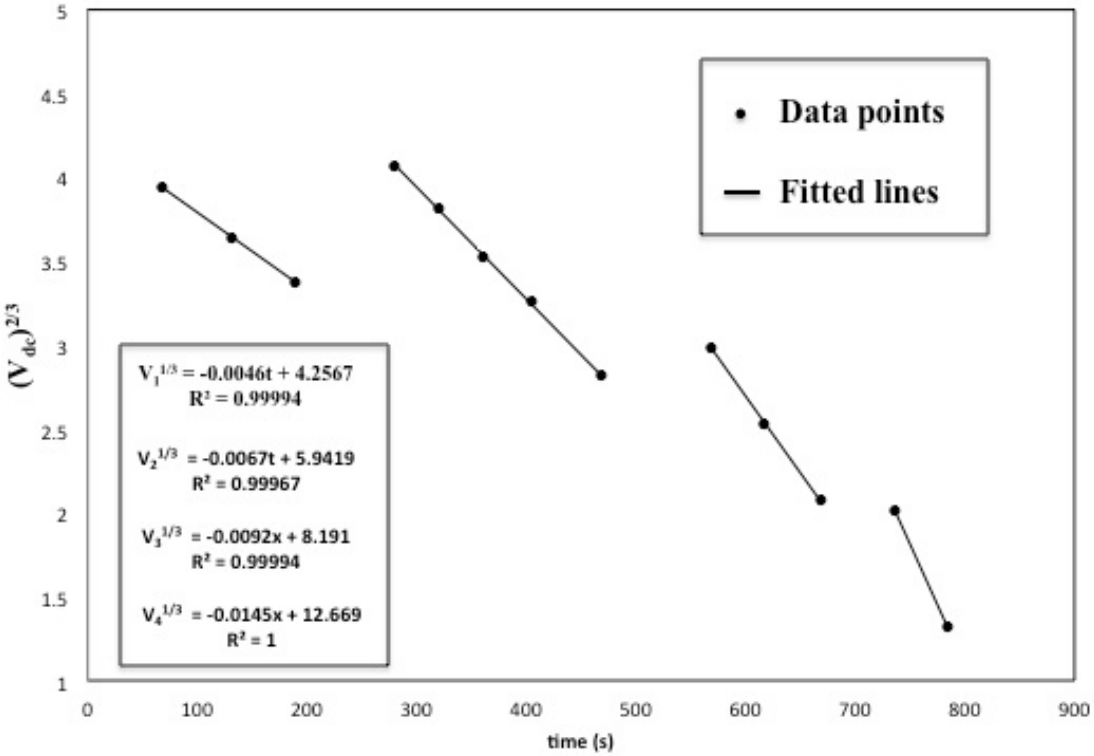

Figure A1.5: $V_{dc}{}^{2/3}$ Vs time plot of a pure DEG droplet at 25.3 ^{0}C and different discontinuities representing multiple droplet break-ups.

during evaporation are also noted. The voltage versus time data shown in figure A1.3 is fitted to the above equation 4.13 to obtain $V_{dc}{}^{2/3}$ as a linear function of time as shown in figure A1.5.

Now, using equation A1.11, assuming that the charge remains constant prior to an explosion, each distinct resonance peak with a unique size parameter can be related to the voltage as,

$$x_i = k\, V_{dc,i}^{1/3}\,, \qquad \text{for i = 1 to N} \tag{A1.14}$$

Also, since resonance peaks with same order occur at a Δx distance,

$$x_i = x_1 - (i-1)\Delta x \tag{A1.15}$$

Substituting equation 4.13 in equation 4.12 and subtracting from x_1, yields,

$$(i-1)\Delta x \; = k\left(V_{dc,1}^{1/3} - V_{dc,i}^{1/3}\right) \tag{A1.16}$$

The plot of $(i-1)$ Vs $(V_{dc,1}^{1/3} - V_{dc,i}^{1/3})$ yields a straight line with the slope given by $\Delta x/k$. An example plot is shown in figure A1.6. Since, Δx, for a given refractive index, can be calculated from equation 4.9, therefore, k is estimated. In this way k is estimated for each plot of ${V_{dc}}^{2/3}$ versus time after each break-up of the same droplet. The peaks obtained from the experimental spectrum prior to the first break-up and sample calculation steps described above are tabulated in Table A1.1 below.

Table A1.1: Resonance peaks from experimental light scattering spectrum prior to first droplet break-up corresponding to the data obtained for a pure DEG droplet at 25.3 ^{0}C and respective calculations to determine k. (Δx = 0.773954)

i	i-1	resonance peak times (s)	$V_{dc}^{2/3}$	$Vdc^{1/3}$	$\Delta Vdc^{1/3}$	Δx/k	k
1	0	8.9857	4.2154	2.0531	0.0000	0.00954	81.1273
3	2	26.1571	4.1364	2.0338	0.0193		
5	4	43.3429	4.0573	2.0143	0.0389		
9	8	76.3571	3.9055	1.9762	0.0769		
11	10	92.1857	3.8326	1.9577	0.0954		
13	12	108.0143	3.7598	1.9390	0.1141		
15	14	124.4286	3.6843	1.9195	0.1337		
17	16	140.6429	3.6097	1.8999	0.1532		

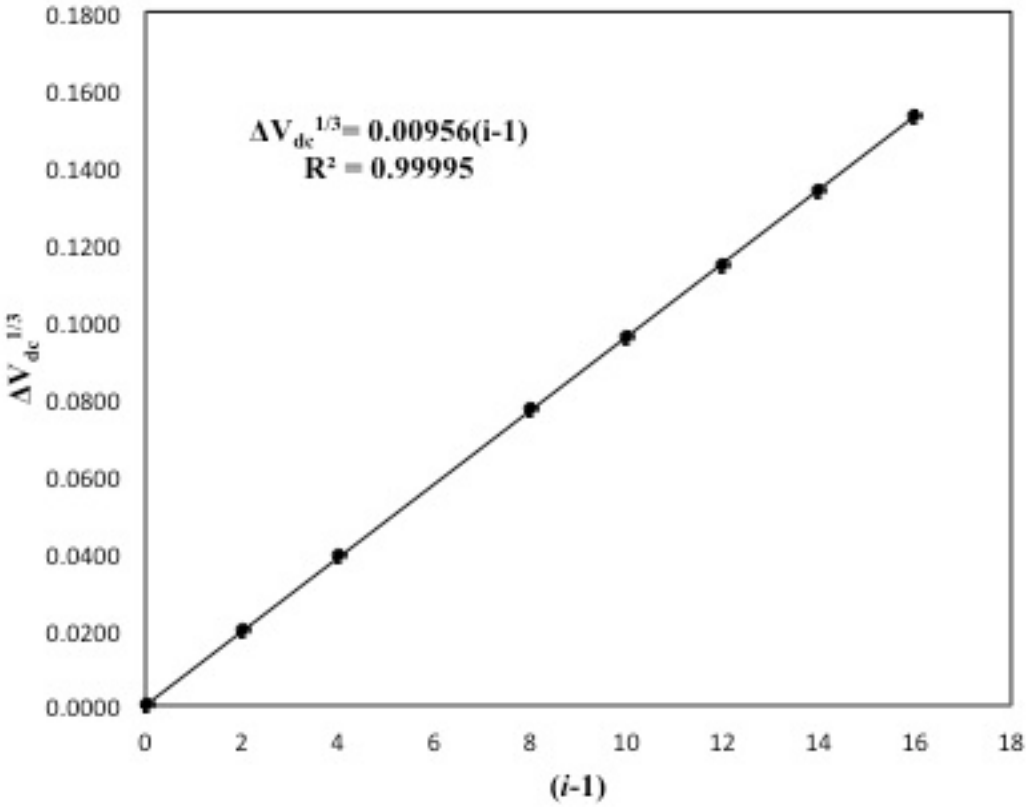

Figure A1.6: Plot of ΔVdc$^{1/3}$ Vs time along with the linear fitted line for a pure DEG drop prior to its first break-up.

From the expression for *k*, it is clear that the charge on the droplet is directly proportional to *k*. Therefore, fractional charge loss due to explosion of the droplet can be written as

$$f_q = 1 - (\frac{k_{after}}{k_{before}})^3 \quad \text{(A1.17)}$$

where k_{before} and k_{after} are the values of *k* prior to and after an explosion. Using this expression, for a charged DEG droplet evaporating under 0% RH and 25.3 ^{0}C yields a charge loss of about 36% after the first droplet break-up and about 31% after the second droplet break-up. This is in agreement to the values of 37% $\pm$ 2% obtained by **Li et. al. (2005)** for a pure DEG droplet evaporating under similar conditions.

A1.3.3 Determination of charge limits on droplets at break-up

Theoretically, for the Rayleigh limit to be valid, the apparent charge on the droplet at explosion must be equal to Rayleigh charge limit given by equation A1.1. Therefore, at droplet explosion, using equation A1.1, A.10 and the relationship between *k* and *q*, we get,

$$(x_b^-)^{3/2} = cV_{dc,b}^- \tag{A1.18}$$

with

$$c = \frac{6C_0}{\rho g z_0}\sqrt{\frac{2\pi^3\epsilon_0\gamma}{\lambda^3}} \tag{A1.19}$$

In equation A1.18, x_b^- and $V_{dc,b}^-$ are the values of the corresponding size parameter and voltage just prior to the break-up of the droplet. It should be noted here that *c* is a function of surface tension and for a droplet that is free of contaminants should yield a constant value for every explosion it undergoes.

Now, Using equations A1.13 and A1.11, the size parameter is calculated for corresponding peak occurrence times and the square of the size parameter is plotted against time. This data is fitted to equation A1.4 and the slope of the equation is equal to the co-efficient of evaporation (size parameter squared/s) as shown in the figure A1.7 below. The regressed equation gives a value of 30.276 for the evaporation rate whereas that obtained by Tu (2000) was around 37 for a pure DEG droplet evaporating under same conditions.

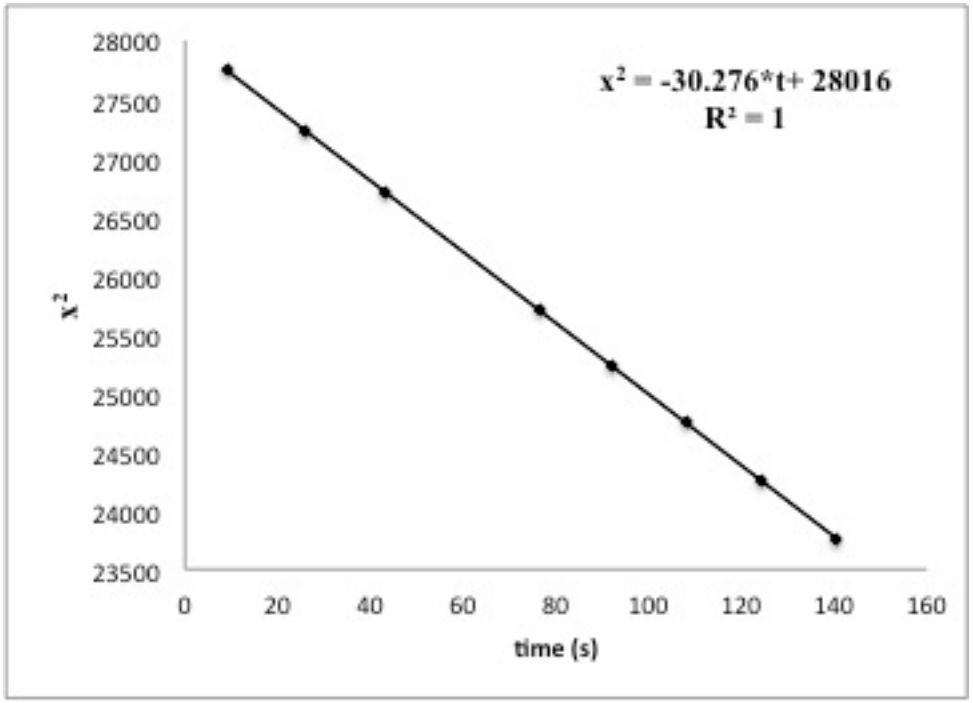

Figure A1.7: Plot of square of the size parameter with time prior to first droplet break-up of a pure DEG droplet.

Evaporation rate of the droplet can be determined much precisely by using an alignment procedure described in detail by Tu (2000). From the experimental light scattering spectra in figure A1.4 (a), occurrences of resonance peaks are tabulated. These resonance peaks are compared with the theoretical resonances generated. The set of theoretical resonances with the least alignment error is chosen as the optimum data set for a given refractive index. The size parameters corresponding to peak times and the constant α in equation A1.4 are obtained. It is to be noted here that the alignment procedure used here relates the square of the size parameter to a second order polynomial w.r.t. time even though in equation A1.4, x^2 is linear in time. This is because of the fact that minute

variations in the gas phase and slight impurities in the droplet leads to an error in the order of t^2. The resonance peaks along with the aligned theoretical size parameter values and their functional relationship is given in Table A1.2 for a pure DEG droplet with refractive index of 1.443 evaporating at a temperature of 25.3 ^{0}C.

Table A1.3: Resonances observed from an experimental run of pure DEG droplet correlated with theoretical results.

observed times	size parameter	peak width	mode no	order no	mode	time error
176.76336	149.14034	0.02377	156	10	2	0.18159
199.3906	147.60067	0.02992	154	10	2	0.03176
221.85163	146.05974	0.0373	152	10	2	-0.1329
244.14647	144.48818	0.00458	154	9	2	0.10518
265.96644	142.95821	0.00614	152	9	2	0.02063
287.62021	141.42679	0.00817	150	9	2	-0.07702
308.96531	139.89389	0.01078	148	9	2	-0.04631
330.29855	138.3595	0.01409	146	9	2	-0.18523
351.31125	136.82361	0.01825	144	9	2	-0.18648
372.16962	135.28623	0.02341	142	9	2	-0.21787
393.50286	133.67577	0.00219	144	8	2	0.04503
412.77044	132.20713	0.03739	138	9	2	0.27391
433.78314	130.62422	0.00414	140	8	2	0.06244
453.67991	129.09619	0.00563	138	8	2	0.03607
512.06436	124.50252	0.01341	132	8	2	0.13809
531.32007	122.968	0.01758	130	8	2	-0.00082
550.25524	121.43183	0.02282	128	8	2	-0.01094
569.02422	119.89403	0.02931	126	8	2	-0.04845
587.47266	118.35466	0.03724	124	8	2	0.03879
605.9211	116.8138	0.0468	122	8	2	-0.07236
624.36954	115.23149	0.00502	124	7	2	0.08385
642.01071	113.70419	0.00688	122	7	2	0.1824
659.66376	112.17513	0.00933	120	7	2	0.07427
677.1506	110.64425	0.01253	118	7	2	-0.06349
694.47124	109.11152	0.01667	116	7	2	-0.23212
refractive index, m = 1.443 regression relation, $x^2 = 25863.9 - 20.5867t + 6.92065 * 10^{-4}t^2$ std error in time (s) = 0.1268						

A1.4 Results and Discussions

In the present work, we have studied pure droplets of DEG and droplets of DEG doped with polyethylene glycol (PEG, 10000). PEG was dissolved in couple of drops of water before mixing with DEG so that the solution droplet is homogeneous. As soon as a drop is generated, water evaporates in a few milliseconds and PEG would precipitate out. The weight fraction of PEG in DEG was 0.86%. The resulting colloidal solution droplet was allowed to evaporate under 0% RH and 25.3 ^{0}C. The resonances observed and the correlated theoretical results for one such doped DEG droplet is shown in Table A1.4. The evaporation rates obtained in Table A1.3 for a pure DEG droplet and in Table A1.4 for a DEG droplet contaminated with PEG were similar. This shows that the evaporation rate of the droplet is not affected by low concentrations of the polymer. Charge limits on several droplets of DEG and DEG doped with PEG were calculated according to the analysis of section A1.3.3 above.

Table A1.4: Observed resonance peaks and correlated theoretical data for a DEG drop contaminated with trace amounts of PEG

observed times	x,size parameter	peak width	mode no	order no	mode	time error
36.62	156.05212	0.00755	165	10	2	0.04333
57.92	154.51857	0.00989	163	10	2	0.09384
79.2	152.98364	0.01285	161	10	2	-0.14299
99.84	151.44735	0.01654	159	10	2	-0.04266
120.18	149.90968	0.02112	157	10	2	0.05897
140.5	148.37067	0.0267	155	10	2	-0.11433
160.18	146.83037	0.03345	153	10	2	0.06078
179.84	145.28883	0.04149	151	10	2	-0.03276
199.52	143.72338	0.00531	153	9	2	-0.14992
218.24	142.19268	0.00709	151	9	2	-0.03645
236.62	140.66053	0.00939	149	9	2	0.14696
272.76	137.59175	0.01605	145	9	2	0.33705
290.82	136.05511	0.02069	143	9	2	0.04978
308.88	134.43775	0.00186	145	8	2	0.39939
326.62	132.91343	0.00258	143	8	2	-0.26505
375.98	128.33159	0.00654	137	8	2	0.12762
392.42	126.80119	0.00878	135	8	2	-0.21005
408.56	125.26915	0.01167	133	8	2	-0.48436
424.04	123.73547	0.01538	131	8	2	-0.333
439.52	122.20013	0.02006	129	8	2	-0.41395
454.68	120.66314	0.02589	127	8	2	-0.40542
483.06	117.58441	0.0418	123	8	2	0.8654
498.56	115.99449	0.00428	125	7	2	0.3001
512.74	114.46806	0.00589	123	7	2	0.21969
526.62	112.93989	0.00802	121	7	2	0.22344
540.48	111.40992	0.01083	119	7	2	0.03322
560.48	109.11152	0.01667	116	7	2	0.14032
573.72	107.57694	0.02193	114	7	2	0.04205
refractive index, m = 1.443 regression relation, $x^2 = 25164 - 22.0348t - 2.88117 * 10^{-3}t^2$ std error in time (s) = 0.269						

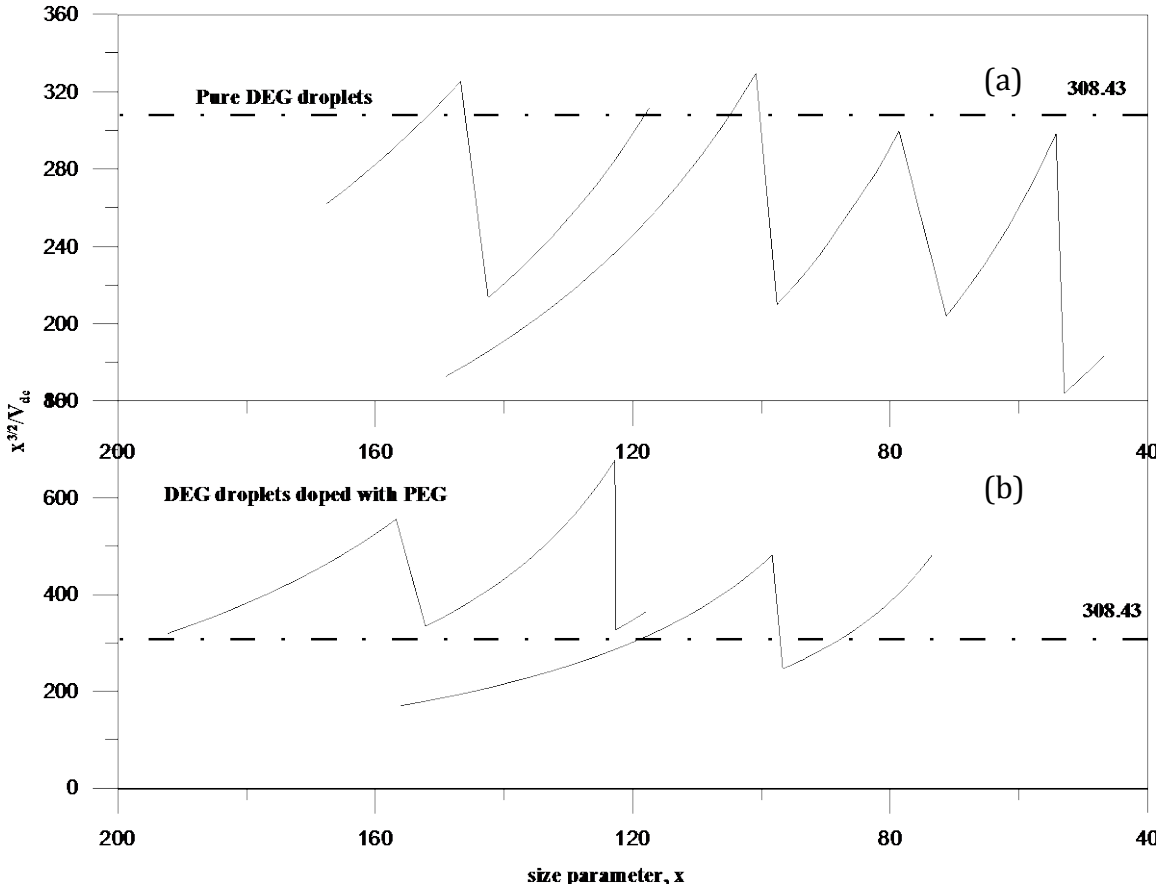

Figure A1.8: Charge limits Vs size parameter plots for different droplets of (a) DEG and (b) DEG contaminated with PEG during evaporation.

A plot of size parameter versus the charge limit values $(x_b^-)^{3/2}/V_{dc}$ is plotted for couple of droplets of DEG and DEG and PEG in figure A1.8. Theoretical Rayleigh limit for DEG droplets were calculated to be 308.43. This is shown as doted lines in the plots. General trend of such a plot shows that as the droplet evaporates (reduction in size parameter) the charge on the droplet increases and then once a certain charge is attained, it explodes. Once the droplet explodes, it again starts to evaporate and the process is repeated. For pure DEG droplets, each explosion occurs at the same limit and satisfies the Rayleigh instability. For DEG droplets doped with PEG, the charge limits predicted were

higher than that of the Rayleigh limit for a pure DEG drop. Also, it was expected that the charge limit would increase significantly as the droplet evaporated and the concentration of the contaminant increased. In our results, even though a general higher trend of charge limit was observed, for one drop the charge limit remained unchanged and for the other it increased slightly when compared to the first explosion. Due to lack of statistical data, the actual amount of increase in charge limits cannot be concluded.

A1.5 Conclusions

Charge limits on droplets of DEG and DEG doped with PEG during their explosions were studied by suspending a single droplet in an electrodynamic balance. The sizes of the droplets at different time instances are obtained from experimental light scattering spectrum using a rigorous alignment procedure. It was found that DEG droplets doped with a polymer can hold higher charge and explode at higher values than their theoretical Rayleigh limit.

Statistically significant data set needs to be obtained for estimation of the charge limit values. Also, different polymers with varying molecular weight can be studied for better understanding of such systems.

REFERENCES

1. Abadio, F. D. B., Domingues, A. M., Borges, S. V., & Oliveira, V. M. (2004). Physical properties of powdered pineapple juice—effect of malt dextrin concentration and atomization speed. *Journal of Food Engineering*, *64*(3), 285-287.
2. Agarwal, S., & Speyerer, C. (2010). Degradable blends of semi-crystalline and amorphous branched poly (caprolactone): Effect of microstructure on blend properties. *Polymer, 51*(5), 1024-1032.
3. Ajji, A., & Utracki, L. A. (1996). Interphase and compatibilization of polymer blends. *Polymer Engineering & Science*, *36*(12), 1574-1585.
4. Alhnan, M. A., & Basit, A. W. (2011). Engineering polymer blend microparticles: an investigation into the influence of polymer blend distribution and interaction. *European Journal of Pharmaceutical Sciences, 42*(1), 30-36.
5. Barba, A., Dalmoro, A., d'Amore, M., & Lamberti, G. (2012). Controlled Release of Drugs fromMicroparticles Produced by Ultrasonic Assisted Atomization Based on Biocompatible Polymers. *Chemical and Biochemical Engineering Quarterly, 26*(4), 345-353.
6. Barnes, M., Kung, C.-Y., Lermer, N., Fukui, K., Sumpter, B., Noid, D., & Otaigbe, J. (1999). Homogeneous polymer blend microparticles with a tunable refractive index. *Optics letters*, *24*(3), 121-123.
7. Berglund, R. N., & Liu, B. Y. (1973). Generation of monodisperse aerosol standards. *Environmental Science & Technology*, *7*(2), 147-153.
8. Biskos, G., Vons, V., Yurteri, C. U., & Schmidt-Ott, A. (2008). Generation and sizing of particles for aerosol-based nanotechnology. *Kona Powder Particle J,26*, 13-35.

9. Bock, N., Woodruff, M. A., Hutmacher, D. W., & Dargaville, T. R. (2011). Electrospraying, a reproducible method for production of polymeric microspheres for biomedical applications. *Polymers, 3*(1), 131-149.
10. Brenn, G. (2004). Concentration fields in drying droplets. *Chemical Engineering & Technology, 27*(12), 1252-1258.
11. Brenn, G., Wiedemann, T., Rensink, D., Kastner, O., & Yarin, A. L. (2001). Modeling and experimental investigation of the morphology of spray dryed particles. *Chemical Engineering & Technology, 24*(11), 1113-1116.
12. Campoy-Quiles, M., Ferenczi, T., Agostinelli, T., Etchegoin, P. G., Kim, Y., Anthopoulos, T. D., & Nelson, J. (2008). Morphology evolution via self-organization and lateral and vertical diffusion in polymer: fullerene solar cell blends. *Nature materials, 7*(2), 158-164.
13. Cao, Y., Zhang, J., Feng, J., & Wu, P. (2011). Compatibilization of immiscible polymer blends using graphene oxide sheets. *ACS Nano, 5*(7), 5920-5927.
14. Chang, M.-W., Stride, E., & Edirisinghe, M. (2010). A new method for the preparation of monoporous hollow microspheres. *Langmuir, 26*(7), 5115-5121.
15. Chapleau, N., & Favis, B. (1995). Droplet/fibre transitions in immiscible polymer blends generated during melt processing. *Journal of materials science, 30*(1), 142-150.
16. Charlesworth, D. H., & Marshall, W. R. (1960). Evaporation from drops containing dissolved solids. *AIChE Journal, 6*(1), 9-23.
17. Chegini, G., & Ghobadian, B. (2007). Spray Dryer Parameters for Fruit Juice Drying. *World Journal of Agricultural Sciences, 3*(2).

18. Chen, X. D., & Lin, S. X. Q. (2005). Air drying of milk droplet under constant and time-dependent conditions. *AIChE Journal, 51*(6), 1790-1799.

19. Davis, E. J., & Bridges, M. A. (1994). The Rayleigh limit of charge revisited: light scattering from exploding droplets. *Journal of aerosol science, 25*(6), 1179-1199.

20. Desai, K. G. H., & Jin Park, H. (2005). Recent developments in microencapsulation of food ingredients. *Drying technology, 23*(7), 1361-1394.

21. Devarakonda, V., & Ray, A. K. (2003). Effect of inter-particle interactions on evaporation of droplets in a linear array. *Journal of aerosol science*, *34*(7), 837-857.

22. Devarakonda, V., Ray, A. K., Kaiser, T., & Schweiger, G. (1998). Vibrating orifice droplet generator for studying fast processes associated with microdroplets. *Aerosol science and technology*, *28*(6), 531-547.

23. Duft, D., Lebius, H., Huber, B. A., Guet, C., & Leisner, T. (2002). Shape oscillations and stability of charged microdroplets. *Physical review letters,89*(8), 084503.

24. Dwivedi, C., & Dutta, V. (2012). Size controlled synthesis and photocatalytic activity of anatase TiO hollow microspheres. *Applied Surface Science*, *258*(24), 9584-9588.

25. Ehtezazi, T., Washington, C., & Melia, C. (1999). Determination of the internal morphology of poly (D, L-lactide) microspheres using stereological methods. *Journal of controlled release, 57*(3), 301-314.

26. Emerson, J. A., Toolan, D. T., Howse, J. R., Furst, E. M., & Epps III, T. H. (2013). Determination of Solvent–Polymer and Polymer–Polymer Flory–Huggins Interaction Parameters for Poly (3-hexylthiophene) via Solvent Vapor Swelling. *Macromolecules, 46*(16), 6533-6540.

27. Erdmann, N., Betti, M., Stetzer, O., Tamborini, G., Kratz, J., Trautmann, N., & Van Geel, J. (2000). Production of monodisperse uranium oxide particles and their characterization by scanning electron microscopy and secondary ion mass spectrometry. *Spectrochimica Acta Part B: Atomic Spectroscopy*, *55*(10), 1565-1575.
28. Esen, C., & Schweiger, G. (1996). Preparation of monodisperse polymer particles by photopolymerization. *Journal of colloid and interface science*,*179*(1), 276-280.
29. Esen, C., Kaiser, T., Borchers, M., & Schweiger, G. (1997). Synthesis of spherical microcapsules by photopolymerization in aerosols. *Colloid and Polymer Science*, *275*(2), 131-137.
30. Eslamian, M., Ahmed, M., & Ashgriz, N. (2006). Modelling of nanoparticle formation during spray pyrolysis. *Nanotechnology*, *17*(6), 1674.
31. Eslamian, M., Ahmed, M., & Ashgriz, N. (2009). Modeling of solution droplet evaporation and particle evolution in droplet-to-particle spray methods. *Drying Technology*, *27*(1), 3-13.
32. Fang, Z-P., Wang, G-l., Cai, G-P., Xu, C-W., & Qian, J. (2000). STUDY ON THE MORPHOLOGY OF POLYVINYL CHLORIDE/POLYSTYRENE BLENDS BY ELECTRON MICROPROBE ANALYSIS, *Chinese Journal of Chemical Engineering*, *18*(5), 437-441.
33. Favis, B. D., & Therrien, D. (1991). Factors influencing structure formation and phase size in an immiscible polymer blend of polycarbonate and polypropylene prepared by twin-screw extrusion. *Polymer*, *32*(8), 1474-1481.

34. Forrest, J. A., Dalnoki-Veress, K., Stevens, J. R., & Dutcher, J. R. (1996). Effect of free surfaces on the glass transition temperature of thin polymer films. *Physical review letters*, *77*(10), 2002.

35. Freitas, S., Merkle, H. P., & Gander, B. (2004). Ultrasonic atomisation into reduced pressure atmosphere—envisaging aseptic spray-drying for microencapsulation. *Journal of controlled release*, *95*(2), 185-195.

36. Frey, D. D., & King, C. J. (1986). Effects of surfactants on mass transfer during spray drying. *AIChE journal*, *32*(3), 437-443.

37. Friend, J. R., Yeo, L. Y., Arifin, D. R., & Mechler, A. (2008). Evaporative self-assembly assisted synthesis of polymeric nanoparticles by surface acoustic wave atomization. *Nanotechnology*, *19*(14), 145301.

38. Gao, Z., Grulke, E. A., & Ray, A. K. (2007). Synthesis of monodisperse polymer microspheres by photopolymerization of microdroplets. *Colloid and Polymer Science*, *285*(8), 847-854.

39. Guo, B., Tay, S. W., Liu, Z., & Hong, L. (2012). Embedding of Hollow Polymer Microspheres with Hydrophilic Shell in Nafion Matrix as Proton and Water Micro-Reservoir. *Polymers*, *4*(3), 1499-1516.

40. Handscomb, C. S., & Kraft, M. (2010). Simulating the structural evolution of droplets following shell formation. *Chemical Engineering Science*, *65*(2), 713-725.

41. Hecht, J. P., & King, C. J. (2000). Spray drying: influence of developing drop morphology on drying rates and retention of volatile substances. 1. Single-drop experiments. *Industrial & engineering chemistry research*, *39*(6), 1756-1765.

42. Hhunter, H., Ph. D. Thesis, University of Kentucky (2010).

43. Hunter, H. C., & Ray, A. K. (2009). On progeny droplets emitted during Coulombic fission of charged microdrops. *Physical Chemistry Chemical Physics, 11*(29), 6156-6165.

44. Jayanthi, G. V., Zhang, S. C., & Messing, G. L. (1993). Modeling of solid particle formation during solution aerosol thermolysis: the evaporation stage.*Aerosol Science and Technology*, *19*(4), 478-490.

45. Jukes, P. C., Heriot, S. Y., Sharp, J. S., & Jones, R. A. (2005). Time-resolved light scattering studies of phase separation in thin film semiconducting polymer blends during spin-coating. *Macromolecules*, *38*(6), 2030-2032.

46. Kamino, T., Yaguchi, T., Konno, M., Ohnishi, T., & Ishitani, T. (2004). A method for multidirectional TEM observation of a specific site at atomic resolution. *Journal of electron microscopy*, *53*(6), 583-588.

47. Kietzke, T., Neher, D., Kumke, M., Ghazy, O., Ziener, U., & Landfester, K. (2007). Phase separation of binary blends in polymer nanoparticles. *Small*, *3*(6), 1041-1048.

48. Kim, E. H.-J., Chen, X. D., & Pearce, D. (2009). Surface composition of industrial spray-dried milk powders. 2. Effects of spray drying conditions on the surface composition. *Journal of food engineering*, *94*(2), 169-181.

49. Leong, K. (1987). Morphological control of particles generated from the evaporation of solution droplets: theoretical considerations. *Journal of Aerosol Science*, *18*(5), 511-524.

50. Leong, K. (1981). Morphology of aerosol particles generated from the evaporation of solution drops. *Journal of Aerosol Science*, *12*(5), 417-435.

51. Li, K.-Y., Tu, H., & Ray, A. K. (2005). Charge limits on droplets during evaporation. *Langmuir, 21*(9), 3786-3794.

52. Li, H., & Hu, G. H. (2001). The early stage of the morphology development of immiscible polymer blends during melt blending: compatibilized vs. uncompatibilized blends. *Journal of Polymer Science Part B: Polymer Physics, 39*(5), 601-610.

53. Liu, B. Y. (1976). *Fine particles: Aerosol generation, measurement, sampling, and analysis*: Elsevier.

54. Liu, J., Rasheed, A., Dong, H., Carr, W. W., Dadmun, M. D., & Kumar, S. (2008). Electrospun Micro- and Nanostructured Polymer Particles. *Macromolecular Chemistry and Physics, 209*(23), 2390-2398.

55. Liu, J., Rasheed, A., Dong, H., Carr, W. W., Dadmun, M. D., & Kumar, S. (2008). Electrospun Micro- and Nanostructured Polymer Particles. *Macromolecular Chemistry and Physics, 209*(23), 2390-2398.

56. Mezhericher, M., Levy, A., & Borde, I. (2007). Theoretical drying model of single droplets containing insoluble or dissolved solids. *Drying Technology,25*(6), 1025-1032.

57. Mezhericher, M., Levy, A., & Borde, I. (2009). Modeling of droplet drying in spray chambers using 2D and 3D computational fluid dynamics. *Drying Technology, 27*(3), 359-370.

58. Mitchell, J., Snelling, K., & Stone, R. (1987). Improvements to the vibrating orifice aerosol generator. *Journal of Aerosol Science, 18*(3), 231-243.

59. Moghadam, S. H., Dinarvand, R., & Cartilier, L. H. (2006). The focused ion beam technique: a useful tool for pharmaceutical characterization. *International journal of pharmaceutics*, *321*(1), 50-55.

60. Mokarian-Tabari, P., Geoghegan, M., Howse, J. R., Heriot, S. Y., Thompson, R. L., & Jones, R. A. L. (2010). Quantitative evaluation of evaporation rate during spin-coating of polymer blend films: Control of film structure through defined-atmosphere solvent-casting. *The European Physical Journal E*, *33*(4), 283-289.

61. Mokarian-Tabari, P., Geoghegan, M., Howse, J., Heriot, S., Thompson, R., & Jones, R. (2010). Quantitative evaluation of evaporation rate during spin-coating of polymer blend films: Control of film structure through defined-atmosphere solvent-casting. *The European Physical Journal E*, *33*(4), 283-289.

62. Na, X. M., Gao, F., Zhang, L. Y., Su, Z. G., & Ma, G.-H. (2012). Biodegradable microcapsules prepared by self-healing of porous microspheres. *ACS Macro Letters*, *1*(6), 697-700.

63. Nešić, S., & Vodnik, J. (1991). Kinetics of droplet evaporation. *Chemical Engineering Science*, *46*(2), 527-537.

64. Newby, B. M. Z., & Composto, R. J. (2000). Influence of lateral confinement on phase separation in thin film polymer blends. *Macromolecules*, *33*(9), 3274-3282.

65. Okuyama, K., & Wuled Lenggoro, I. (2003). Preparation of nanoparticles via spray route. *Chemical Engineering Science*, *58*(3), 537-547.

66. Pingali, K. C., Rockstraw, D. A., & Deng, S. (2005). Silver nanoparticles from ultrasonic spray pyrolysis of aqueous silver nitrate. *Aerosol Science and technology*, *39*(10), 1010-1014.

67. Pinnick, R., & Auvermann, H. (1979). Response characteristics of Knollenberg light-scattering aerosol counters. *Journal of Aerosol Science, 10*(1), 55-74.

68. Qian, C., Mumby, S. J., & Eichinger, B. (1991). Phase diagrams of binary polymer solutions and blends. *Macromolecules, 24*(7), 1655-1661.

69. Rama Rao, G., Lopez, G. P., Bravo, J., Pham, H., Datye, A. K., Xu, H., & Ward, T. L. (2002). Monodisperse Mesoporous Silica Microspheres Formed by Evaporation-Induced Self Assembly of Surfactant Templates in Aerosols. *Advanced materials, 14*(18), 1301-1304.

70. Rathod, S., Rama Rao, G., Andrzejewski, B., López, G. P., Ward, T. L., Brinker, C. J., & Datye, A. K. (2003). *Monodisperse mesoporous microparticles prepared by evaporation-induced self assembly within aerosols.* MRS Proceedings

71. Richardson, H. E., Wittenberg, C., Cross, F., & Reed, S. I. (1989). An essential G1 function for cyclin-like proteins in yeast. *Cell, 59*(6), 1127-1133.

72. Risbud, M., Hardikar, A., & Bhonde, R. (2000). Growth modulation of fibroblasts by chitosan-polyvinyl pyrrolidone hydrogel: Implications for wound management?. *Journal of biosciences, 25*(1), 25-30.

73. Schmidt-Hansberg, B., Sanyal, M., Klein, M. F., Pfaff, M., Schnabel, N., Jaiser, S., . . . Scharfer, P. (2011). Moving through the phase diagram: morphology formation in solution cast polymer–fullerene blend films for organic solar cells. *Acs Nano, 5*(11), 8579-8590.

74. Schmidt-Hansberg, B., Sanyal, M., Klein, M. F., Pfaff, M., Schnabel, N., Jaiser, S., Schabel, W. (2011). Moving through the phase diagram: morphology formation in

solution cast polymer–fullerene blend films for organic solar cells. *Acs Nano*, *5*(11), 8579-8590.

75. Schneider, J., & Hendricks, C. (1964). Source of Uniform- Sized Liquid Droplets. *Review of Scientific Instruments*, *35*(10), 1349-1350.
76. Scott, C. E., & Macosko, C. W. (1995). Morphology development during the initial stages of polymer-polymer blending. *Polymer*, *36*(3), 461-470.
77. Seydel, P., Blömer, J., & Bertling, J. (2006). Modeling Particle Formation at Spray Drying Using Population Balances. *Drying Technology*, *24*(2), 137-146.
78. Seydel, P., Sengespeick, A., Blömer, J., & Bertling, J. (2004). Experiment and Mathematical Modeling of Solid Formation at Spray Drying. *Chemical Engineering & Technology*, *27*(5), 505-510.
79. Shabde, V. S., & Hoo, K. A. (2006). Design and operation of a spray dryer for the manufacture of hollow microparticles. *Industrial & engineering chemistry research*, *45*(25), 8329-8337.
80. Sharma, A., Jana, A. H., & Chavan, R. S. (2012). Functionality of Milk Powders and Milk- Based Powders for End Use Applications—A Review. *Comprehensive Reviews in Food Science and Food Safety*, *11*(5), 518-528.
81. Shine, A. D. (1994). Precipitation of homogeneous polymer mixtures from supercritical fluid solutions, US patent no.- 5,290,827
82. Shultz, A. R., & Young, A. L. (1980). DSC on freeze-dried poly (methyl methacrylate)-polystyrene blends. *Macromolecules*, *13*(3), 663-668.

83. Siepmann, F., Siepmann, J., Walther, M., MacRae, R., & Bodmeier, R. (2008). Polymer blends for controlled release coatings. *Journal of controlled release, 125*(1), 1-15.

84. Sloth, J., Kiil, S., Jensen, A. D., Andersen, S. K., Jørgensen, K., Schiffter, H., & Lee, G. (2006). Model based analysis of the drying of a single solution droplet in an ultrasonic levitator. *Chemical Engineering Science, 61*(8), 2701-2709

85. Smith, J. N., Flagan, R. C., & Beauchamp, J. (2002). Droplet evaporation and discharge dynamics in electrospray ionization. *The Journal of Physical Chemistry A*, *106*(42), 9957-9967.

86. Solval, K. M., Sundararajan, S., Alfaro, L., & Sathivel, S. (2012). Development of cantaloupe juice powders using spray drying technology. *LWT-Food Science and Technology*, *46*(1), 287-293.

87. Sullad, A. G., Manjeshwar, L. S., & Aminabhavi, T. M. (2010). Polymeric blend microspheres for controlled release of theophylline. *Journal of applied polymer science*, *117*(3), 1361-1370.

88. Sumpter, B. G., Noid, D. W., & Barnes, M. D. (2003). Recent developments in the formation, characterization, and simulation of micron and nano-scale droplets of amorphous polymer blends and semi-crystalline polymers. *Polymer, 44*(16), 4389-4403.

89. Sun, R., Lu, Y., & Chen, K. (2009). Preparation and characterization of hollow hydroxyapatite microspheres by spray drying method. *Materials Science and Engineering: C, 29*(4), 1088-1092.

90. Taflin, D. C., Ward, T. L., & Davis, E. J. (1989). Electrified droplet fission and the Rayleigh limit. *Langmuir*, *5*(2), 376-384.

91. Taflin, D. C., Zhang, S. H., Allen, T., & James Davis, E. (1988). Measurement of droplet interfacial phenomena by light- scattering techniques. *AIChE journal*,*34*(8), 1310-1320.

92. Tom, J. W., & Debenedetti, P. G. (1991). Formation of bioerodible polymeric microspheres and microparticles by rapid expansion of supercritical solutions.*Biotechnology progress*, *7*(5), 403-411.

93. Hauhua Tu, Ph. D. Thesis, University of Kentucky, 2001

94. Utracki, L. A. (2002). Compatibilization of polymer blends. *The Canadian Journal of Chemical Engineering*, *80*(6), 1008-1016.

95. Vehring, R. (2008). Pharmaceutical particle engineering via spray drying. *Pharmaceutical research*, *25*(5), 999-1022.

96. Vehring, R., Foss, W. R., & Lechuga-Ballesteros, D. (2007). Particle formation in spray drying. *Journal of Aerosol Science*, *38*(7), 728-746.

97. Walheim, S., Böltau, M., Mlynek, J., Krausch, G., & Steiner, U. (1997). Structure formation via polymer demixing in spin-cast films. *Macromolecules*,*30*(17), 4995-5003.

98. Walker, T. A., Raghavan, S. R., Royer, J. R., Smith, S. D., Wignall, G. D., Melnichenko, Y., Spontak, R. J. (1999). Enhanced Miscibility of Low-Molecular-Weight Polystyrene/Polyisoprene Blends in Supercritical CO2. *The Journal of Physical Chemistry B*, *103*(26), 5472-5476.

99. Walton, D. (2002). Spray- Dried Particle Morphologies. *Developments in Chemical*

Engineering and Mineral Processing, 10(3- 4), 323-348.

100. Wang, H., & Composto, R. J. (2000). Understanding morphology evolution and roughening in phase-separating thin-film polymer blends. *EPL (Europhysics Letters), 50*(5), 622.

101. Wang, J., Zhang, H., Yang, X., Jiang, S., Lv, W., Jiang, Z., & Qiao, S. Z. (2011). Enhanced water retention by using polymeric microcapsules to confer high proton conductivity on membranes at low humidity. *Advanced Functional Materials, 21*(5), 971-978.

102. Watkins, J. J., Brown, G. D., RamachandraRao, V. S., Pollard, M. A., & Russell, T. P. (1999). Phase separation in polymer blends and diblock copolymers induced by compressible solvents. *Macromolecules, 32*(23), 7737-7740.

103. Werner, S. R., Edmonds, R. L., Jones, J. R., Bronlund, J. E., & Paterson, A. H. (2008). Single droplet drying: Transition from the effective diffusion model to a modified receding interface model. *Powder Technology, 179*(3), 184-189.

104. Xuan and Yang (1985). Studies of the crystallization behavior in the crystalline/amorphous polymer blends: poly (ethylene oxide)/poly (methyl methcrylate) and poly (ethylene oxide)/ poly (methyl methcrylate), *Chinese Journal of Chemical Engineering, 3*(3), 280-288.

105. Yang, Y.-T., Chen, C.-T., Yang, J.-C., & Tsai, T. (2010). Spray-dried microparticles containing polymeric micelles encapsulating hematoporphyrin. *The AAPS journal, 12*(2), 138-146.

106. Zammarano, M., Maupin, P. H., Sung, L. P., Gilman, J. W., McCarthy, E. D., Kim, Y. S., & Fox, D. M. (2011). Revealing the interface in polymer nanocomposites. *ACS nano*, *5*(4), 3391-3399.

107. Zhang, H., & Takeoka, S. (2012). Morphological evolution within spin-cast ultrathin polymer blend films clarified by a freestanding method. *Macromolecules*, *45*(10), 4315-4321.

108. Zhou, H., Fang, J., Yang, J., & Xie, X. (2003). Effect of the supercritical CO on surface structure of PMMA/PS blend thin films. *The Journal of supercritical fluids*, *26*(2), 137-145.

VITA

Venkat Narayan Rajagopalan was born in Chennai, Tamil Nadu, India. After finishing his high school from Delhi Public School, Mathura, UP, India in 2000, he joined University of Madras, Chennai, India. In May, 2004 he received his Bachelor of Technology degree in Chemical Engineering and then entered Anna University, Chennai, India to pursue a Master of Technology degree in Chemical Engineering from there. After receiving his degree in May 2006, he joined Central Electrochemical Research Institute (CECRI), Chennai, India as a Senior Research Fellow and then in August 2007 joined the Graduate School at the University of Kentucky for pursuing his doctoral degree.